A Multidimensional Study of *Streptomyces* Morphogenesis and Development

PROEFSCHRIFT

ter verkrijging van de graad van doctor
aan de Universiteit Leiden,
op gezag van de Rector Magnificus prof. mr. C.J.J.M. Stolker
voorzitter van het College voor Promoties
in het openbaar te verdedigen op
woensdag 27 november 2013
klokke 12:30

door
Katherine Anna Celler
geboren te Vancouver, Canada
30 juli, 1985

PROMOTIECOMMISIE

Promotor:	Prof. dr. G.P. van Wezel
Overige leden:	Prof. dr. J. Brouwer
	Prof. dr. ir. A.J. Koster
	Prof. dr. ir. M.C.M. van Loosdrecht
	Prof. dr. H.P. Spaink
	Prof. dr. hab. J. Zakrzewska-Czerwińska

Enabling new technology

This research was supported by the Dutch Technology Foundation STW, which is part of the Netherlands Organisation for Scientific Research (NWO) and partly funded by the Ministry of Economic Affairs (project number 10379).

Printing of this thesis was partially sponsored by the Stichting tot Bevordering van de Elektronenmicroscopie in Nederland (SEN).

Printed by Smart Printing Solutions, Gouda, the Netherlands.

‘‘There’s a lot of beauty in ordinary things -’’

Pam Halpert, the office

TABLE OF CONTENTS

Chapter 1

General Introduction and Outline of Chapter Contents

GENERAL INTRODUCTION

Streptomycetes are Gram-positive multicellular soil-dwelling bacteria which are commercially used as natural producers of antibiotics, anticancer agents and immunosuppressants, as well as many industrial enzymes (Hopwood 2007). Similarly to fungi, they carry out a complex developmental life cycle, forming highly structured multicellular colonies composed of physiologically distinct hyphae (Miguelez *et al.* 2000). This life cycle starts with the germination of a spore, from which one or more germ tubes emerge. A complex mycelial network is formed as the hyphae grow and branch to form what is called the vegetative or substrate mycelium (Chater and Losick 1997). Growth occurs by tip extension, during which newly synthesized wall material is incorporated at the hyphal apex (Gray *et al*. 1990). In Streptomyces, the combination of tip growth and branching results in exponential growth of the organism (Jakimowicz and van Wezel 2012).

Nutrient depletion and other stresses (heat, drought, competing microbes) are considered the major triggers for the onset of aerial mycelium formation in the soil and also on solid-grown cultures in the laboratory environment. At this point, hydrophobic vegetative hyphae break through the moist surface of the soil or agar and grow into the air (Claessen *et al.* 2006). Multiple cell division occurs, whereby up to 100 septa are formed more or less simultaneously, and the multigenomic aerial hyphae are converted into chains of unigenomic spores. These spores then disseminate to start the formation of new colonies in more favorable conditions.

In liquid-grown cultures, on the other hand, most streptomycetes only grow vegetatively. Hyphae grow and branch, taking on a variety of morphological shapes, from dense pellets to small fragmented mycelia. In general, the morphology of liquid-culture pellets is a determining factor for productivity during industrial fermentations of filamentous organisms (van Wezel *et al.* 2009), with larger clumps favoring antibiotic production in *Saccharopolyspora erythraea* (Wardell *et al.* 2002), and fragmentation stimulating enzyme production by *Streptomyces lividans* (van Wezel *et al.* 2006). The understanding and control of mycelial morphology is thus key for optimization of industrial fermentations (Celler *et al.* 2012). With this in mind, the purpose of this work was to combine different approaches and techniques to arrive at a better understanding of *Streptomyces* morphogenesis and development, with the ultimate aim to improve *Streptomyces* as a production platform in industrial biotechnology (Figure 1).

A natural starting point for the study of morphogenesis is the cytoskeleton, or cellular scaffolding, which helps to maintain and change cell shape, but also plays an important role

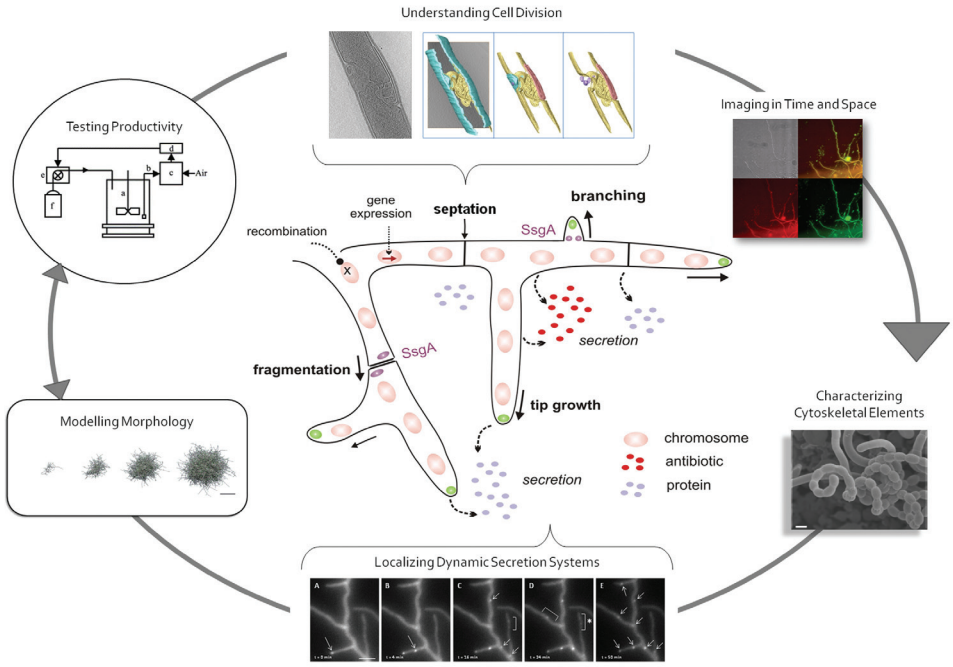

Figure 1**. **The systems biology of growth and production.

The basis of morphogenesis is the cytoskeleton, a dynamic collection of proteins which helps to maintain and control cell shape, but also influences intracellular trafficking and cell division. As the Streptomyces mycelium grows, branching frequency, tip growth rate and fragmentation of hyphae are influenced and controlled by the combination of cytoskeletal proteins and growth conditions. Novel imaging techniques, such as cryo-correlative light and electron microscopy and specifically tomography, can provide fundamental insight into vegetative cell division and its effect on development within a pellet. At the same time, fluorescent live imaging in time and space is an invaluable tool to better understand and localize dynamic secretion systems. Combining the multi-scale information gained can lead to improved morphological models and provide a test drive for the fermentation process. The aim is to improve Streptomyces as a production platform in industrial biotechnology.

in many dynamic cellular processes such as intracellular trafficking and cell division. Until recent years, the cytoskeleton was believed to be a feature unique to eukaryotic organisms, but this perspective was overturned when homologs of all three known eukaryotic cytoskeletal elements - actin, tubulin, and intermediate filaments (IFs) - were identified in prokaryotes and implicated in major cell functions, including growth, morphogenesis, cell division, DNA partitioning and cell motility (Graumann 2007; Cabeen and Jacobs-Wagner 2010). In addition, new elements have been identified which have no apparent eukaryotic counterparts, such as the Walker A-Type ATPases or the bactofilins (Koonin 1993; Kühn *et al.* 2010).

Multidimensional imaging techniques have contributed to new insights and demonstrated the astonishing complexity of the bacterial intracellular world, demonstrating cytoskeletal proteins forming filaments or patches, often rapidly translocating in a directed manner to respond to the many changing functions of the cell. The recent advances made towards understanding the role of cytoskeletal proteins in controlling bacterial shape and division, with particular emphasis on modern imaging approaches, are reviewed in **CHAPTER 2**.

Experiments to identify the localization of proteins in cells, such as for the cytoskeletal proteins described above, is often performed by tagging the protein with a fluorescent reporter such as eGFP (green fluorescent protein). Nowadays, *in vivo* multidimensional fluorescence microscopy enables the collection of very large data sets showing the directed spatial relocation of dynamic proteins in three-dimensional time lapse movies. Automated analysis and particle tracking are necessary to facilitate physical parameter estimation and large-scale analysis of localization experiments and/or object dynamics. To tackle this problem, we developed a particle tracking algorithm to specifically deal with tracking of fluorescently-tagged proteins in *Streptomyces*. It involves the application of a series of image filtering methods for optimal foci detection with subsequent nearest-neighbour tracking to link detections into tracks that can be analyzed. The algorithm was submitted to the Particle Tracking Challenge of the IEEE International Symposium on Biomedical Imaging (ISBI) in 2012 (Chenouard *et al.*, *submitted for publication*). Using the software allowed us to provide a mathematical tracking analysis of diffusion-limited foci in vegetative and aerial hyphae of *Streptomyces*.

The algorithm was applied to analyze the dynamic localization of TatA, the most abundant unit of the Tat (twin-arginine translocation) complex. The Tat pathway transports folded proteins across the bacterial cytoplasmic membrane and is a major route of protein export in *Streptomyces*. A better understanding of where and when secretion takes place in hyphae can lead to important insights for strain-improvement and rational process design. TatA localizes dynamically before colocalizing with TatBC to form an active translocation complex. **CHAPTER 3** provides a quantitative analysis of TatA movement, revealing the dynamics of complex assembly at different stages as well as the total time needed to arrive at the final stage in localization, roughly 2 µm behind the tip. Our easy-to-use particle tracking package should allow for the study of the dynamics of many other proteins and protein complexes in these fascinating multicellular microorganisms.

At higher magnification, the application of electron microscopy to *Streptomyces* hyphae provides a unique opportunity to visualize and increase fundamental understanding of morphogenesis, capturing the ultrastructure of tip growth, branching, and cell division

at nanometer resolution. Unlike other electron microscopy techniques, cryo-electron tomography (cryo-ET) enables the collection of structural information under conditions that are directly relevant to the native state of the cell (Subramaniam 2005). We applied cryo-ET to better understand vegetative cell division and its effect on development within a pellet. In fact, during the *Streptomyces* life cycle, two distinct forms of cell division occur. In aerial hyphae, cell division occurs by septation, where thick, double-layer sporulation septa are formed. During septation, a significant amount of cell-wall material is synthesized and remodeled during the metamorphosis of unicellular prespore compartments into mature spores (McCormick 2009). In vegetative hyphae, on the other hand, cell division occurs by the formation of crosswalls at irregular intervals of roughly 5-10 µm. These crosswalls delimit the syncytial cells, but do not constrict, and do not lead to cell fission. Much is known about aerial septation, but little was known of vegetative division. Using the new Netherlands Centre for Electron Nanoscopy (NeCEN) 300 keV Titan microscope to image hyphae at the high resolution of 10 nm, we discovered that crosswall formation is preceded by the formation of large membrane structures delimiting hyphae.

To identify the membrane components and better understand their function, we developed cryo-correlative light and electron tomography (cryo-CLET). Cryo-CLET correlates the images acquired by fluorescence light microscopy and electron tomography, enabling selective labeling and identification of cellular components as well as DNA and mapping of these lower resolution data onto high resolution tomograms. Using a combination of cryo-CLET and live fluorescent light microscopy, we discovered that the membranes, enriched in phosphatidylglyderol and cardiolipin, dynamically localize during development, and play a major role in division-site selection and nucleoid occlusion in *Streptomyces* hyphae. A better understanding of vegetative cell division can lead to new insight into mycelial differentiation and morphogenesis, as well as fragmentation. **CHAPTER 4** discusses these results.

As mentioned previously, morphology and productivity in filamentous organisms are closely connected. Morphological modeling is a valuable tool to predict optimal fermentation conditions, applicable in, for example, strain improvement approaches. Such a form of modeling should include important biological details, such as the correlation between gene expression and protein localization on the one hand, and growth and product formation on the other. Combining different modeling approaches, a structured, 3D morphological modeling framework for rational design of *Streptomyces* species was developed and is described in **CHAPTER 5**. The initial development of an interactive 3D web implementation (using HTML5 and WebGL) of the Matlab model are described in **CHAPTER 6**. The objective is to ultimately create an interactive model which can be a test-drive for the fermentation

process, where several input variables (such as bulk oxygen concentration, growth rate or morphological parameters such as distance between branches or maximum branch length) can be adjusted to arrive at an optimal production strain.

Finally, perhaps due to their filamentous growth and multicellular nature, *Streptomyces* have a particularly wide range of coiled-coil proteins, proposed to be cytoskeletal in nature. Based on sequence analysis, streptomycetes may have more than ten IF-like elements, and preliminary mutational analysis suggests specific functions for a number of these proteins in the control of cell integrity, growth, development, protein secretion and DNA segregation. **CHAPTER 7** discusses the functional analysis of two pairs of cytoskeletal genes: SCO2259, SCO2260 and SCO3285, SCO3286 and their effects on sporulation-specific cell division.

A general conclusion to this thesis is provided in **CHAPTER 8**.

Chapter 2

A Multidimensional View of the Bacterial Cytoskeleton

Katherine Celler, Roman I. Koning, Abraham J. Koster
and Gilles P. van Wezel

Journal of Bacteriology. 2013 Apr; 195(8):1627-36

ABSTRACT

The perspective of the cytoskeleton as a feature unique to eukaryotic organisms was overturned when homologs of the eukaryotic cytoskeletal elements were identified in prokaryotes and implicated in major cell functions, including growth, morphogenesis, cell division, DNA partitioning, and cell motility. FtsZ and MreB were the first identified homologs of tubulin and actin, respectively, followed by the discovery of crescentin as an intermediate filament-like protein. In addition, new elements were identified which have no apparent eukaryotic counterparts, such as the deviant Walker A-type ATPases, bactofilins, and several novel elements recently identified in streptomycetes, highlighting the unsuspected complexity of cytostructural components in bacteria. *In vivo* multidimensional fluorescence microscopy has demonstrated the dynamics of the bacterial intracellular world, and yet we are only starting to understand the role of cytoskeletal elements. Elucidating structure-function relationships remains challenging, because core cytoskeletal protein motifs show remarkable plasticity, with one element often performing various functions and one function being performed by several types of elements. Structural imaging techniques, such as cryo-electron tomography in combination with advanced light microscopy, are providing the missing links and enabling scientists to answer many outstanding questions regarding prokaryotic cellular architecture. Here we review the recent advances made toward understanding the different roles of cytoskeletal proteins in bacteria, with particular emphasis on modern imaging approaches.

When the term 'cytoskeleton' was first coined in 1931 (Wintrebert 1931), cytoskeletons were thought to consist of fibrous structural elements within a cell which, like the bones in our body, exist to provide reinforcement. It gradually became clear, however, that the cytoskeleton is not so much a static structural system like spokes in a wheel but is rather a highly dynamic system responsible for major processes in the cell, including muscle contraction (Banga and Szent-Györgyi 1942), the beating of cilia (Gibbons and Rowe 1965), chromosome segregation (Inoué and Sato 1967), cell division (Schroeder 1972), phagocytosis (Kaplan 1977), and organelle transport (Brady 1985; Vale *et al*. 1985), besides providing cell structure.

Still, it was a widely held notion that the cytoskeleton, consisting of microtubuli, microfilaments, and intermediate filaments (IFs), with cross-linking and other associating proteins providing additional levels of complexity (Alberts *et al.* 2002), is a feature unique to eukaryotic cells. The existence of a multifunctional cytoskeleton in bacteria became generally accepted only in the last decade, when the concept of bacterial cells as sacculi of freely diffusible proteins was overturned, and it was established that they, in fact, contain homologs of all known eukaryotic cytoskeletal elements (Graumann 2007; Margolin 2009; Young 2010). FtsZ (a tubulin homolog [Bi and Lutkenhaus 1991]) and MreB (an actin homolog [Jones *et al.* 2001]) were the first to be characterized; later, crescentin, the first intermediate filament (IF)-like protein, was discovered in *Caulobacter crescentus* (Ausmees *et al*. 2003). Currently, there are also newly identified elements with no eukaryotic counterparts, namely, the deviant Walker Amotif ATPases (Koonin 1993) and bactofilins (Kühn *et al.* 2010), clear evidence of the complexity of the bacterial cytoskeleton, while many elements are likely still to be discovered.

On the cellular scale, much has been learned about the cytoskeleton based on fluorescence light microscopy (fLM) studies and, in recent years, also via atomic force microscopy (AFM), which has been applied for the study of live cells as well as of isolated membrane proteins or microtubules (Hamon *et al.* 2010), by measurement of surface properties. On the molecular scale, X-ray crystallography and nuclear magnetic resonance (NMR) spectroscopy are providing valuable structural information. In fact, rather than sequence similarity analyses, the main methods used for identification of prokaryotic cytoskeletal elements have been based on a combination of crystal structures, *in vitro* properties, and *in vivo* functional behavior (Cabeen and Jacobs-Wagner 2010). Bridging the gap between cellular and molecular structural studies (Figure 1), cryo-electron tomography (cryo-ET) is taking its place as an important part of the imaging arsenal, providing structural information about protein complexes under conditions directly relevant to the native state of the cell (Subramaniam 2005; Koning and Koster 2009; Tocheva *et al.* 2010; McIntosh *et al.* 2005; Lučič *et al.* 2005). Combining tomography with the

aforementioned imaging methods provides the multiscale and multidisciplinary approach needed to understand how cytoskeletal proteins function within the context of the cell.

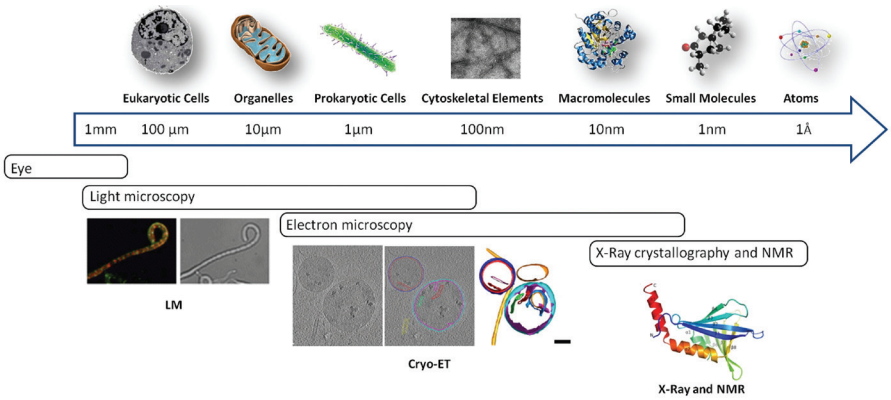

Figure 1. Resolution ladder demonstrating imaging techniques which can be used at different scales.
Light microscopy (LM) can be used to image the live localization of proteins tagged with fluorescent reporters to obtain dynamic information; at higher resolution, cryo-electron tomography (cryo-ET) can provide structural information about the localization of, for example, cytoskeletal elements within the cell. Crystal structures of the proteins of interest can be obtained via X-ray crystallography or nuclear magnetic resonance spectroscopy. LM images adapted from reference (Willemse et al. 2011) with permission from Cold Spring Harbor Laboratory Press; cryo-ET images adapted from reference (Koning and Koster 2009) with permission from Elsevier; X-ray and NMR images adapted from reference (Xu et al. 2009) with permission from the American Society for Biochemistry and Molecular Biology.

In this review, we focus on the different roles of the major cytoskeletal proteins and demonstrate ways in which multiscale imaging techniques have provided insight into the organization and spatial arrangement of cytoskeletal filaments. In addition, we highlight their function in the morphologically unusually complex mycelial *Streptomyces*, where many of the elements take on new and distinct roles. We believe that streptomycetes are a good illustration of the flexibility of core cytoskeletal protein motifs, where one type of element can perform various functions and one function can be performed by several types of elements (Graumann 2007; Cabeen and Jacobs-Wagner 2010). The review is nonexhaustive, and for detailed information on specific filament-forming proteins in bacteria we refer the reader to excellent reviews elsewhere (Graumann 2007; Cabeen and Jacobs-Wagner 2010; Shih and Rothfield 2006; Michie and Löwe 2006; Ingerson-Mahar and Gitai 2012).

DETERMINING (AND MAINTAINING) BACTERIAL CELL SHAPE

Bacteria have a wide variety of shapes, from the more common spherical and rod shapes to spiral, square, and filamentous shapes, and the molecular basis underlying cell shape is complex (Margolin 2009; Young 2010; Cabeen and Jacobs-Wagner 2005). Maintaining shape throughout cell growth and division is important if cells are to proliferate. In most bacteria, the external peptidoglycan (PG) wall, or murein sacculus, is responsible for maintaining cell shape by providing a rigid protection against osmotic pressure. Some bacteria, however, lack a cell wall and still maintain clearly defined shapes, ranging from the cocci of *Acholeplasmato* the tapered flask-like shape of some *Mycoplasma* species and the spiral shape of *Spiroplasma* species (Cabeen and Jacobs-Wagner 2005). It is little wonder that a wide variety of shape-defining and -maintaining cytoskeletal elements, forming a variety of superstructures (Pilhofer and Jensen 2013), must exist to enable this diversity.

MreB AND MreB-LIKE PROTEINS

In rod-shaped bacteria, mutation of *rodA*, *rodZ*, and *mreBCD* resulted in loss of shape, with formation of round cells that eventually die (Jones *et al.* 2001; Figge *et al.* 2004; Kruse *et al*. 2003; Defeu Soufo and Graumann 2003). Their structural analysis identified MreB as an actin homolog (van den Ent *et al.* 2001). Gram-negative bacteria apparently have a single *mreB* gene, typically in an operon with *mreC* and *mreD*, while genomes of Gram-positive bacteria encode up to three MreB-like proteins (MreB, Mbl, and MreBH in *Bacillus subtilis*). Imaging of MreB-green fluorescent protein (MreB-GFP) revealed patches localized in a spiral-like fashion along the long axis of cells, which was explained by MreB aiding in peptidoglycan deposition (Jones *et al.* 2001; Dye *et al.* 2005; Srivastava *et al.* 2007; Vats and Rothfield 2007) (Figure 2). Recent experiments, however, contradicted the notion of the existence of continuous helices and suggested rather a model whereby MreB moves circumferentially around the cell, perpendicular to its length, with synthesis complexes moving independently of each other in both directions (Garner *et al.* 2011). Inhibition of peptidoglycan synthesis blocks filament motion within 10 to 30 s, suggesting that PG synthesis drives the motion of MreB—and not vice versa. In fact, though previous studies have suggested that MreB dynamics are driven by its own polymerization, MreB rotation around the long axis of the cell requires the assembly of the peptidoglycan cell wall (van Teeffelen *et al.* 2011). Total internal reflection fluorescence microscopy visualized the dynamic relationship between MreB paralogs and the cell-wall synthesis machinery in *Bacillus* (Domínguez-Escobar *et*

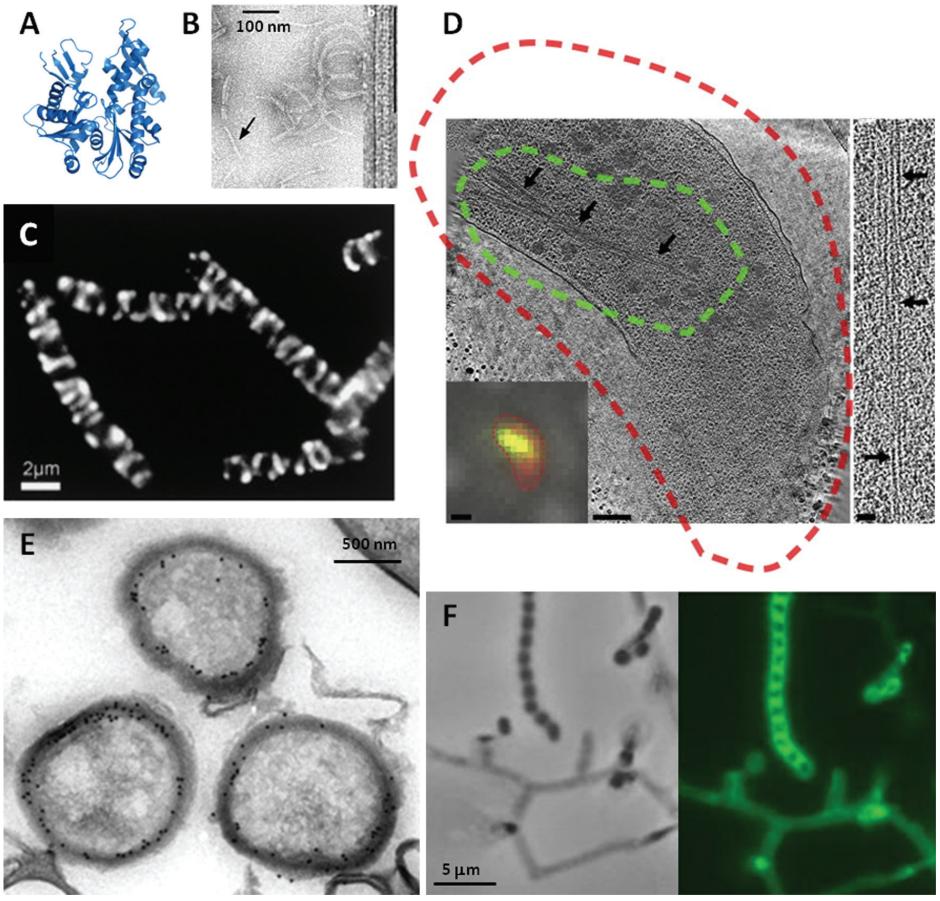

Figure 2. Structure and microscopy of MreB. *(A and B) The fold of prokaryotic MreB is similar to that its eukaryotic counterpart, actin (A), and MreB assembles into actin-like filaments (B). (C) The seemingly helical localization of an (MreB-like) Mbl-GFP fusion protein in cells in rod-shaped B. subtilis is now called into question (Margolin 2012; Swulius et al. 2011; Swulius and Jensen 2012). (D) In fact, though cytoplasmic MreB filaments are visible in tomograms, no helical filaments were seen in several rod-shaped bacteria, and helical filaments seen in E. coli were shown to be an artifact of the N-terminal YFP tag. In panel D, a tomographic slice through a Vibrio cholerae cell overexpressing GFP-MreB is shown. The cryo-fLM inset shows the cell stained with membrane dye FM 4-64 (red) and expressing GFP-MreB (green); dashed lines in the main image represent the fluorescent signal boundaries. On the right side, a 15-nm-thick tomographic slice through an MreB bundle not fused to GFP is shown.The scale bars represent 1m in the fLM inset, 200 nm in the cryo-electron tomography slice, and 50 nm in the higher-magnification inset. In Streptomyces coelicolor, MreB is not essential for vegetative growth but is essential for spore integrity and has been shown by immunoelectron microscopy (E) and fluorescence microscopy (F) to localize to the spore envelope. Panel B adapted from (van den Ent et al. 2001) with permission from the Nature Publishing Group; panel C from (Jones et al. 2001) with permission from Elsevier Ltd.; panel D from (Swulius et al. 2011) with permission from Elsevier Ltd.; and panels E and F from (Mazza et al. 2006) with permission from John Wiley and Sons.*

al. 2011; Vats *et al.* 2009), and similar patch-like localizations of MreB and dynamics were found in *Escherichia coli* and *Caulobacter crescentus*, suggesting that the behavior is widely conserved. These studies sparked a large debate. Is the helical organization the natural configuration that a filamentous structure on the inner surface of a cylinder will assume? Or are the localization patterns an artifact of images taken with long exposure times? Or is helical localization perhaps due to the effect of fluorescent fusions on tagged proteins? It is now becoming clear that different imaging techniques are required to corroborate the observed localization patterns (Margolin 2012). Cryo-electron tomography corroborated the absence of long (80-nm) MreB filaments near or along the inner membrane of six different rod-shaped bacteria, although use of correlative cryo-light and electron tomography of GFP-MreB allowed the identification of cytoplasmic MreB bundles, showing that MreB is indeed detectable by cryo-ET (Swulius *et al.* 2011). The same researchers later demonstrated that helical localization may be induced by fluorescent tagging: cryo-ET on *E. coli* cells producing native and yellow fluorescent protein (YFP)-tagged MreB demonstrated that MreB localizes in a helix when it is N-terminally tagged with YFP, while, when tagged with mCherry within an internal loop, it localizes in the same manner as native MreB (Swulius and Jensen 2012).

COILED-COIL PROTEINS: INTERMEDIATE FILAMENTS IN BACTERIA?

If MreB is mainly involved in maintaining the rod shape, some intermediate filament-like proteins act to control other bacterial shapes. Crescentin (CreS), bearing remarkable architectural and biochemical relatedness to eukaryotic IF proteins, was the first to be identified in this class; other IF-like proteins include CfpA (Izard *et al.* 2004; You *et al.* 1996), Scc (Mazouni *et al.* 2006), AglZ (Yang *et al.* 2004), and the four Ccrp proteins of *Helicobacter* (Specht *et al.* 2011; Waidner *et al.* 2009), as well as FilP (Bagchi *et al.* 2008) and Scy (Holmes *et al.* 2013) in *Streptomyces*. Because, unlike crescentin, the other proteins do not actually have a high degree of structural similarity to IF proteins and may in fact present a case of convergent evolution (Graumann 2009), they have also been termed coiled-coil rich proteins, or Ccrps.

Crescentin (CreS) forms a filamentous structure at the short axis of the curved bacterium *C. crescentus* (Ausmees *et al.* 2003). Deletion of the creS gene turns curved *C. crescentus* cells into straight rods, demonstrating that crescentin is required for the curved (crescent) cell shape. Cryo-electron tomography of *C. crescentus* revealed multiple filament bundles, which fall into four major classes based on their shape and location (inner curvature, cytoplasmic, polar, and ring-like [Ausmees *et al*. 2003]). Bundles, however, persisted in crescentinless

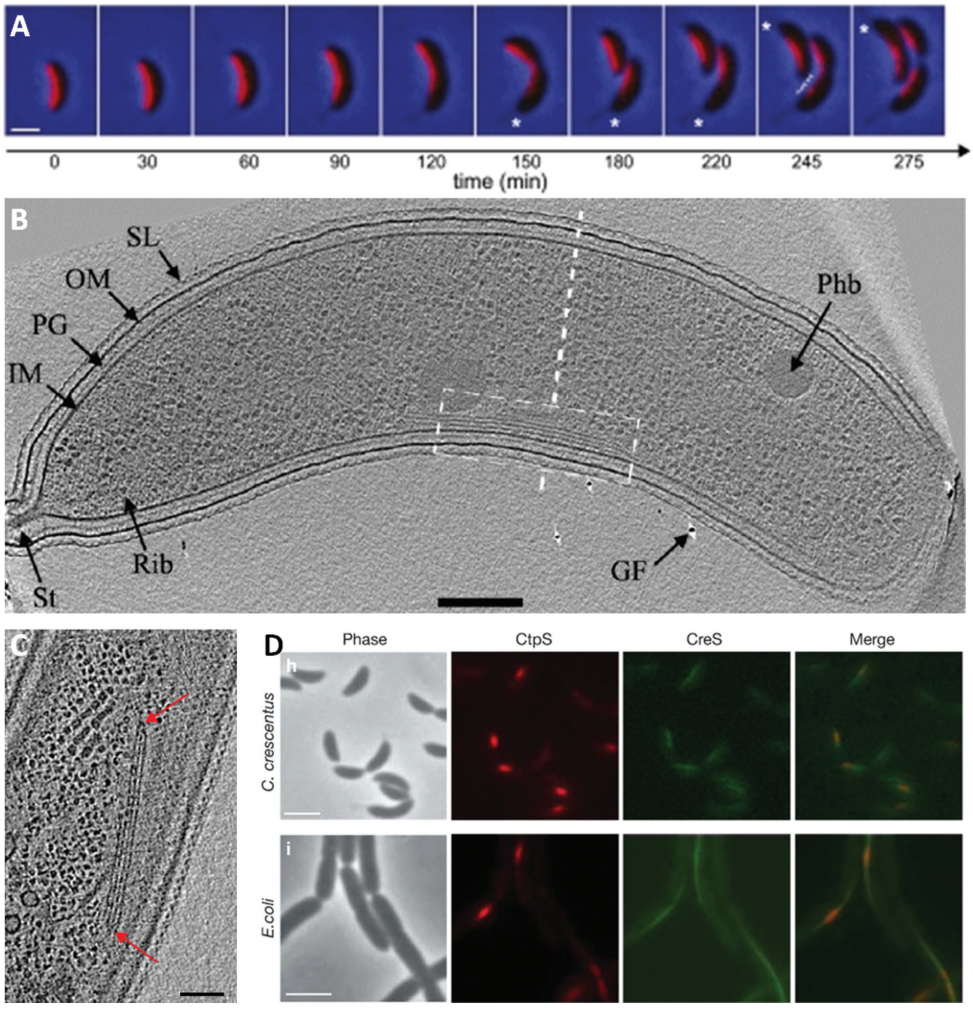

Figure 3. Discovery of metabolic enzyme CtpS as a novel filament-forming protein in Caulobacter crescentus. *(A) A time-lapse series of images of the GFP-labeled crescentin structure (red; laid over phase-contrast images) during the course of the cell cycle shows crescentin localizing to the short axis of curved C. crescentus cells. (B and C) Cryo-ET confirmed the presence of filament bundles (B), though bundles were still present in a crescentin deletion strain (C). This led to the discovery of metabolic enzyme CtpS as a novel filament-forming protein in C. crescentus. (D) CtpS and CreS colocalize. Bars, 1m (A), 200 nm (B), 50 nm (C), and 2 m (D). Structural features in panel B: SL, surface layer; OM, outer membrane; PG, peptidoglycan layer; IM, inner membrane; St, stalk; Rib, probable ribosome; GF, gold fiducial used to align images; Phb, putative poly-β-hydroxybutyrate granule. Panel A adapted from (Charbon et al. 2009) with permission from Cold Spring Harbor Laboratory Press; panel B adapted from (Briegel et al. 2006) with permission from John Wiley and Sons; panels C and D adapted from (Ingerson-Mahar et al. 2010) with permission from the Nature Publishing Group.*

mutants and in cells treated with A22, a compound with causes depolymerization of MreB filaments (Gitai *et al.* 2005), suggesting that they are composed of as-yet-unidentified cytoskeletal elements. This led to the identification of the metabolic enzyme CtpS as a novel filament-forming protein in *C. crescentus*, interacting dynamically with CreS to regulate cell curvature (Figure 3). The bifunctionality of CtpS filaments, which have a metabolic as well as a morphogenic role, demonstrates that protein polymerization may serve different functions within different cell contexts. Polymerization may have initially occurred for nonstructural, regulatory reasons— and the development of cytoskeletal and structural function of some proteins occurred later, during diversification and evolution. The four coiled-coil proteins of *Helicobacter pylori* (Ccrp48, Ccrp59, Ccrp1142, and Ccrp1143) have all been shown to be essential for the maintenance of proper (spiral) cell shape (Specht *et al.* 2011; Waidner *et al.* 2009). Deletion of these genes results in almost straight chained cells; in addition, though flagella are not affected, motility is reduced. All four Ccrps have different multimerization and filamentation properties and different types of smallest subunits and do not copurify, suggesting that the filaments have different though complementary roles (Yang *et al.* 2004).

The *Streptomyces* cytoskeletal element Scy was recently proposed to control polarized growth in existing hyphal tips, as well as to promote new tip formation during branching (Holmes *et al.* 2013). Deletion of *scy* affects polarized growth and, as a consequence, also hyphal geometry, resulting in irregular hyphal width, short hyphal length, and aberrant branching. FilP, encoded from a gene immediately downstream of *scy*, is important for the stability of filamentous hyphae and for correct DNA segregation (Bagchi *et al.* 2008), again underlining the versatile architecture of IF-like proteins, offering different solutions for a variety of cytoskeletal tasks. Characterization of these coiled-coil proteins was performed by analyzing protein architecture and sequence conservation and, in the case of FilP, by AFM to analyze the rigidity of wild-type hyphae and deletion mutants; cryo-ET should allow visualization of such filaments in situ. In fact, *Streptomyces* hyphae are ideally suited for study with whole-cell cryo-electron tomography, as they are thinner than 500 nm — almost half the width of unicellular bacteria such as *E. coli* and *B. subtilis* — and therefore within the range of permissible thickness for ET. Moreover, other than those already identified, streptomycetes may have many more cytostructural elements, and preliminary mutational analysis suggests specific functions for a number of the large coiled-coil proteins found in these organisms in the control of cell integrity, growth, development, protein secretion, and DNA segregation (our unpublished data). It will be interesting to see if cryo-ET can reveal these elements within the hyphae. Indeed, despite their expected significant width (eukaryotic IFs are around 10 nm wide), to date, no confirmed intermediate filament-like structures (of

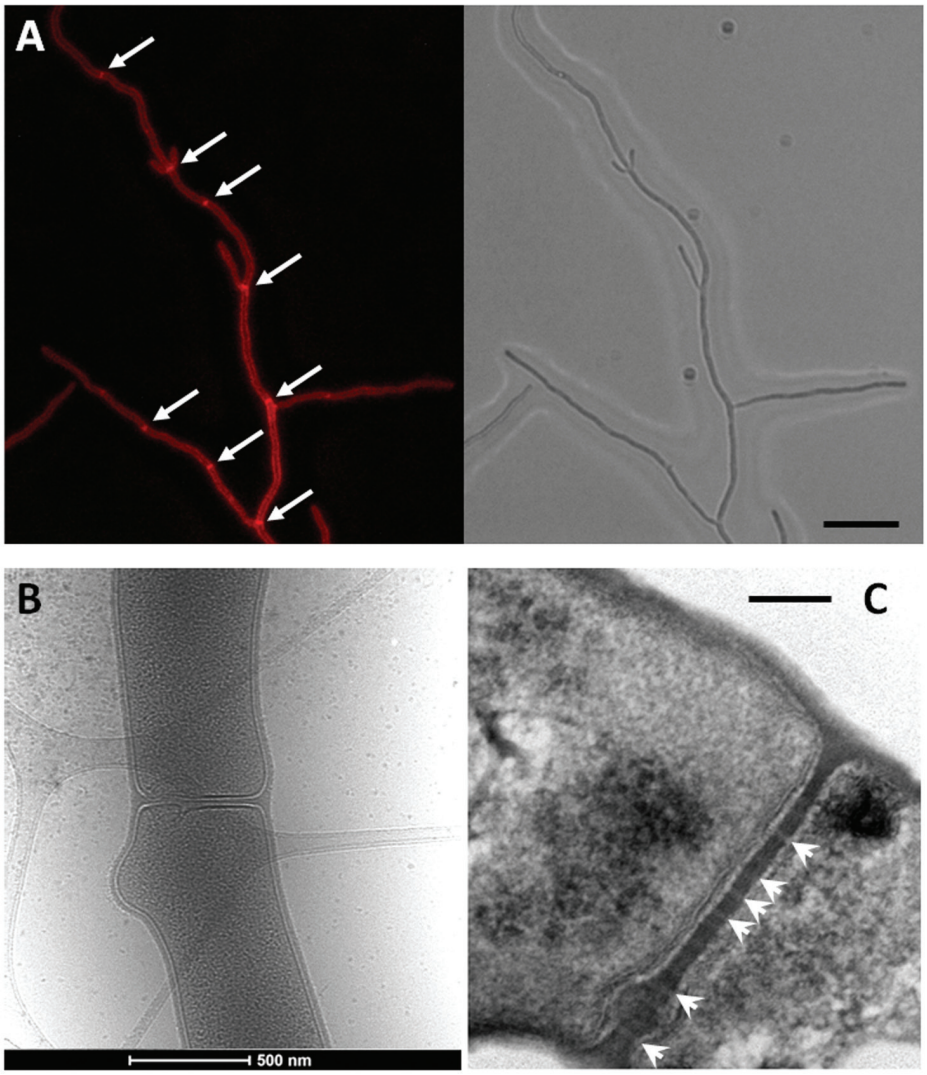

Figure 4. Cross-wall formation in Streptomyces coelicolor.

(A) Cross walls (arrows) are formed at irregular intervals in vegetative hyphae of Streptomyces, and their structure and control of their localization are still poorly understood.Left, fluorescence micrograph after staining with the membrane dye FM5-95; right, corresponding light image. Bar, 5 m. (B) Electron micrograph of a cross wall at higher resolution. (C) Transmission electron micrograph of a complete cross-wall with likely channels (arrowheads; apparent as lighter sections) and a bulge. Bar, 100 nm. It should be noted that cross walls may not all have channels. Figure 4C adapted from (Jakimowicz and van Wezel 2012) with permission.

CreS or others) have been unequivocally identified in tomograms of bacteria. Confirmation of the existence of prokaryotic IFs by, for example, high-resolution imaging combined with fluorescence microscopy is therefore eagerly awaited.

OTHER ROLES FOR MreB AND THE IF-LIKE PROTEINS

Difficult as it may be to group the intermediate filament-like proteins based on their structural similarity, it is even more difficult to classify them based on their function. Though several have an important role in shape control in non-rod-shaped bacteria, others have diverse roles in, for example, cell division (CfpA) or motility (AglZ). In a similar fashion, MreB and its homologs not only function to dictate rod shape but also play a role in motility (discussed below) (Mauriello *et al.* 2010; Kürner *et al.* 2005), chromosome segregation (Gitai *et al*. 2005; Defeu Soufo and Graumann 2005), establishing cell polarity (Gitai *et al.* 2004), and providing stability to the spore coat wall in *Streptomyces* (Mazza *et al.* 2006). In *Myxococcus xanthus*, filament-forming proteins AglZ and, interestingly, MreB are involved in (adventurous) A-type motility, a type of gliding for which the mechanism is not yet well understood. Many models were proposed (Wolgemuth *et al*. 2002; Mignot 2007), but the latest results indicate that A-motility involves distributed motors and focal adhesion complexes, involving up to 40 proteins in a large multiprotein structural complex (Nan and Zusman 2011; Mignot *et al*. 2007). Coiled-coil protein AglZ localizes in clusters at the leading cell pole and, as the cell moves, is transported toward the lagging cell pole, where clusters are disassembled (Mignot *et al*. 2007). These clusters are associated with A-motility motors that are hypothesized to power motility by coupling movement on a rigid cytoskeletal filament with adhesion complexes on the surface (Sun *et al*. 2011). Recently, MreB, in cooperation with MglA, a Ras-like GTPase, was shown to be critical for the proper positioning and stabilization of polar motility proteins and the focal adhesion complexes (Mauriello *et al*. 2010). A-type gliding motion of *M. xanthus* is thus actually remarkably similar to eukaryotic cell migration. In the mollicute *Spiroplasma melliferum*, propulsion is also assisted by the action of MreB filaments: two types of filaments were found arranged in three parallel ribbons underneath the cell membrane, with the two outer ribbons built of fibril protein and the inner ribbon suggested to be composed of MreB (Kürner *et al.* 2005). The structural data suggest a model explaining propulsion of helical mollicutes by means of coordinated length changes of the ribbons. In the filamentous actinomycetes, which grow by apical extension, MreB homologs occur only in species that differentiate by forming an aerial mycelium and spores, with a less pronounced and nonessential role during

vegetative growth (Mazza *et al*. 2006). The absence in other apically growing actinomycete genera such as corynebacteria and mycobacteria suggests that the function of MreB is directly related to the way bacteria elongate and divide (reviewed in reference Letek *et al.* 2012). In *Streptomyces*, the main function of MreB is to provide stability to the spore wall, which is corroborated by the dense crowding of the inner spore wall by MreB, as shown by immunoelectron microscopy (immuno-EM), suggesting that a large part of the spore wall is associated with MreB molecules (Mazza *et al.* 2006). Deletion of the paralogous *mbl* also compromises spore-wall integrity (Heichlinger *et al.* 2011). Detailed biochemical analysis of MreB and Mbl in streptomycetes should teach us more about the diverse roles these proteins can play in non-rod-shaped bacteria.

CELL DIVISION AND THE TUBULIN ANCESTOR FtsZ

Although some of the IF-like proteins assist in cell division processes, the major cell players in binary cell division are the Fts proteins, originally identified through analysis of temperaturesensitive mutants that fail to divide (the term fts, for filamentous temperature sensitive, was coined by Van de Putte and colleagues [Van de Putte *et al.* 1964]). Upon completion of chromosome segregation (influenced by MreB in *E. coli*, *Caulobacter*, and *B. subtilis* [Kruse *et al.* 2003; Gitai *et al*. 2005; Defeu Soufo and Graumann 2005]), the bacterial protein FtsZ directs the formation of the cytokinetic ring. A guanosine triphosphatase (GTPase) that is widely conserved and located within a cluster of genes involved in division and cell wall (dcw) synthesis, FtsZ polymerizes to form a scaffold of cell division proteins (the Z-ring) at the midplane of dividing cells. Interestingly, while in eukaryotes the cytokinetic ring is formed by actin, FtsZ is a structural homolog (and ancestor) of tubulin (Bi and Lutkenhaus 1991; Erickson 1995; Löwe and Amos 1998). The highly conserved FtsZ protein is found in virtually all bacteria and archaea (Michie and Löwe 2006), with only a few exceptions (Bernander and Ettema 2010).

CLUES FROM IMAGING OF CELL DIVISION

Cryo-ET imaging of bacterial cell division recently provided new insight into FtsZ localization. Cryo-ET images of dividing *C. crescentus* cells showed short, separated, arc-like filaments of FtsZ and not a complete ring or spiral (Li *et al*. 2007). In fact, the formation of FtsZ arcs was reported previously (Addinall and Lutkenhaus 1996) as a stage in ring maturation. Cryo-ET revealed irregularly spaced protofilaments of FtsZ, seemingly connected to the inner

membrane by other electron-dense protein complexes. Some were curved and others were straight, suggesting that, as speculated (Erickson *et al.* 1996; Lutkenhaus and Addinall 1997; Erickson 1997), FtsZ generates the constricting force for cell division itself through the nucleotide-hydrolysis-driven conformational change from straight to curved protofilaments.

Cross-wall formation in *Streptomyces* may, however, prove to be an exception to this model. Indeed, cell division in *Streptomyces* is remarkable. Not only is its division controlled in an entirely different manner, but it is also the only organism known to grow without cell division; the creation of a knockout mutant of *ftsZ* in *S. coelicolor* is an important event in cell biology (McCormick *et al*. 1994). Availability of null mutants for the canonical cell division genes such as *ftsEX*, *ftsI*, *ftsL*, *ftsQ*, *ftsW*, and *ftsZ* makes *Streptomyces* an important object for cell division studies (Jakimowicz and van Wezel 2012; McCormick 2009). Additionally, in *Streptomyces* two types of cell division occur: in aerial hyphae, septation results in formation of spores which can separate to disperse, and in vegetative hyphae, cross-walls form at irregular intervals, do not constrict, and do not result in cell fission (Figure 4). Amazingly, most canonical cell division proteins such as FtsI and FtsW are not even required for cross-wall formation. This suggests an entirely different cell division mechanism, whereby another pair consisting of a SEDS (shape, elongation, division, and sporulation) protein and a cognate class B penicillin-binding protein (PBP) may carry out septum synthesis (McCormick 2009; Bennett *et al.* 2009). This is something that has so far gained very little attention. One explanation is that because cross walls do not constrict but, rather, form semipermeable barriers that separate connecting compartments, the main function of the divisome is to mediate the activation of Z-ring contraction and that FtsZ does not generate a constricing force if other divisome components are absent. It will be interesting to see what role FtsZ plays in cross-wall formation.

OTHER TUBULIN HOMOLOGS

Although FtsZ is clearly the most common tubulin homolog, other bacterial tubulin homologs exist, including TubZ and RepX in *Bacillus* (Larsen *et al*. 2007; Tinsley and Khan 2006) and BtubA and BtubB in *Prosthecobacter* (Sontag *et al.* 2005; Schlieper *et al.* 2005). TubZ and RepX are plasmid-encoded proteins that play an important role in maintaining the stability of the plasmids that encode them and are therefore discussed in the following section. In contrast to TubZ, BtubA and BtubB are more closely related to eukaryotic alpha- and beta-tubulin than to any other bacterial protein, forming heterodimers which polymerize into protofilaments *in vitro*. Based on comparative modeling data, and because

microtubules were not found in thin EM sections, researchers initially predicted that BtubA and -B protofilaments are unlikely to form microtubule-like structures (Jenkins *et al*. 2002). When the ultrastructure of BtubA and BtubB was recently revisited using cryo-ET, however, it was shown that these proteins indeed assemble to form microtubules — consisting of five protofilaments instead of the 13 found in eukaryotes (Pilhofer *et al.* 2011) — but with the same basic architecture. Their existence suggests that microtubule organization may have originated in bacteria, although horizontal transfer of the eukaryotic tubulins cannot be ruled out.

POSITIVE CONTROL OF CELL DIVISION AND THE SsgA-LIKE PROTEINS

In bacteria that divide by binary fission, FtsZ is the first protein to localize at the midcell position at the onset of cell division, followed by the subsequent recruitment of the other cell division components (de Boer 2010). For details on prokaryotic cell division and the cell division machinery, we refer the reader to excellent reviews published elsewhere (for instance, references Margolin 2009; Young 2010; de Boer 2010; Adams and Errington 2009; Dajkovic and Lutkenhaus 2006). In *E. coli* and *Bacillus*, septum-site localization and stabilization of the Z-ring require, among others, FtsA and ZipA (Hale and de Boer 1997; Pichoff and Lutkenhaus 2002; RayChaudhuri 1999), ZapA (Gueiros-Filho and Losick 2002), and SepF (Hamoen *et al*. 2006), and the positioning and timing of septum formation involve the action of negative-control systems such as Min, which prevents Z-ring assembly at the cell poles (Marston et al. 1998; Raskin and de Boer 1997), and nucleoid occlusion (NOC), which prevents formation of the Z-ring over nonsegregated chromosomes (Bernhardt and de Boer 2005; Woldringh *et al.* 1991; Wu and Errington 2004; Wu and Errington 2012).

Remarkably, division site selection during sporulation in *Streptomyces*, where up to a hundred septa are constructed almost simultaneously in the long aerial hyphae (Jakimowicz and van Wezel 2012; McCormick 2009), appears to be positively controlled. Similar positive control of cell division was also recently described in another multicellular bacterium, namely, the fruiting body forming *Myxococcus xanthus*, where FtsZ is recruited by the ParA-like protein PomZ (Treuner-Lange *et al.* 2013). In *Streptomyces*, division is mediated via the SsgA-like proteins, a family of small proteins that occur exclusively in morphologically complex actinomycetes and play a role in the control of morphogenesis (Traag and van Wezel 2008; Noens et al. 2005), with SsgA and SsgB required for sporulation (Keijser *et al.* 2003; van Wezel *et al.* 2000). During sporulation-specific cell division, FtsZ is actively recruited by the membrane-associated divisome component SsgB, which also stimulates

FtsZ polymerization *in vitro* (Willemse *et al.* 2011). The technique of Förster fluorescence resonance energy transfer combined with fluorescence lifetime imaging (FRET-FLIM), a powerful tool for the *in vivo* imaging and calculation of distances between proteins or between a protein and another cellular component such as the membrane, cell wall, or DNA (Alexeeva *et al.* 2010; Miyawaki *et al.* 1997), revealed that SsgB indeed interacts closely with FtsZ and with the membrane (Willemse *et al*. 2011). In turn, SsgB is guided to future septum sites by its paralog SsgA, a multifunctional protein that directly activates cell division (van Wezel *et al*. 2006) but also other events relating to cell-wall remodeling such as germination and branching (Noens *et al.* 2007). SsgB (and probably also SsgA) forms multimeric complexes, with the crystal structure of SsgB revealing a bell-shaped trimer (Xu *et al.* 2009). Whether or not SsgA-like proteins should be regarded as cytoskeletal elements themselves is yet unclear. Another interesting aspect of the control of division in *Streptomyces* is that reaching a threshold level of FtsZ expression appears to be the decisive step in the onset of division (Flärdh et al. 2000), and enhanced expression of FtsZ indeed overrules many sporulation (*whi*) mutants (Willemse *et al.* 2012). This again points at a different way of decision making toward the initiation of division. The concept of positive control of division apparently violates the general idea that in nature all major checkpoints are negatively regulated (Alberts *et al*. 2002). However, positive division control is probably less expensive in terms of ATP (e.g., not requiring the energy-consuming oscillation of the Min proteins). In the case of *Streptomyces*, occasional defective spores in a long spore chain are less consequential than mistakes during binary fission, which could be considered an advantage of a multicellular lifestyle (Jakimowicz and van Wezel 2012). Having said that, PomZ is required for binary fission in *M. xanthus* (Treuner-Lange *et al*. 2013), while FtsZ can also localize (though inefficiently) to division sites in the absence of Min and NOC in *B. subtilis* (Rodrigues and Harry 2012). It remains to be seen how widespread active FtsZ recruitment in unicellular bacteria actually is (Monahan and Harry 2013).

ON PAR: THE CYTOSKELETON AND CHROMOSOME SEGREGATION

As we have seen, components of the cytoskeleton play an important role in guiding the spatiotemporal dynamics that govern the assembly of cellular components into higher-order structures. Chromosome and plasmid segregation is a good case in point. Segregation is mediated by tripartite partitioning systems (Gerdes *et al*. 2010; Leonard *et al*. 2005), which consist of a cytoskeletal nucleotide triphosphatase that provides the energy (ParA, ParM, or TubZ), a DNA-binding protein that forms higher-order nucleoprotein complexes

with the DNA (ParB, ParG, or ParR), and a centromere site (*parC*, *parS*, or *parH*) close to the origin of replication (*ori*) that is recognized by dimers of the respective DNA binding proteins (Gerdes *et al.* 2010; Leonard *et al*. 2005). Interestingly, the cytoskeletal partitioning NTPases all have different structural folds, suggesting that convergent evolution resulted in these different elements (and solutions) for the general problem of DNA separation. ParM is an actin family ATPase (van Den Ent *et al*. 2002; Møller-Jensen *et al*. 2002), TubZ is a tubulin homolog (thus hydrolyzing GTP) (Larsen *et al*. 2007), and ParA is a deviant Walker A-type Cytoskeletal ATPase (WACA) protein (Koonin 1993), a bacterial cytoskeletal element that has no eukaryotic counterparts. ParM forms dynamic, actin-like filaments that segregate plasmids in a mitosis-like process. In *E. coli*, cryo-ET was used to identify small bundles of three to five intracellular ParM filaments located close to the nucleoid, confirming that plasmid-segregating ParM filaments are associated with the nucleoid (Salje *et al*. 2009). A recent model suggests that antiparallel ParM filaments work together to drive plasmid segregation (Gayathri *et al*. 2012). TubZ assembles into highly dynamic, linear polymers with directional polymerization that are involved in plasmid segregation and move by a process called treadmilling. This treadmilling has so far been observed only in eukaryotes and involves assembly at one end of the filament and disassembly at the other, with, as a result, the net movement of the filament. Yet, unlike the hollow cylinders formed by tubulin, TubZ forms a two-stranded doubly helical filament which much more resembles actin-like ParM, which is also doubly helical. ParA functions by fuelling ParB, which in turn forms higher-order nucleoprotein complexes at partitioning (*parS*) sites near the chromosomal origin of replication, or *oriC* (Hayes and Barilla 2006; Leonard *et al.* 2004). In rod-shaped bacteria, ParB complexes actively transfer the *oriC* proximal chromosomal region to the cell poles after completion of DNA replication. ParA most likely attaches to a chromosome with bound ParB and then pulls the chromosome across the cell by depolymerizing (Gerdes *et al.* 2010; Banigan *et al*. 2011; Ptacin *et al.* 2010). It may also play a role in the control of chromosome replication, since *B. subtilis* ParA directly affects the function of replication initiator DnaA (Murray and Errington 2008; Scholefield et al. 2012). However, the cytoskeletal role of ParA is as yet controversial, and the filaments produced *in vitro* (Hui *et al*. 2010) have not yet been unequivocally established *in vivo*.

FUTURE PERSPECTIVES

In the span of a few years, we have made leaps and bounds toward understanding the mechanisms behind bacterial shape and structure. Twenty years ago, bacterial cytoskeletal elements were unknown; today, actin, tubulin, and intermediate-filament homologs, as well as novel cytoskeletal elements with no apparent eukaryotic counterparts, have all been identified in bacteria. The examples provided in this review demonstrate the vast plasticity and wide variety of roles taken on by prokaryotic cytoskeletal proteins and illustrate how multiscale imaging techniques are leading to new insights and improving our understanding of how bacterial cells function.

To come even closer to an understanding of the complex interactions that occur within the molecular landscape of the cell, static structural information must be coupled with *in vivo* dynamic studies. For this, correlative approaches are necessary. In correlative light and electron microscopy, proteins tagged with a fluorescent reporter, such as enhanced GFP (eGFP), or cell components stained with a selective dye can be directly identified on an EM grid and a tilt series acquired at the location of interest. This should enable mapping of cytoskeletal proteins onto high-resolution images created by electron microscopy, preferably in three dimensions (Plitzko *et al*. 2009; Briegel *et al.* 2010; Sartori *et al.* 2007; van Driel *et al*. 2009; Schwartz *et al.* 2007). In addition, to catch dynamic structural changes, using a rapid-transfer system, samples can be cryoimmobilized once a physiological state has been observed in the cell (Müller-Reichert *et al.* 2007). In this way, the missing links needed to resolve physical models for bacterial growth, division, or propulsion can be determined. Adding the insight provided by correlative methods to the multiscale data of other techniques, we can get even further toward understanding the relationship between the structure of cytoskeletal elements and their position within the cell and function. Given the centrality of the cytoskeleton in regulating and executing key cellular processes, this would mark a great milestone in the field of cell biology.

ACKNOWLEDGMENTS

We are very grateful to Grant Jensen, William Margolin, and the anonymous referees for their valuable comments on the manuscript. G.P.v.W. acknowledges support from the Netherlands Technology Foundation STW (VICI grant 10379). A.J.K. and R.I.K. acknowledge funding from the Dutch funding sources Cyttron II 20559 and NIMIC SSM06002 supporting the development of correlative imaging tools.

Chapter 3

Single Particle Tracking of Dynamically Localizing TatA Complexes in *Streptomyces* Species

Katherine Celler, Gilles P. van Wezel, Joost Willemse

Biochemical and Biophysical Research Communications. 2013 Aug; 438(1):38-42

ABSTRACT

The Tat (twin-arginine translocation) pathway transports folded proteins across the bacterial cytoplasmic membrane and is a major route of protein export in the mycelial soil-dwelling bacterium *Streptomyces*. We recently examined the localization of Tat components (TatABC) in time-lapse imaging and demonstrated that all three components colocalize dynamically with a preference for apical sites. Here we apply an in-house single particle tracking package to quantitatively analyze the movement of the TatA subunit, the most abundant of the Tat components. Segmentation and analysis of trajectories revealed that TatA transitions from free to confined movement and then to fixed localization. The sequence starts with a mixed punctate and dispersed localization of TatA oligomers, which then develop into a few larger still foci, and finally colocalize with TatBC to form a functional translocation system. It takes 15-30 min for the Tat export complex to assemble and most likely become active. With this study we provide the first example of quantitative analysis of dynamic protein localization in *Streptomyces*, which is applicable to the study of many other dynamically localizing proteins identified in these complex bacteria.

INTRODUCTION

In recent years, high resolution cell-biology techniques have revealed that, despite their small size, bacteria have a complex internal organization (Celler *et al.* 2013; Lopez and Kolter 2010; Margolin 2009). Molecular crowding within cells results in a dynamic equilibrium of components (Ellis 2001), leading to their non-uniform spatial distribution (Capoulade *et al.* 2011). This necessitates diffusion or active transport to areas where proteins can function, such as in nuclear organization, cell division or differentiation (McCormick and Flärdh 2012; Figge *et al.* 2004). *In vivo* multidimensional fluorescence microscopy allows scientists to visualize these processes which often display rapid and directed spatial relocation of proteins in three-dimensional time lapse movies (Mika and Poolman 2011; Meyer and Dworkin 2007; Shapiro *et al.* 2009). Taking cell division proteins as an example, these have been seen oscillating from one end of the cell to the other, forming rings across its midsection, or focal complexes at specific intracellular sites (Erickson *et al.* 2010; Hu and Lutkenhaus 1999; Noens *et al.* 2007; Raskin and de Boer 1999). To better understand these modes of action, and the lifespan of cellular proteins, quantitative measurements of protein abundance and dynamics are necessary.

A challenging subject for the study of dynamic protein localization is the Gram-positive filamentous soil bacterium *Streptomyces*. These mycelial organisms are used as natural producers of a large number of commercially important secondary metabolites, enzymes, and other secreted protein products (Hopwood 2007; Horinouchi 2007). In most bacteria the Sec pathway is the predominant route for protein export, but the streptomycetes encode an unusually large numbers of Tat (twin-arginine translocation) substrates (Palmer and Berks 2012; Müller and Klösgen 2005; Widdick *et al.* 2006). During fermentation, growth of hyphae is a balance of tip extension, branching frequency and fragmentation (Celler *et al.* 2012; Nieminen *et al.* 2013), all of which affect the efficiency of production and secretion. Fragmentation of hyphae strongly enhances protein secretion (van Wezel *et al.* 2006), which correlates well with our observation that the components of the Tat pathway in *Streptomyces* localize at the apical sites of hyphae (Willemse *et al.* 2012). A better understanding of where and when secretion takes place in the hyphae can lead to important insights for strain-improvement and rational process design.

The *Streptomyces* Tat machinery consists of TatA, TatB and TatC proteins (Widdick *et al.* 2006; Schaerlaekens *et al.* 2001), functional homologs of proteins found in Gram-negative bacteria such as Escherichia coli (Hicks *et al.* 2006). The tetrameric TatA is the most abundant component of the Tat complex (Jack *et al.* 2001) and many copies of this monotopic

membrane protein are believed to cluster around a substrate-bound TatBC complex to bring about the transport of a folded protein across the membrane, with an average of ~25 TatA subunits per complex (Dabney-Smith *et al.* 2006; Leake *et al.* 2008; Mori and Cline 2002).

Analysis of the Tat complex using live imaging revealed that the proteins localize surprisingly dynamically throughout the life cycle (Willemse *et al.* 2012). The dynamic localization of the separate components, however, creates difficulty in understanding their biological implication. Quantitative description and modeling of these movements by single particle tracking is therefore necessary to better understand complex assembly in time and space. Here we provide a detailed analysis of the dynamics of the TatA component of the Tat protein export pathway, using an in-house foci tracking package which was developed in the frame of the Particle Tracking Challenge of the International Symposium on Biomedical Imaging (ISBI) in 2012 (Chenouard *et al.*, *submitted for publication*). Specific questions we wished to address were (1) whether TatA undergoes different stages of motion prior to colocalization with TatB and TatC; (2) if so, what are the durations of these transitional stages; and (3) what is the time it takes for the complex to assemble.

This is the first mathematical tracking analysis of diffusion-limited foci in vegetative and aerial hyphae of *Streptomyces*, which can be applied to study the movement of many other dynamic proteins in these complex microorganisms.

MATERIALS AND METHODS

Strains and culturing conditions

Strain BRO3 is a derivative of *Streptomyces coelicolor* FM145, a variant of *S. coelicolor* M145 with reduced autofluorescence (Willemse and van Wezel 2009). BRO3 produces TatA-eGFP from the native chromosomal location (FM145, *tatA*::*tatA*-eGFP). Construction of the strain is described elsewhere (Willemse *et al.* 2012). To culture samples for live imaging, uncoated µ-dishes (Ibidi GmbH) were perforated at the side while closed tightly, and subsequently were semi-filled with SFM medium (Kieser *et al.* 2000). These dishes were inoculated with 1 µL of spores at a concentration of 109 spores/mL, turning the lid so that it was supported on the vents, allowing for gas exchange, and were sealed off by two layers of Parafilm to prevent drying of the medium. Samples were incubated at 30 °C for 48 hours before being transferred to the live imaging microscope. Temperature was controlled with a p-insert heating block and kept at 30 ºC, and allowed to calibrate for one hour before commencing imaging.

Data collection

Fluorescence microscopy

Fluorescence and corresponding light micrographs were obtained with a Zeiss Observer inverted fluorescence microscope (with an Hamamatsu CCD camera at a resolution of 78 nm/pixel) as described (Willemse and van Wezel 2009; Jyothikumar *et al.* 2008). The green fluorescent images were created using 470/40-nm bandpass excitation and 525/50 bandpass detection. All images were background-corrected setting the signal outside the hyphae to 0 to obtain a sufficiently dark background. These corrections were made using Axiovision software 4.8.

Time-lapsed (live) imaging

Imaging was performed with a Zeiss Observer A1 microscope with a Hamamatsu EM-CCD C9100-02 camera as described (Willemse *et al.* 2011). Images were taken at 2 minute intervals with an exposure time of 100 ms. In order to minimize focal drift, the microscope stage and imaging chamber were allowed to equilibrate for 60 min before imaging. Initially z-stacks of 5 images with a focal depth of 0.5 µm were taken to prevent out-of-focus movement of the hyphae. These image sequences were then z-projected using the average z-stack projection method implemented in ImageJ.

Computer programs

The particle tracking algorithm was submitted to the Particle Tracking Challenge (http://bioimageanalysis.org/track/) of the 2012 International Symposium on Biomedical Imaging (http://www.biomedicalimaging.org/2012/), in which the performance of existing and newly developed particle tracking algorithms was tested against synthetic image sets with ground truth data. The methods and results of the challenge have been described (Chenouard *et al.*, *submitted for publication*). For details on the algorithm see the Supplemental Methods. The algorithm was implemented in the Java programming language (Sun Microsystems Inc., Santa Clara, CA) in the form of a plug-in for ImageJ (National Institutes of Health, Bethesda, MD), the computer-platform independent public domain image analysis program inspired by NIH-Image. ImageJ version 1.46o was used with the Java 1.7 compiler.

RESULTS AND DISCUSSION

We focused on TatA complex assembly as a whole, which occurs at a timescale several orders of magnitude greater than the fast movement of individual proteins. To capture an entire localization sequence (with an initial estimated duration of roughly 30-60 minutes) prior to bleaching of the samples, we took images for up to 3.5 hours at 2 minute intervals. Since mobility data suggests that cytosolic diffusion occurs at a time scale two orders of magnitude faster than membrane diffusion, we observed the dynamics of slow-moving membranebound macrocomplexes, and not the cytosolic fraction of TatA. *Streptomyces coelicolor* FM145, a derivative from the wild-type strain with reduced autofluorescence (Willemse and van Wezel 2009), was used for the localization studies, allowing imaging of the fluorescently labeled proteins at significantly higher signal to noise ratio. In 18 time lapse imaging movies of diffusion-limited TatA-eGFP, roughly 1500 foci were tracked from the onset of imaging to final localization. Foci tracked/detected in only two consecutive frames were not taken into account. The distribution of tracks (Figure 1) demonstrates that short tracks predominate, with roughly half of all tracks corresponding to 10 or less consecutive frames.

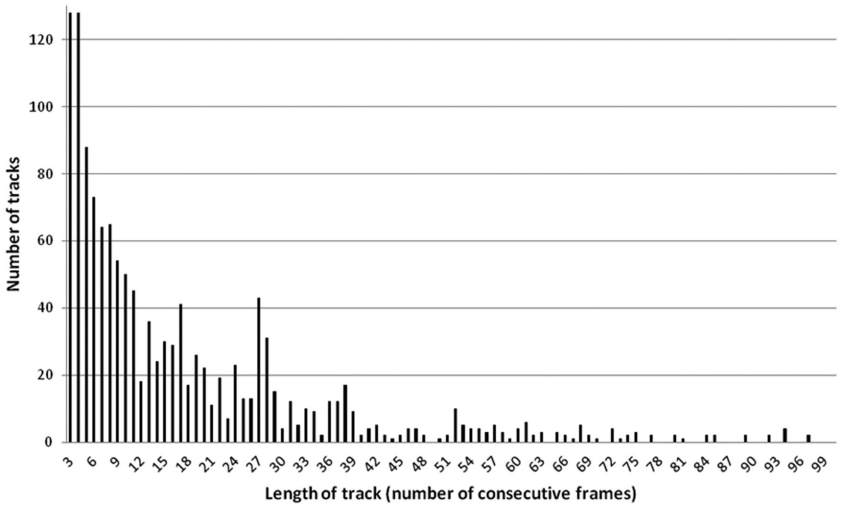

***Figure 1**. The distribution of tracks per track length demonstrates that short tracks predominate, with roughly 25% of TatA-eGFP foci tracked in three, four or five consecutive frames. These short tracks are of the many small TatA oligomers which race through the hyphae before agglomerating and forming larger complexes. Foci tracked in only two frames were not taken into account by the software. Roughly 50% of tracks are 10 consecutive frames or shorter.*

Our previous study revealed increased amounts of localization in aerial hyphae, and imaging was therefore performed on early aerial hyphae after 48 hours of growth. At this point, many hyphae had already stopped growing due to crowding in the sample, but occasionally extending tips were still observed. In the growing hyphae, the Tat complex was seen following the tips. The broad range of stoichiometries exhibited by TatA suggests that dynamic polymerization and depolymerization occurs during assembly (Leake *et al.* 2008). This is evident in our time lapse sequences, where protein complexes display different types or stages of movement prior to fixed localization (ex. Fig. 2 and Supplemental Video 1). At the start of imaging, mainly dispersed fluorescence is seen, with gradually many faint foci appearing to 'race' along the hyphae. During this fast movement, several strong fluorescent foci become visible localizing (mainly) near the tips at roughly a 2 µm distance. Over the course of the time lapse, the faint foci either fade or merge with larger stable fluorescent foci. These faint foci have short tracks lasting only 3-4 frames or 6-8 minutes. Particle tracking highlights these tracks as brief directed bursts of motion. The larger foci remain stationary, or wobble before stabilizing.

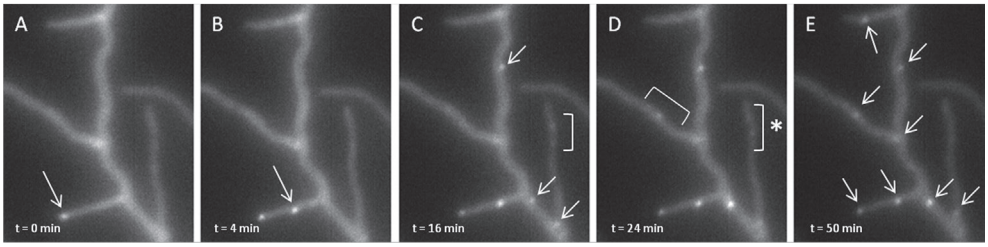

***Figure 2**. TatA-eGFP localizes dynamically in a Streptomyces hypha showing different stages of movement (frames taken from Supplemental Video 1). The initial localization is diffuse (A), though one focal point of TatA-eGFP localised to a branch tip can already be seen at this point in time (arrow). A second focus appears during live imaging (B), and around 15 minutes after the start multiple small foci are observed (C), some of which are clearly evident in the still frame (arrows), and some appearing as faint traveling foci in the time lapse (bracket). Foci continue to travel as they dynamically localise (D). Some foci ultimately fade again (bracket denoted by *) while others persist. In the final frame (E), multiple fixed localizations of the now stably localised protein are observed (arrows). Scale bar, 5 µm. Imaging was started at 49 hours post inoculation (48 hours of growth, with one hour of incubation time in the microscope). This time was deemed t=0.*

A large variation in fluorescence intensity is seen over the course of imaging. Initial faint foci assemble over the course of the time lapse imaging to form complexes with increased fluorescent intensity, likely reflecting natural protein oligomerization.

Although formation of protein complexes can be enhanced by an eGFP fusion, which may affect protein functionality (Landgraf *et al.* 2012), we previously demonstrated that the TatA fusion is fully functional, restoring secretion of Tat substrates to wild-type levels. For full functional analysis of the TatA fusion product and Tat complex formation we refer to our previous work (Willemse *et al.* 2012).

Supplemental Video 2 shows another representative example of dynamic localization. The final image from the time lapse is presented (Fig. 3A), with the detected TatA-eGFP tracks projected onto the image. Despite the fading of foci due to the imaging, three tracks could be followed for the entire duration (one hour) of the movie. The trajectories of these tracks were plotted (Fig. 3B), demonstrating representative trajectories of a still focus, a rapidly traveling focus (which becomes confined after 10 minutes) and a wobbling focus.

Plotting of the mean square displacement (MSD, see Supplemental Data S1) versus time for these tracks (Fig. 3C) facilitated classification of the different modes of motion observed. In this case, MSD curves reflect the global changes that occur during complex assembly, and not rapid-scale protein dynamics. In the case of the wobbling focus, the MSD is irregular anddoes not show a clear trend towards a particular mode of diffusion. The trajectory of the traveling focus appears to consist of two different stages, namely an initial phase of rapid diffusion followed by a phase of slower diffusion. The still focus has an MSD curve with a slope of zero. Analysis was done for the first half of time lags for these curves, or 30 minutes, to minimize error.

Supplemental Video 3 shows a third example of the dynamic localization patterns described above (for still images see Fig. 4). The tracks of detected foci projected onto the image (Fig. 4A). In this movie, focus 1 (circled in Fig. 4B) hardly moves over the length of the time-lapse; the MSD curve has a slope of zero. Focus 2 initially moves at greater speed (in the direction of the arrow, Fig. 4B) than the other foci in a seemingly directed manner. It then stalls before continuing motion and later settling in a fixed position; from its MSD curve (Fig. 4C) the focus is seen to undergo different motion regimes. The multiple foci labeled in a region 3 seem to wobble and by eye fall into the same category of motion. When their MSD is plotted, however, it is clear that they have different rates of diffusion.

We obtained a sufficiently large number of ‘full tracks’ to obtain reliable insight into how TatA complexes localize, starting with diffuse localization, followed by assembly and finally settlement. Track lengths for TatA-eGFP in the movies varied from foci linked in a few consecutive frames to tracks that could be followed for several hours (> 90 linked foci). Our observations from the live imaging experiments suggest that the categories of motion exhibited by TatA (still, traveling or wobbling) are stages in a single localization sequence.

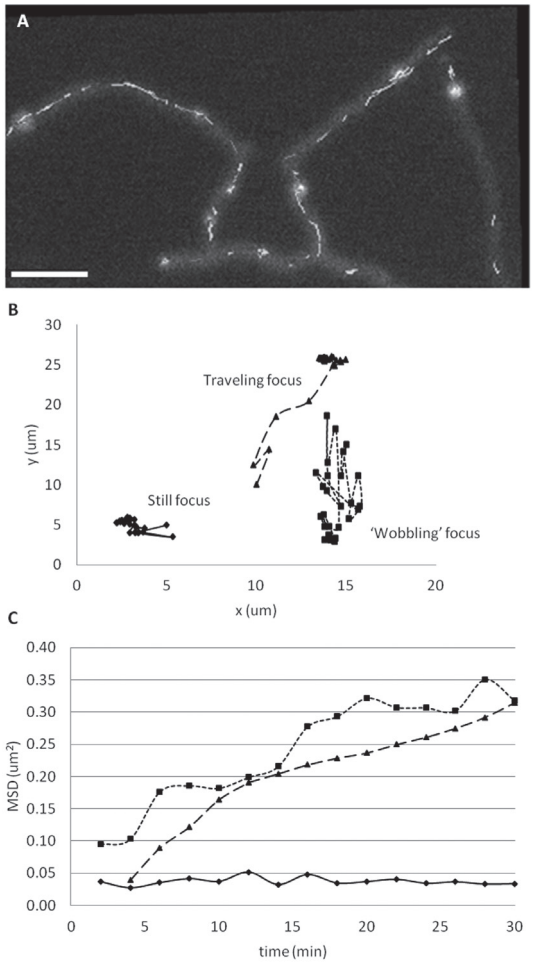

***Figure 3**. A trajectory and MSD analysis of dynamic TatA-eGFP localization in a Streptomyces hypha provides evidence for different stages of localization (frame taken from Supplemental Video 2). TatA-eGFP tracks projected onto the frame demonstrate that dynamics occur throughout entire hyphae (A). Scale bar, 5 µm. Foci could be classified into those that are still, traveling and wobbling (B); the displacement of these foci is plotted on an x-y plot, with tracks starting at (5,5), (10,10) and (15,15) respectively. The still focus stays close to its origin; the traveling focus appears to move rapidly in a directed fashion for the first part of its trajectory and then to localise; the wobbling focus has a more random trajectory. The MSD is plotted versus time for the foci shown (C). Only the first half of the curve (total time 60 min) is plotted and taken into consideration to minimise error. The still focus has a slope of zero. The traveling focus has an MSD curve with two regimes: fast, followed by slower diffusion. Linear trend lines are fitted to these two regimes. The MSD of the wobbling focus has an upward trend, but no conclusions can be drawn on the diffusion.*

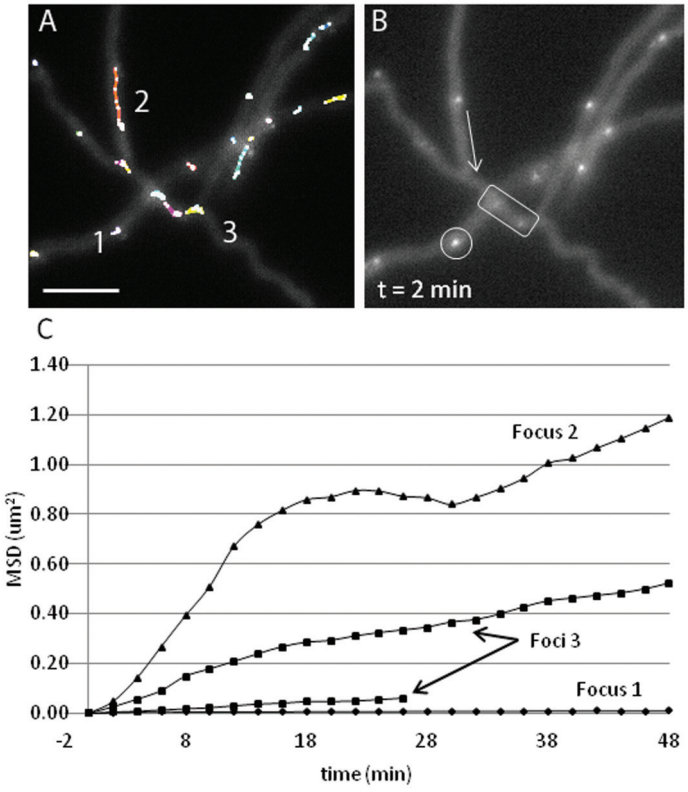

***Figure 4**. TatA-eGFP localizes dynamically in a Streptomyces hypha showing different stages of movement (frames taken from Supplemental Video 3). Detected tracks of the foci are projected onto the frame with different colours (A). Some foci are still (1), some travel linearly before stalling, continuing motion, and then become still (2) and some wobble backwards and forwards (3). For clarity, the still focus is circled, the direction of travel of focus 2 is shown with an arrow, and the portion of a hyphae where several foci (foci '3') are wobbling is denoted by a rectangle (B). Scale bar, 5 µm. The MSD is plotted versus time for the foci presented (C). Only the first half of each curve is plotted and taken into consideration to minimise error. The MSD of the still focus is zero. The traveling focus, which travels quickly, stalls, and then continues motion until localizing has an MSD with different regimes. Two foci from region 3 show different rates of diffusion.*

Proteins may be observed in each of the different stages of motion in a single time lapse since dynamics within the hyphae are not synchronized. Short tracks represent foci that fade or fuse at the onset of imaging, while longer tracks undergo dynamic transition through all stages of movement. The latter start with dispersed localization, with faint foci likely

consisting of only a few TatA tetramers, followed by confined movement when tetramers oligomerize, and finally a fixed localization, at which point TatA multimers most likely colocalize with TatBC to form a functional translocation system. By taking into account only the foci that undergo all of the above stages of localization, the average time for a focus of TatA to assemble and find its proper position was estimated at between 15-30 minutes (Supplemental Figure 1).

This localization time may be indicative of the time required for an active TatABC transport complex to assemble. The current model for the Tat mechanism postulates that TatA polymerizes in response to substrate binding to the TatBC complex. The decrease in mobility during localization supports this idea and most likely represents the formation of a TatABC complex which actively transports proteins outside the bacterial cell (Leake *et al.* 2008). Our time lapse imaging in *Streptomyces* supports the notion that Tat component dynamics are very complex, with the proteins undergoing various phases of motion (and consequently rates and modes of diffusion) during localization.

Previous studies on localization of the replisome machinery in *Streptomyces* observed that most apically localized DNA replisomes were more than 1.5 µm from the tip (Ruban-Ośmiałowska *et al.* 2006), settling at a position on average 5.32 (±2.00) µm from the tip (Wolański *et al*. 2011). Our unpublished data by high resolution electron microscopy further suggest that the very tips of hyphae are a ribosome-free area, which could also explain why the Tat complex localizes near, but not at the tip. Ribosomes are known to localize near the nucleoids, and these data would confirm a model coupling transcription with translation and subsequent secretion of certain protein products by the Tat system.

To the best of our knowledge, our analysis of TatA dynamics is the first example of a quantitative analysis of dynamic protein localization in *Streptomyces*. Study of other dynamically localizing fluorescent proteins will provide more insight into the biochemical details of protein assembly and localization. Tracking single proteins in the cell and analyzing their trajectories will significantly increase our understanding of dynamic behavior of proteins *in vivo*.

ACKNOWLEDGEMENTS

We are grateful to the organizers of the ISBI Particle Tracking Challenge 2012 for stimulating discussions. We would like to thank Tracy Palmer for providing us with the TatA-eGFP fusion constructs and for her helpful comments on the manuscript. This work was supported by a VICI grant from the Netherlands Applied Research Council (STW) to GPvW.

Supplemental Material - Supplemental Data S1

Plotting the mean-square displacement as a function of time interval can be used to characterize particle movement by determining whether diffusion is Brownian, active or constrained (Figure S1), and to calculate the diffusion coefficient. The mean square displacement is defined as:

$$MSD(t) = (r^2(t)) = (|r_i(t) - r_i(0)|^2) \quad (i)$$

where $r_i(t)$ is the position of foci i at time t and the brackets represent an average on the time steps and foci. The MSD describes the average of the squared distances between a particle's start and end position for time intervals of a certain length t in a trajectory, and gives an indication of an object's pattern of motion (de Bruin, Ruthardt et al. 2007). Normal diffusion (or Brownian motion) is indicated by a linear dependence of ($r^2(t)$) on the time interval and can be described by:

$$MSD(t) = (r^2(t)) = 4D\Delta t \quad (ii)$$

where D is the diffusion coefficient, and the factor 4 is specific for 2-dimensional diffusion. Confined diffusion is indicated by an asymptotic behavior at large Δt and normal diffusion at small Δt. It can be described by:

$$MSD(t) = (r^2(t)) = (r_c^2(t))\left[1 - A_1 \exp\left(-\frac{4A_2 D\Delta t}{(r_c^2(t))}\right)\right] \quad (iii)$$

where ($r^2(t)$) is the size of the confinement, and constants A_1 and A_2 are determined by the confinement geometry. Active transport is described by a quadratic dependence of the MSD on Δt:

$$MSD(t) = (r^2(t)) = v^2\Delta t^2 + 4D\Delta t \quad (iv)$$

where v is the velocity of the directed motion (drift). The MSD curves for Brownian diffusion, constrained diffusion and active transport are given in Figure S1.

The accuracy of the MSD curve is affected by the time differences: the longer the MSD, the fewer time points that can be taken into account to calculate the MSD value. Analysis of MSD curves is therefore only possible for the initial portions of the curves, typically for the first third of all points, N. This results in an artificial increase in the MSD curve of a stalling focus because the average squared displacement can no longer be determined for the final

frames of the movie where the focus remains still. A certainty measure was therefore added to the plug-in to allow the user to set the minimum of number of data points needed to create the MSD curve.

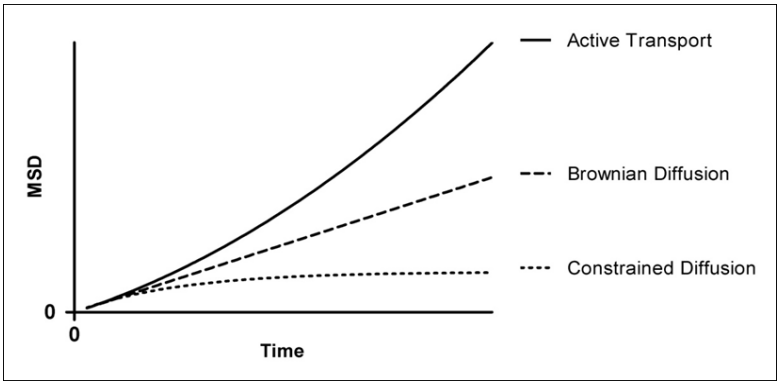

***Figure S1**. Mean-square displacement (MSD) curves for active transport, Brownian and constrained diffusion.*

Supplemental Video, SV1

Time lapse of TatA-eGFP localizing dynamically in a *Streptomyces* hyphae. The video consists of 28 frames taken at an interval of 2 minutes between frames and plays at 6 frames per second. Total imaging time was 56 minutes. For a reference of scale, refer to Figure 1.

Supplemental Video, SV2

Time lapse of TatA-eGFP localizing dynamically in a *Streptomyces* hyphae. The video consists of 29 frames taken at an interval of 2 minutes between frames and plays at 6 frames per second. Total imaging time was 58 minutes. For a reference of scale, refer to Figure 2.

Supplemental Video, SV3

Time lapse of TatA-eGFP localizing dynamically in a *Streptomyces* hyphae. The video consists of 49 frames taken at an interval of 2 minutes between frames and plays at 6 frames per second. Total imaging time was 98 minutes. For a reference of scale, refer to Figure 3.

Supplemental Figure 1

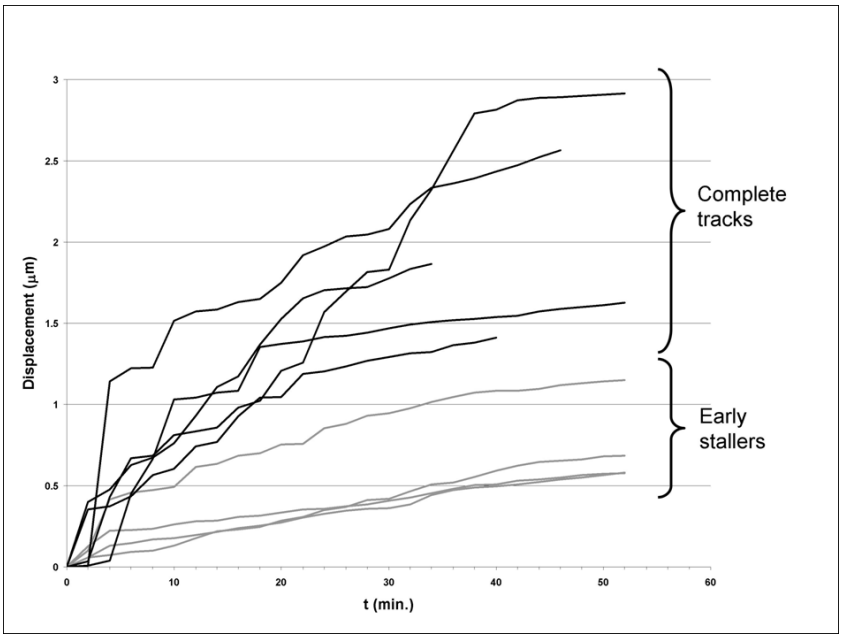

Supplemental Figure 1. *Total displacement plotted for TatA-eGFP foci with foci stalling (localizing) at different times. Visual inspection of TatA movement reveals different patterns of movement; in some cases, TatA is already assembled into a focus at the start of the movie ('early stallers'), while in others, focus assembly occurs during the time-lapse movie ('late stallers'). The assembled foci wobble, and stall at a time prior to those that assemble during the experiment, with different total displacement for each group. Averaging the curves resulted in an estimated assembly time of 15-30 minutes. The curves of complete tracks and foci already assembled at the start of imaging ('early stallers') are indicated.*

Supplemental Method - Particle Tracking

A particle tracking method consists of two steps: (1) particle detection and (2) particle linking. Image analysis starts with detection of cells or fluorescent particles by segmentation. This involves partitioning of a digital image into multiple sets of pixels, and then assigning labels to these pixels such that pixels with the same label share visual characteristics. In this way, the outline of cells or fluorescent foci can be determined. Once images are segmented, a tracking algorithm is needed in order to follow a cell or focus from image to image. Here we describe our image analysis (particle detection) and tracking (particle linking) algorithm.

DETECTION

To detect particles in the images, several filtering steps are applied to enhance the contrast between natural autofluorescence and the observed particle fluorescence. The initial step for noise reduction is a Gaussian filter (σ =1 pixel), which keeps the particles intact while the noise is diffused throughout the image. After this, two processing steps are possible, depending on the SNR in the image. For high SNRs, a top-hat filter is applied to detect and emphasize foci that are brighter than the background. The result is an image in which the background has been equalized and the foci of interest have been intensified. Based on this image, a thresholding procedure is applied, in which the cut-off intensity (above which objects are considered true particles) can be manually chosen by the user. Setting the threshold correctly is a vital part of the algorithm. In the competition, the chosen threshold values were 30 (for SNR = 7), 20 (for SNR = 4), and an automatically determined level (using the auto-thresholding function of ImageJ) with a constant added (for SNR = 1 or 2, where the constant was 10 for high-density, 12 for mid-density, and 15 for low-density images), respectively. Thresholded objects that are either too large (in this study 500 pixels or larger) or too small (less than the expected minimum size of typically 6-10 pixels depending on SNR) are filtered out. Objects located close to each other are separated using a watershed-based splitting operation, using the Euclidean distance transform. For low-SNR images, a similar approach is taken, leaving out the top-hat filter. In noisier images, this levels the background only slightly compared to the objects of interest, since these generally consist of several intensity peaks in nearby pixels. Finally, the subpixel position of each thresholded particle region is taken to be the center of mass.

LINKING

To track detected particles from frame to frame, a modified nearest-neighbor algorithm is used. Initially, the image space is divided into blocks (of tunable size, in this study 1 pixel in 2D cases, and 1 voxel in 3D cases), using a regular grid. Starting with the first frame, each particle is labeled according to the block containing its coordinates. In the next frame, the same grid is created, and the particles in that frame too are labeled according to their corresponding block. Then, each particle is linked with the particle in the previous frame that is nearest in its neighborhood, defined by the surrounding blocks (initially ± 1 block in each dimension). If multiple particles are detected, the closest one is chosen, and if none is found, the neighborhood is iteratively extended in all dimensions (to ± n blocks, n = 1 ...N, with N a user-defined maximum range, typically 10). If the particles cannot be tracked within this distance, a gap-closing step is applied. This ensures that if particles disappear in a certain frame, and then reappear again, tracking continues. Gap closing is performed by running the tracking procedure on frame t - 2, and then continuing backwards along frames until the particle is 'found' again. Thus in a sense, particles are not tracked forwards, but backwards. The user may choose how many frames backwards to search. In this study the backwards tracking parameter was set to 3 frames. Disappearing of particles may occur due to noise or if a particle moves out of focus. Newly appearing particles are labeled as new objects and tracked thereafter in subsequent frames. If particles are tracked forward to the same particle in the next frame, the event is identified as a fusion. This is done based on particle area. It was estimated that a fusion consisting of two particles has 1.5 times the average area of a single particle, and that a fusion of three particles has 1.5 times the area of a fusion of two particles. These larger objects can be tracked back to two or three parents if these are detected in the neighborhood. Splitting particles are also detected, with both daughter particles tracking back to the same parent based on directionality. This is based on the assumption that on short time scales, tracks follow a straight path. Finally, it is possible in this method to eliminate single detections or short tracks. In the present study, single detections and tracks shorter than 3 frames were filtered out.

Chapter 4

Intracellular Membrane Structures Mediate Crosswall Formation and Nucleoid Occlusion in *Streptomyces*

Katherine Celler, Roman I. Koning, Joost Willemse,
Abraham J. Koster and Gilles P. van Wezel

Manuscript in preparation.

ABSTRACT

During the bacterial cell cycle, chromosome replication and segregation is tightly regulated and coordinated with septum formation to guarantee the survival of progeny. The cytokinetic machinery is highly conserved, with subtle variations, and stabilizing and destabilizing factors cooperate to properly position the cell division apparatus at mid-cell. Yet the precise mechanisms that initiate divisome formation coordinated with nucleoid segregation are still largely unknown. Here we show that intracellular membrane structures play a major role in division-site selection and nucleoid occlusion in *Streptomyces* hyphae. Cross-membranes, consisting of a heterogeneous distribution of lipids, create a chromosome-free area to ensure that septum formation can occur without damaging DNA. Crosswalls are then seen to form in these cross-membrane structures, away from the nucleoid. The membranes fully colocalize with - and are dependent on - the division scaffold protein FtsZ, which highlights the subtle interplay between membrane and cell wall formation during the initiation of cell division.

INTRODUCTION

Within the bacterial cell, several control systems cooperate to ensure that chromosomes are faithfully separated and not damaged during the formation of a cell division septum. In rod-shaped bacteria, the combined action of the Min system and nucleoid (chromosome) occlusion ensures the precise positioning of the division machinery at mid-cell (Rothfield *et al*. 2005; Harry *et al*. 2006; Barak and Wilkinson 2007; Wu and Errington 2012). The Min system prevents FtsZ assembly at the cell poles, while nucleoid occlusion prevents the formation of the Z-ring over the nucleoids, with Z-ring formation therefore occurring at the mid-cell by default. Yet though division is much less efficient in cells lacking these systems, neither the Min system nor the Noc/SlmA nuclear occlusion proteins are essential in *E. coli* or *B. subtilis* (Wu and Errington 2004; Bernhardt and de Boer 2005). What exactly initiates the formation of the divisome at cell centre remains unclear, and several lines of evidence suggest that there are additional mechanisms at work.

A recently proposed model suggests that DNA replication at the chromosomal origin of replication (*oriC*) triggers the accumulation of an as-of-yet unidentified positive signal at mid-cell which activates Z-ring formation (Moriya *et al*. 2010). Complementary studies on the distribution of phopholipids in the bacterial membrane have shown that their heterogeneous distribution results in regions enriched in particular lipids at cell poles - as well as at the cell centre. In fact, lipid heterogeneity is critical for the spatial and temporal organization of cells (Fishov and Woldringh 1999; Nishibori *et al.* 2005; Barak *et al.* 2008; Fishov and Norris 2012). Lipid domains play a crucial role in the specific localization of proteins and protein complexes and are important for cellular function, influencing signal transduction, secretion, as well as cell division and development (Mileykovskaya and Dowhan 2005; Matsumoto *et al.* 2006; Barak and Muchová 2013). Phospholipid composition at a particular location affects the chemical and physical properties of a membrane, as well as its curvature (Lenarcic *et al.* 2009; Ramamurthi *et al.* 2009) and electric potential (Strahl and Hamoen 2010), effectively determining when and where proteins and protein complexes specifically localize. In fact, lipid domains may bind amphitropic proteins responsible for selection and recognition of the division site (Mileykovskaya and Dowhan 2005; Barak *et al.* 2008). Evidence exists that the phopholipid composition at mid-cell is optimal for initiation of DNA replication and Z-ring positioning, suggesting that a dynamic protein-lipid interaction may act as the positive trigger for Z-ring formation (Norris *et al.* 2004; Mileykovskaya and Dowhan 2005; Saxena *et al.* 2013).

In the long hyphae of streptomycetes there is no mid-cell. Positioning of the divisome therefore poses a difficult problem: where should a septum be formed in a branching, multinucleoid and filamentous cell? These multicellular soil-dwelling bacteria grow as a syncytial vegetative mycelium separated by crosswalls (Wildermuth and Hopwood 1970). During the reproductive phase, they produce chains of spores in aerial hyphae, following a complex cell division event whereby long ladders of Z-rings are produced in a short time span (Flärdh and Buttner 2009). Interestingly, while the *Streptomyces* cell division machinery resembles that of unicellular bacteria, the canonical control systems like Min, Noc and SulA are missing, perhaps redundant and therefore lost in hyphae because of the absence of a mid-cell reference point (McCormick 2009; Jakimowicz and van Wezel 2012). This implies that an entirely different mechanism of controlling septum-site localization and nucleoid occlusion is present in these bacteria. We recently showed that septum-site localization during sporulation-specific cell division in aerial hyphae is positively controlled, with FtsZ recruited by the SsgB protein (Willemse *et al.* 2011), which in turn depends on its paralogue SsgA. SsgA is a cell division activator protein, and the number of septa formed in the hyphae directly correlates to the expression level of SsgA (van Wezel *et al.* 2000a; van Wezel *et al.* 2006). In aerial hyphae, SsgA plays an important role in the correct localization of the FtsZ-recruiting SsgB in time and space (Willemse *et al.* 2011). SsgA and SsgB belong to the family of the SsgA-like proteins or SALPs, which occur exclusively in morphologically complex actinomycetes (Noens *et al.* 2005; Traag and van Wezel 2008). The way these proteins find the future sites of septation is as of yet unknown.

In vegetative hyphae, cross-walls form at irregular intervals to delimit multigenomic compartments. These compartments usually have an irregular number of chromosomes, and contain replication machinery in different stages of assembly and disassembly, sometimes within the same compartment (Ruban-Ośmiałowska *et al*. 2006). Unlike aerial septa, crosswalls do not constrict the cell, and do not result in cell fission, effectively constituting a completely different form of cell division in this microorganism. Notably, many canonical divisome components, such as FtsI and FtsW, which are required for septal peptidoglycan synthesis in *E. coli* (Wang *et al.* 1998), are not required for crosswall formation. This suggests an entirely different mechanism, where another pair of proteins consisting of an SEDS (shape, elongation, division, and sporulation) protein and a cognate class B penicillin-binding protein (PBP) may carry out septum synthesis (Bennett *et al.* 2009; McCormick 2009). Here we show that crosswall formation is preceded by the formation of large membrane structures delimiting hyphae. These membrane structures form during development, localizing either in small sites along the cell wall, at tips, or within hyphae,

compartmentalizing the vegetative mycelium. The large delimiting membranes, which we have dubbed cross-membranes, appear to be essential for FtsZ recruitment prior to the formation of a crosswall. The membranes play a dominant role in nucleoid occlusion, creating a chromosome-free area prior to septum synthesis and ensuring that cell division can occur without damaging the chromosomes.

RESULTS

Live imaging reveals dynamic membrane localization in Streptomyces vegetative hyphae

As the Min and Noc/SlmA control systems are missing in streptomycetes, and the SsgA-like proteins SsgA and SsgB play only a minor role in the control of crosswall formation, we set out to discover what governs vegetative division and how DNA damage is prevented. Lipid domains enriched in cardiolipin, an anionic negative-curvature phospholipid, have recently been implicated in cell division processes, hypothesized to be responsible for selection and recognition of the division site (Mileykovskaya and Dowhan 2005; Barak and Wilkinson 2007). We therefore performed live imaging experiments on *Streptomyces* hyphae grown in a medium containing FM 5-95 and 10-N-nonyl acridine orange (NAO) to investigate the dynamics of membrane and cardiolipin localization during crosswall formation. FM5-95 stains anionic phospholipids, including phosphatidylglycerol (PGL), while NAO allows for visualization of cardiolipin.

Imaging demonstrated that membrane localization is highly dynamic and complex. Membranes could be seen associating and dissociating along the hyphae within an hour, at times forming large cross-membrane structures, localizing to the tip, or forming small foci at the cell wall. Simultaneously, punctate localization of cardiolipin assemblies occurred throughout vegetative hyphae. Both membrane and cardiolipin phospholipids localized highly dynamically (Figure 1 and Supplemental Movie S1). Interestingly, typically after roughly 12 hours of growth, a flash of cardiolipin was seen propagating through the hyphae. Within 20 minutes this distributed localization faded, to be replaced by discrete membrane localization. Large membrane agglomerates (ranging from one to several µm in length, red arrow in Figure 1) grew and subsequently shrunk in the regions of localization; within the span of an hour, the membranes faded again, and were accompanied by forming cardiolipin assemblies.

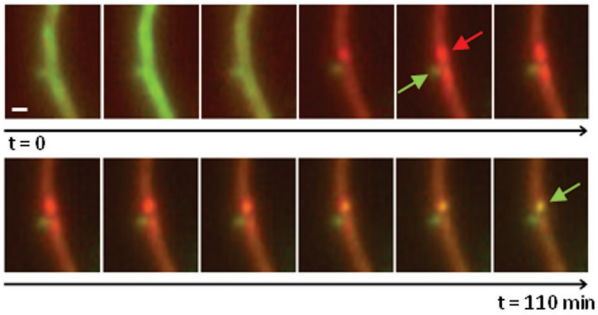

Figure 1. *Membrane and cardiolipin localization within hyphae is highly dynamic (stills taken from Supplemental Video S1). Rapid translocation of cardiolipin (green) is seen within Streptomyces coelicolor hyphae, followed by diffused localization of this phospholipid. Membranes (red) next appear within the hyphae and are recruited to the future site of a crosswall (red arrow), while cardiolipin can be seen localizing steadily at the tip of a newly forming branch (green arrow). Membranes expand and then coalesce and disappear. By the end of the time lapse, membrane localization is replaced by cardiolipin. S. coelicolor was grown in a medium containing FM5-95 (staining negatively charged phospholipids in the plasma membrane) and NAO (preferentially staining cardiolipin) and live imaging was started after 12 hours of growth, with a time lapse of 10 minutes between images. Scale bar, 0.5* μm.

Cross-membranes localize to the sites where crosswalls are formed

Intrigued by the membrane localization dynamics, we set out to investigate the underlying mechanism and structure of the observed membrane patches in more detail and at higher resolution using cryo-electron microscopy (cryo-EM). Cryo-EM on vitrified *Streptomyces* liquid culture samples of early mycelia revealed the presence of a vast and intricate intracellular membrane system within hyphae. As in live imaging, membranes were seen either at small regions along the cell wall, at tips, or as large structures completely delimiting hyphae (the cross-membranes) (Figure 2). Often the observed membranes consisted of bundles of tube-like structures, extending from the cytoplasmic membrane. Searching for crosswalls, we discovered that in samples grown for 14 hours or more, crosswalls had completely formed (Figure 2I), whereas at earlier time points, membrane material was more plentiful, and crosswalls were scarce (Figure 2A-G). Interestingly, in these younger samples, the start of cell wall invagination could sometimes be seen within cross-membrane structures (Figure 2H), suggesting that these are the sites of crosswall formation. Examining samples at different time points suggested that crosswalls form rapidly, in line with earlier live imaging experiments (Jyothikumar *et al*. 2008). While in 10 hr samples hardly any crosswalls or cross-membranes were present, in 12 hr samples such membranes were abundant, sometimes associated with septum synthesis. After 14 hrs, many crosswalls had

been completed. In these and older (20-24 hr) samples, membranes could sometimes still be found, though they were not as abundant. This strongly suggests that once started, cell-wall formation is completed rapidly. Since we have never seen incomplete crosswalls in the absence of cross membranes, it is likely that the crosswalls are associated with - and likely formed within - membrane assemblies.

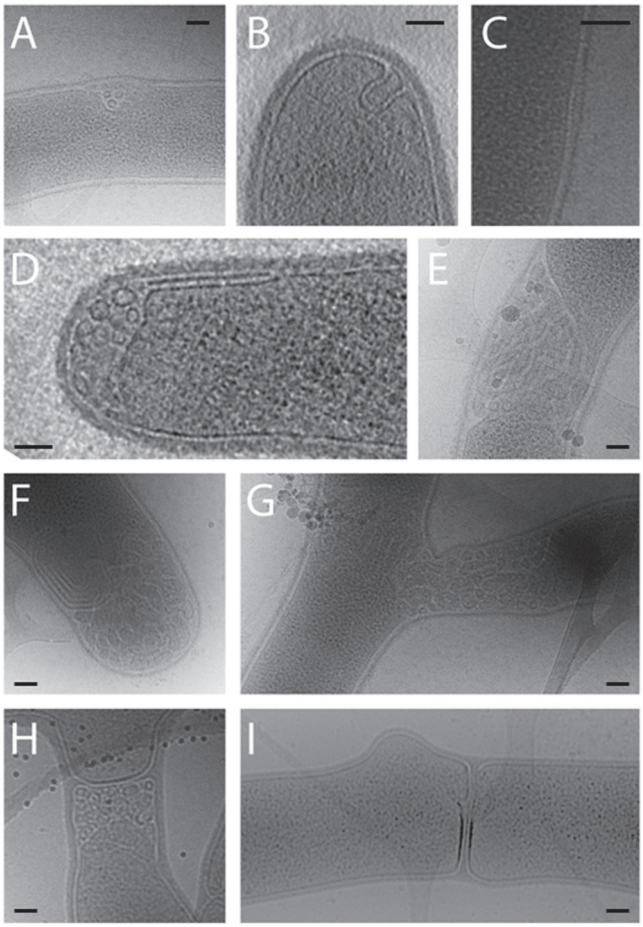

Figure 2. *Diverse intracellular membrane structures are found in Streptomyces sp. Membranes localize at the sides of hyphae in small or large blurbs (A,C,E) or to tips (B,D,F). Cell delimiting cross-membranes can also be found, with membrane tubes creating large intracellular structures (E,G). In some instances, cell wall can be found within these membrane structures (H), suggesting that crosswalls are initiated in membranes. In later stages of growth, complete crosswalls are seen (I). Scale bars, 100 nm.*

Membranes create a chromosome-free area, mediating nucleoid occlusion

Intrigued by the cell wall invaginations within cross-membrane structures, we sought to obtain a more detailed and three-dimensional view of the onset of crosswall formation. Since membrane patches, and specifically the CL rafts, localized transiently in time and space, depending on growth stage, and because the membrane and CL patches localized closely together, we developed correlative light and electron microscopy (CLEM) for use in streptomycetes. Cryo-CLEM correlates the images acquired by cryo-fluorescence light microscopy and cryo-electron microscopy, including tomography, enabling selective labeling and identification of membrane components, as well as DNA, and direct mapping of these lower resolution data onto high resolution tomograms.

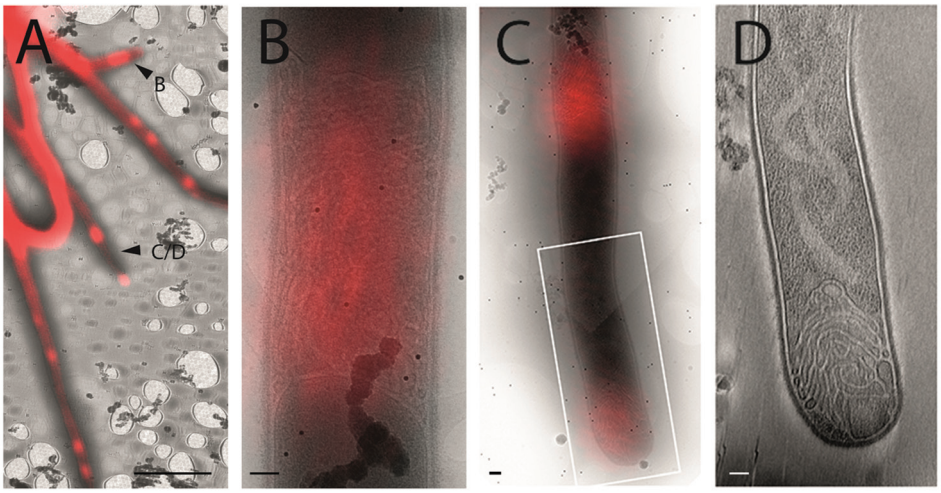

Figure 3. *Cryo-CLEM on Streptomyces stained for membranes with FM5-95. An overlaid fLM (red) and cryo-EM overview image (A) shows FM5-95 staining patches along the hyphae. Cryo-EM of the locations identified by boxes in (A) indicates that at the positions of fluorescent staining, large internal membranes can be found (B,C). A tomographic slice through the membrane-filled tip shown in (C) reveals the partly tubular shape of the membranes (D). Chromosomal DNA can be seen forming a curve following the tip. Scale bars, 5 μm (A), 100 nm (B-D).*

We stained for membranes using fluorescent dye FM5-95, and found that the large membrane formations observed in tomograms correlate directly to areas stained by FM5-95 in the light microscopy images, and are therefore likely to be enriched in PGL. Staining allowed us to identify cross-membranes as well as membrane-filled apical sites (Figure 3). Chromosomal DNA, in tomograms evidenced by a finely textured region devoid of ribosomes and other macromolecular complexes, could be seen between small membrane blebs, or

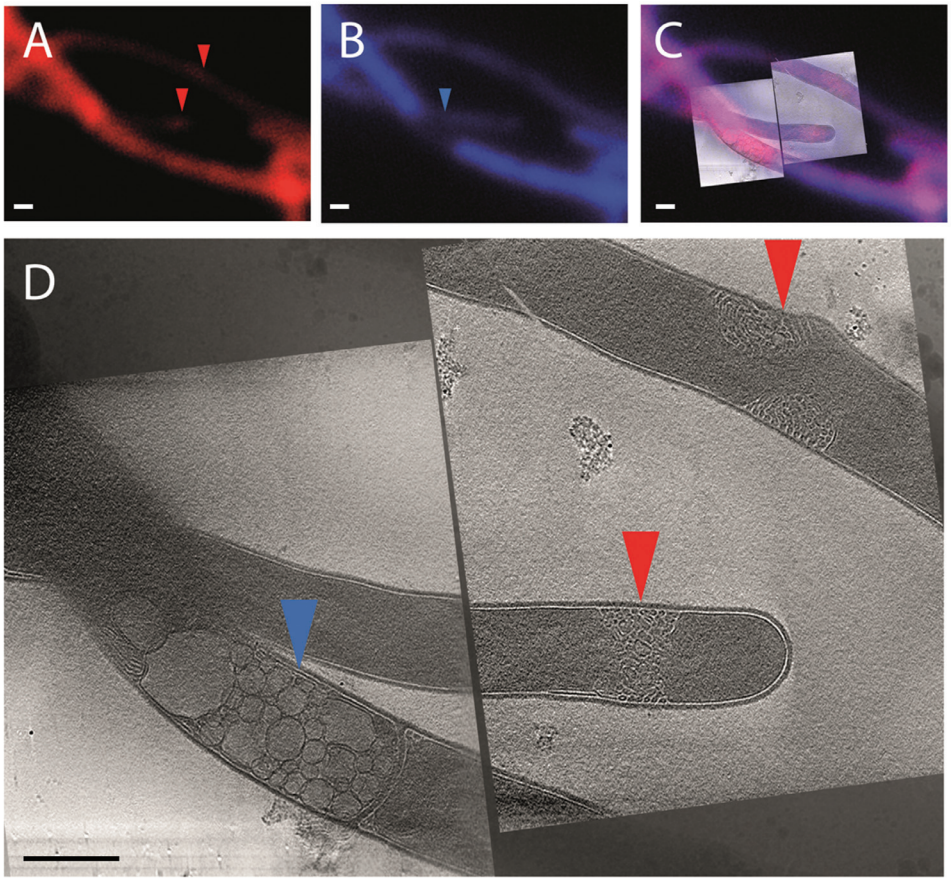

Figure 4. *Cryo-CLEM on Streptomyces stained for membranes (using stain FM5-95) and DNA (using stain DAPI) demonstrates that patches of membrane stain coincide with tubular membrane structures in hyphae (red arrows in A and D). Large gaps in the DNA staining coincide with vesicles near a crosswall (blue arrows in B and D). An overlay of the fLM and cryo-EM images is given in (C). Tomographic slices through two adjoining tomograms show the membranes localizing at the sides of a hyphae, near a forming branch (upper right), or near a tip (lower right) (D). At the new branch point, new cell wall invagination can be seen within the membranes. Scale bars, 0.5 μm.*

behind a membrane-filled tip (Figure 3D and Supplemental Video S2). This provided the first evidence that DNA and membranes structures may be mutually exclusive.

To analyze this further, membrane staining was combined with 4',6-diamidino-2-phenylindole (DAPI) to visualize chromosomes. As in the case of the membrane-filled apical sites, all areas where large cross-membrane or membrane-enriched vesicle structures localized were devoid of DNA, evidenced by a distinct gap in DAPI fluorescence (Figure 4).

Where membranes localized to the hyphal wall, but did not delimit a hyphae, DNA could still be seen passing through the channel between membranes. Together with direct evidence from the native tomograms (Supplemental Video S2), this suggests that the cross-membranes create DNA-free zones, occluding the chromosomal DNA from sites where active cell-wall restructuring takes place in *Streptomyces* vegetative hyphae.

We also stained for cardiolipin with NAO and discovered many cardiolipin-rich zones in vegetative hyphae, which invariably correlated to membrane vesicles observed in the tomograms (Figure 5). These multilayered vesicles appeared in many different shapes and forms were and clearly distinct from the tubular and unilamellar vesicles in cross-

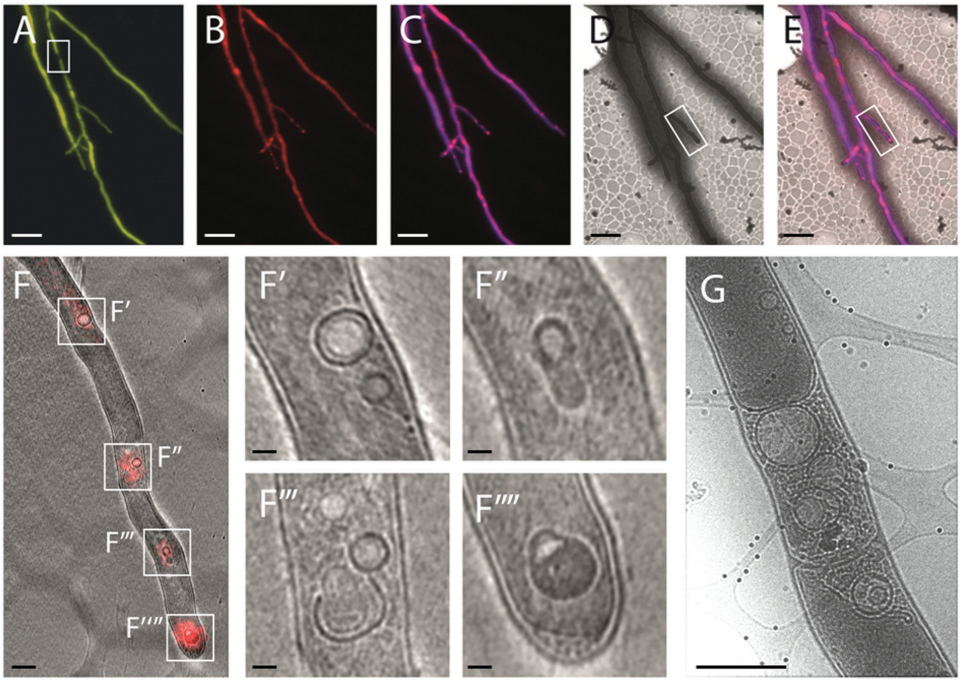

Figure 5. *Cryo-CLEM on Streptomyces stained for cardiolipin (using stain NAO) and DNA (using stain DAPI), demonstrates that cardiolipin forms vesicle-like structures within the hyphae. fLM images of DAPI staining, shown in yellow, for clarity (A) and cardiolipin staining (B) have been overlaid in (C). The EM picture is shown in (D) and an overlay of fLM and EM is provided in (E). At higher magnification, direct correlation can be seen between the staining and intracellular structures rich in cardiolipin (F) - Hyphae shown in (F) is the one denoted by a square in (D.E). A gap in the DNA (denoted by a square in (A)) is filled with membranes and cardiolipin, forming tubes and vesicle-like structures (G). A crosswall can be seen at this location. Scale bars, 5 μm (A-E), 0.5 μm (F,G), 100 nm (F′-F⁗).*

membranes. Co-staining with DAPI revealed that cardiolipin vesicles obstruct DNA localization. Cardiolipin localized either diffusely, or in the vesicle-like structures, directly corresponding to focal points seen in the hyphae (Figure 5B,F). Such structures were also routinely seen in unstained samples; intracellular formations are therefore not an artifact of staining, which was performed immediately prior to vitrification.

Vesicularization occurs when crosswalls are completed

In addition to membranes, we observed large vesicles adjacent to a newly formed layer of peptidoglycan (PG) in cryo-electron tomograms (Figures 4D, 5G). PG deposition occurred preferentially at one side of the membrane structures. These vesicles were low in electron density as compared to the cytosol, and hence of different composition. In all cases where PG had formed, vesicles were highly disorganized, forming large and small bubble-like structures, seemingly lodged between a membrane and PG layer exerting pressure on one side, and cytosol on the other. Apparently, once PG is deposited, vesicularization of the lipid tubes occurs as excess membrane is gathered, with vesicles coalescing to one another and into the cytoplasmic membrane. The appearance of cardiolipin at the final stage of crosswall formation (as evidenced by our live imaging experiments) likely coincides with vesicularization, with non-bilayer forming cardiolipin acting to help remodel the membrane. This likely marks the final stage in crosswall formation.

FtsZ and cross-membranes colocalize

If membrane structures indeed mark the sites of crosswall formation, that would predict that they may also mark the sites Z-ring formation is initiated. In a previous study, we demonstrated that during sporulation-specific cell division in *Streptomyces*, FtsZ is actively recruited by the membrane-associated divisome component SsgB (Willemse *et al.* 2011). Interestingly, though the *S. coelicolor ssgB* mutant does not form sporulation septa, cross-membranes do still form in vegetative hyphae (Figure 6A), similarly to the wild-type (Figure 6B) (see also (Willemse *et al.* 2011)). However, in the *ftsZ* mutant, cross-membranes are missing or scarce (Figure 6C), suggesting that membrane localization is largely dependent on FtsZ, and occurs at a greatly decreased rate in the absence of FtsZ. Immunofluorescence microscopy allowed visualization of membranes in a strain harboring FtsZ-eGFP, revealing complete colocalization of FtsZ and phospholipids and further demonstrating their interdependence (Figure 6D). Attempts to covisualize FtsZ-eGFP and cross-membranes in CLEM experiments were as yet unsuccessful, as visualizing eGFP in the cryo-fluorescent stage is not yet possible, and hampered by the green autofluorescence of *Streptomyces* hyphae.

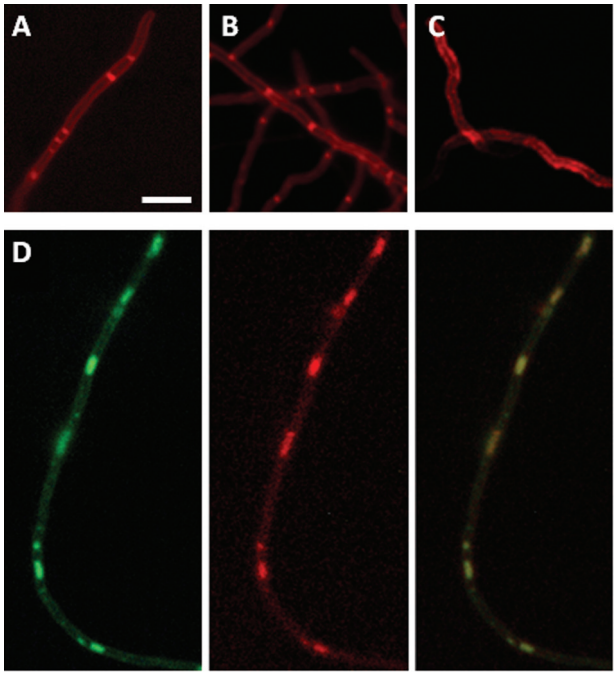

Figure 6. Membrane localization depends on FtsZ.

In an ssgB deletion strain of M145, which does not form sporulation septa in aerial hyphae, cross-membranes still occur (A) in the vegetative mycelium, as evidenced by staining with FM5-95. These membranes are similar to those that form in wild type hyphae (B), though SsgB is not present to bind FtsZ at the sites of septation. In the absence of FtsZ, however, cross-membranes no longer form (C). Colocalization of FtsZ-eGFP (green), with FM5-95 (red) indicates interaction between FtsZ and membranes (D). An overlay of both channels is also shown. Scale bar, 5 μm.

DISCUSSION

The accurate localization of the cell division machinery in time and space is a tightly controlled process that is critical for growth and survival. The canonical view of bacterial cell division is binary fission, which involves finding the precise mid-cell position and coordinating septum synthesis with chromosome replication and segregation to avoid damage to the DNA (Harry *et al.* 2006). The bulk of the experimental information available to us today comes from genetic and biochemical experiments, combined with fluorescence microscopy-based cell biology. Using these techniques, the Min, SulA and NOC negative control systems were discovered, as well as a large number of septum localizing and stabilizing proteins, including FtsA, ZipA, ZapA and SepF (Romberg and Levin 2003; Goehring and Beckwith 2005; Harry *et al.* 2006). All of these proteins are absent in *Streptomyces*, which is readily explained by the absence of a mid-cell reference point in the long multinucleoid hyphae. While sporulation-specific cell division requires a divisome that is highly similar to that in other bacteria, crosswalls require FtsZ and to a lesser extent FtsQ, but their formation is not hampered by the absence of FtsI or FtsW, peptidoglycan-synthesizing proteins in *E. coli*, suggesting that an entirely different mechanism is in place. Using cryo-electron tomography, which allows the visualization of intracellular structures in three dimensions, we discovered an important if not essential role for intracellular membranes in division-site selection and nucleoid occlusion in *Streptomyces* vegetative hyphae. These cross-membranes create a DNA-free zone during the initiation of division, allowing crosswall formation inside these membrane-protected areas. Thus our work for the first time provides insight into the mechanism of nucleoid occlusion in streptomycetes. Furthermore, fluorescence and time-lapsed microscopy demonstrated that the membranes form dynamically and play a major role in the localization of FtsZ. We previously showed that the SsgB protein recruits FtsZ during sporulation-specific cell division in aerial hyphae (Willemse *et al.* 2011), but like for many cell division genes, null mutants of *ssgB* were apparently not affected in crosswall formation. Indeed, during vegetative cell division lipids and FtsZ fully colocalize, suggesting that this is how FtsZ is recruited to septum sites in vegetative hyphae.

Live imaging of young vegetative hyphae grown in a medium containing FM5-95 and NAO demonstrated that localization of P_{GL} and CL-enriched lipids is remarkably rapid and dynamic. After roughly 12 hours of growth, cardiolipin was seen propagating through the vegetative hyphae and localizing diffusely prior to P_{GL} localization, suggesting that cardiolipin is required to recruit membrane synthases to areas where membrane deposition should occur. Some of the larger membranes then created cross-hyphal structures, expanded,

and then began to dissolve, accompanied by renewed CL localization. Examining these formations using CLEM revealed large tubular membrane structures forming in hyphae, completely obstructing DNA localization, and vesicular-like CL deposits associated with the membranes during late stages of division. Thus, by staining for specific membrane components, we may for the first time have identified the structures previously seen in early transmission electron micrographs of *Streptomyces* hyphae and dubbed 'mesosomes' (Glauert and Hopwood 1959; Stuart 1959; Glauert and Hopwood 1960), and which have also been seen in other bacteria (Reusch and Burger 1973). Researchers hypothesized that proliferation of membranes plays a role in enhancing enzymatic activity and is involved in crosswall formation, but the so-called mesosomes were later taken to be an artifact of fixation (Nanninga 1971; Higgins *et al.* 1976; Silva *et al.* 1976). We show that intracellular membranes in fact exist and are prevalent in early vegetative hyphae, playing an important role in cell division.

Although large cross-membranes have a clear role in vegetative cell division, the abundance of lipid structures localized in small blebs adjacent to the cell wall or at apical sites - in addition to those delimiting the hyphae. This implies that lipid structures could also be involved in other cellular functions. Tip-localizing membranes likely tether DivIVA and the tip growth complex, analogous to the fungal Spitzenkörper (Steinberg 2007), and membranes at the sides of hyphae may be actively involved in localizing the secretome (involving the Tat or Sec secretion machineries).

Based on these results, we propose a model of membrane formation in which small membrane tubes found at the hyphal wall either grow in size to enable crosswall formation, or resorb back and disappear (Figure 7). Those that grow in size at sites of crosswall formation coalesce in an asymmetric fashion, fusing from one side of a hyphal wall across to the other. This change of conformation decreases the channel connecting neighboring hyphal compartments, until complete convergence of membrane is seen. Coalescing membranes not only localize a large amount of FtsZ, but also form a barrier to prevent damage to chromosomal DNA as evidenced by the complete gap in DAPI fluorescence whenever cross-membranes are seen. The membranes seem therefore to mediate nucleoid occlusion during crosswall formation. DNA can still be seen passing through this channel at late stages of constriction, until at some point it no longer can pass, and a membrane-filled, chromosome-free area is formed. Our high resolution three-dimensional tomograms support the notion that the structure of the chromosomes controls division site selection (Mannik *et al.* 2012).

Coupled transcription-translation-insertion (transertion) of proteins from segregating chromosomes creates heterogeneous phospholipid domains at the cell centre which allow

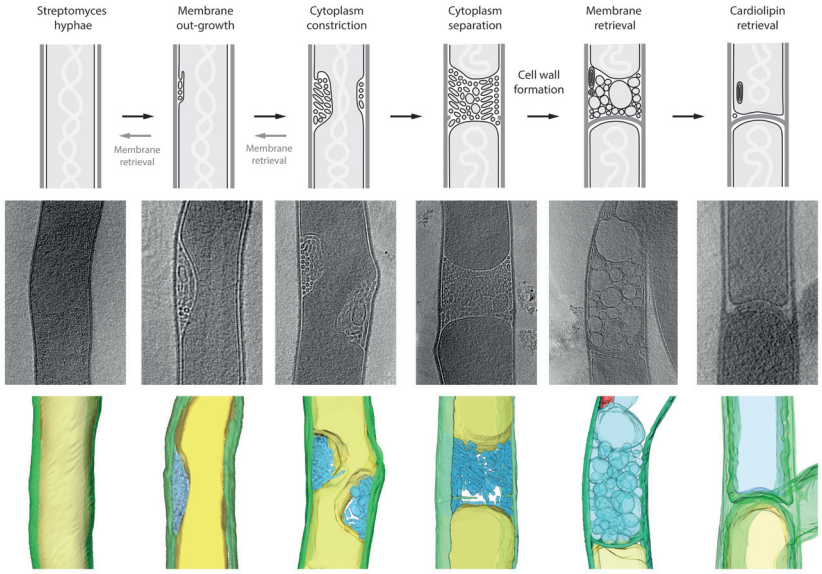

Figure 7. Model to explain crosswall formation in Streptomyces vegetative hyphae.

Initially, during early growth, no intracellular membranes can be seen. Chromosomal DNA can be found uncondensed within hyphae (gray helix). Small membrane blebs at the sides of hyphae appear and disappear continuously (gray arrow). Those that grow, constrict the hyphae, including the DNA, from one side. When membranes have completely converged, the DNA is obstructed. At this point, cell wall deposition can occur. A crosswall forms, and membrane tubes disintegrate into small vesicles that coalesce into larger vesicles. These vesicles eventually coalesce with the cytoplasmic membrane , while simultaneously cardiolipin rich membrane vesicles appear. A fully formed crosswall remains.

membranes to extend into the cytoplasm (Norris *et al.* 2004). The rapid changes observed in membrane formation are likely necessary to create an optimal phospholipid composition - with suitable membrane potential and curvature - for protein recruitment (Matsumoto *et al.* 2006). We show that these membrane tubes are substrate for the dynamic assembly and disassembly of FtsZ. The colocalization of FtsZ and membranes in vegetative hyphae supports a two-way relationship, whereby membranes create an optimal environment for FtsZ localization, while at the same time FtsZ is required for cross-membrane formation. This correlates to observations in *B. subtilis*, where localization of phospholipid synthases to cardiolipin and phosphatidylethanolamine-rich septa also depends on FtsZ (Nishibori *et al.* 2005). Other membrane-associated proteins and phospholipids show the same synergy: overproduction of the proteins results in a compensatory overproduction of membrane,

enriched with the phospholipid composition preferred by the overexpressed protein (Arechaga *et al.* 2000; van den Brink-van der Laan *et al.* 2003; Eriksson *et al.* 2009). In these cells, similar membrane structures have also been observed at high resolution. It is unclear how exactly in *B. subtilis* FtsZ interacts with membranes to induce tube formation, as all proteins which interact with a membrane bilayer do so via an amphipathic α-helix which is missing in FtsZ (Norris *et al.* 2004). It has been hypothesized that C-terminus residues can make intrasubunit contacts in an FtsZ protofilament, or that these residues may extend to make a contact to the next adjacent subunit in a protofilament fostering intersubunit interaction (McCormick 2009). Nevertheless, *in vitro* studies have clearly demonstrated FtsZ interaction with phospholipid structures: FtsZ polymerization is facilitated by cationic lipids (Erickson *et al.* 1996; Lu *et al.* 2001) and in a phosphatidylethanolamine monolayer system, FtsZ can create large rings of up to 500 nm in diameter (the upper limit of a *Streptomyces* vegetative hypha) as well as linear polymers of several microns (Alexandre *et al.* 2002; Lafontaine *et al.* 2007). These observations directly connect to the colocalization of (and likely interaction between) FtsZ and the membrane assemblies we observe in vegetative hyphae.

Sporulation-specific cell division in *Streptomyces* is positively controlled, mediated by SsgA and SsgB, whereby SsgB directly recruits FtsZ to division sites and stimulates its polymerization (Willemse *et al.* 2011). Overproduction of the cell division activator protein SsgA enforces a physical change of vegetative hyphae to structures much more resembling sporogenic aerial hyphae (van Wezel *et al.* 2000a; van Wezel *et al.* 2006). Sporulation-specific cell division is mechanistically similar to binary fission in e.g. *Bacillus*, except that the control of septum-site localization requires different proteins (Jakimowicz and van Wezel 2012). Conversely, vegetative crosswalls do not result in cell fission, and these structures do not depend on *ssgA* or *ssgB*. Remarkably, the same is true for mutants lacking the canonical divisome proteins *ftsI* or *ftsW*, required for septal PG synthesis in most bacteria. Perhaps because crosswalls consist of only a single layer of PG, and not the thicker double-layer which is present in sporulation septa, crosswall formation is an entirely different process as compared to sporulation-specific cell division in aerial hyphae. As discussed above, FtsZ and membranes have a synergistic relationship, and only very few cross-membranes occur in *ftsZ* null mutants of *S. coelicolor.* This apparently correlates to the fact that in rare occasions crosswalls are formed in the same *ftsZ* null mutants (McCormick *et al.* 1994). It is likely that in these cases, crosswalls are the result of fortuitous conditions in which membranes converge unaided and septum synthesis results if the required SEDS and PBP proteins are present.

An important question that needs to be addressed in the future is what controls the spectacular intracellular membranes in *Streptomyces*. Candidate proteins are dynamins and flotillins. Dynamins are GTPases which mechanochemically interact with lipids to assist in membrane remodeling, and two dynamin homologues exist in *Streptomyces* (SCO2684 and SCO2685 in *S. coelicolor)*. Flotillins are associated with lipid rafts in eukaryotes and characterized by the SPFH (Stomatin, Prohibitin, Flotillin and HflK/C) domain of unknown function and extended heptad repeat regions (Hinderhofer *et al.* 2009). *S. coelicolor* encodes for at least six flotillin-domain proteins In *B. subtilis*, the dynamin ortholog DynA plays a role in cell division, colocalizing with FtsZ and affecting Z-ring formation, while flotillin generates a local environment favoring membrane curvature, perhaps assisting in the recruitment of cell division proteins to the division site (Dempwolff *et al.* 2012). It would be interesting to see what role dynamin and flotillin play in the formation of crosswalls, and these proteins are good candidates for generating the membrane tubes that are favored by FtsZ.

Taken together, our work provides evidence that intracellular membranes play a critical role during *Streptomyces* vegetative growth, assisting in positioning of the division machinery in the branching, filamentous hyphae, in the absence of canonical control systems such as Min and Noc/SlmA. We believe that membrane-mediated division is not unique to *Streptomyces*. In fact, though membrane structures are not always evident in high resolution images of *E.coli* and *B. subtilis*, studies show they also play a critical role in the cell division of these organisms. *E. coli* and *B. subtilis* cells compromised in lipid production produce long filamentous cells, indicative of defective cell division (Mileykovskaya *et al.* 1998; Salzberg and Helmann 2008). In *E. coli* cells that are unable to produce phosphatidylethanolamines, FtsZ spirals and ladders are formed not dissimilar to those seen in *Streptomyces* hyphae, but cell constriction does not take place. This aberrant non-fission type of cell division is reminiscent of crosswall formation. It is likely that variations in lipid composition correlate to the different lifestyles of microorganisms and the approaches they have evolved to ensure the correct timing and localization of cell division. It will be interesting to see whether the intracellular membranes implicated in *E. coli* and *B. subtilis* division function in a similar manner as the cross-membranes in *Streptomyces*, and perhaps also play a role in triggering divisome formation, e.g. by activating Z-ring formation. Regardless of how widespread cross-membranes are, the next step will be to discover how their formation is initiated and what dictates their function and dynamics.

EXPERIMENTAL PROCEDURES

Bacterial strains and constructs

E. coli strains were routinely grown in Luria-Bertani medium. *S. coelicolor* and *S. albus* strains were grown on R2YE agar or soya flour mannitol (SFM) agar. Liquid cultures were grown in a 50:50 mixture of tryptone soya broth (TSB; Oxoid) and yeast extract-malt extract (YEME), or 2YT medium supplemented with 10% sucrose. All of the growth medium recipes used are those of (Kieser *et al.* 2000). For fluorescence microscopy, samples from liquid cultures were spotted onto a glass microscope slide before microscopy analysis. Images of vegetative hyphae from solid growth samples were collected from samples that had been inoculated at the acute-angle junction of coverslips inserted at a 45° angle in SFM agar plates.

Strains used in this study include *S. coelicolor* M145 (Kieser *et al.* 2000), obtained from the John Innes Centre strain collection, the *S. albus* subspecies *albus* G. ATCC 25426, as well as strains GSB1 (M145 *ΔssgB* (::aacC4)) (Keijser *et al.* 2003) and K202 (M145 + KF41) (Grantcharova *et al.* 2005).

Microscopy

Fluorescence microscopy

Fluorescence and corresponding light micrographs were obtained with a Zeiss Axioscope A1 upright fluorescence microscope (with an Axiocam Mrc5 camera at a resolution of 37.5 nm/pixel), with, for the green channel, 470- to 490-nm excitation and 515 long-pass detection; and for the red channel, 530- to 550-nm excitation and 590 long-pass detection. The green fluorescent images were created using 470/40-nm bandpass excitation and 525/50 bandpass detection; for the red channel, 550/25-nm bandpass excitation and 605/70 bandpass detection were used. For staining of the cell wall (peptidoglycan), we used TRITC-WGA; for membrane staining, we used FM5-95 (both obtained from Molecular Probes). All images were background-corrected, setting the signal outside the hyphae to 0 to obtain a sufficiently dark background. These corrections were made using Adobe Photoshop CS5.

Time-lapsed (live) imaging

Uncoated μ-Slide 2 × 9 dishes (Ibidi GmbH) were placed at an angle and the central wells semi-filled with SFM medium containing spore solution as well as FM5-95 and NAO stains. The remaining wells were filled with water to maintain humidity in the slide chamber, and the lid was left partially open, allowing for gas exchange, sealed off by two layers of Parafilm to prevent drying of the medium. Samples were incubated at 30 ºC in the microscope stage

overnight and imaged with a Zeiss Observer A1 with a Hamamatsu EM-CCD C9100-02 camera. Images were taken with 10 min intervals for 60 min.

Sample preparation for electron microscopy

A small drop (3 µL) of *Streptomyces* liquid culture was applied to EM grids and vitrified using a vitrobot Mark IV (FEI Company, USA) operated at 22 °C and 100% humidity using 1-2 seconds blotting. Subsequently, the cells were cryo-fixed by plunging into a liquid ethane/propane mixture. Plunge-frozen grids were stored in liquid nitrogen until further use. For cryo-electron tomography, 15 nm colloidal gold particles coupled to protein A (CMRC, Utrecht, The Netherlands) were added to samples as fiducial markers. For correlative light and microscopy work, finder grids were used and samples were stained with FM5-95, NAO and/or DAPI directly before sample application to the grid and subsequent plunge freezing.

Electron microscopy

Cryo electron tomography was performed on a Tecnai 20 FEG operated at 200 kV and a Titan Krios operated at 300 keV (FEI Company). Images were recorded using Explore 3D software on a 2k x 2k camera mounted behind a GIF energy filter (Gatan) operated at a slit width of 20 eV. Cryo electron tomograms of membrane vesicles were recorded with 2° tilt steps between -60° to +60° at a defocus of -5 µm, at magnifications between 1850x (6.6 nm pixels zie) and 8000x (1.64 nm pixel size).

Cryo-correlative light and electron microscopy

Plunge-frozen grids containing fluorescently labeled *Streptomyces* were imaged using a fluorescence microscope equipped with a THMS600 or CMS196 cryo light microscope stage (Linkam, Surrey, UK), in conjunction with a Leitz DMRB (Leica, Wetzlar, Germany), with a 100x dry objective with a working distance of 4.7mm and a numerical aperture (NA) of 0.75. Digital images were recorded with a Leica DFC350FX CCD camera. Following cryo-FM imaging, sample grids were stored in liquid nitrogen until they were used for cryo-EM.

Image analysis and visualization

Tomographic tilt series were processed using IMOD version 4.5 (Kremer *et al.* 1996). Projection images were preprocessed by hot pixel removal and rough alignment by cross-correlation. Final alignment was done using fiducial gold markers. The tomograms were obtained using a weighted back-projection or a simultaneous iterative reconstruction technique. Cryo-electron tomograms were Fourier filtered and denoised with a non-linear

anisotropic diffusion (Frangakis and Hegerl 2001) to enhance the visibility of structures. For 3D surface rendering, the tomographic volumes were imported into AMIRA (FEI) for further processing and representation.

Chapter 5

Structured Morphological Modeling as a Framework for Rational Design of *Streptomyces* Species

Katherine Celler, Cristian Picioreanu, Mark C.M. van Loosdrecht, and Gilles P. van Wezel

Anthonie van Leeuwenhoek. 2012 Oct; 102(3):409-23

ABSTRACT

Successful application of a computational model for rational design of industrial *Streptomyces* design requires a better understanding of the relationship between morphology - dictated by microbial growth, branching, fragmentation and adhesion - and product formation. Here we review the state-of-the-art in modeling of growth and product formation by filamentous microorganisms, and expand on existing models by combining a morphological and structural approach to realistically model and visualize a three-dimensional pellet. The objective is to provide a framework to study the effect of morphology and structure on natural product and enzyme formation and yield. Growth and development of the pellet occur via the processes of apical extension, branching and cross-wall formation. Oxygen is taken to be the limiting component, with the oxygen concentration at the tips regulating growth kinetics and the oxygen profile within the pellet affecting the probability of branching. Biological information regarding the processes of differentiation and branching in liquid cultures of the model organism *Streptomyces coelicolor* has been implemented. The model can be extended based on information gained in fermentation trials for different production strains, with the aim to provide a test drive for the fermentation process and to pre-assess the effect of different variables on productivity. This should aid in improving *Streptomyces* as a production platform in industrial biotechnology.

STATE OF THE ART IN GROWTH MODELING OF FILAMENTOUS MICROORGANISMS

Streptomycetes are Gram-positive mycelial bacteria which are commercially used in the production of natural products such as antibiotics, anticancer agents and immunosuppressants, as well as industrial enzymes (Hopwood 2007). Unlike unicellular bacteria, which grow exponentially by binary fission with a constant generation time (Errington *et al.* 2003), filamentous organisms grow due to the combination of steady hyphal growth and addition of new hyphal tips via branching of the mycelium. During growth, vegetative hyphae are divided into compartments by cross-walls (Chater and Losick 1997). The reproductive phase is initiated by the erection of sporogenic structures called aerial hyphae, which are nonbranching structures that differentiate following a complex cell division event whereby the multigenomic hyphae are converted into chains of unigenomic spores. Aerial hyphae are formed only on solid-grown cultures, giving the colonies their characteristic white and fluffy appearance. Some *Streptomyces* species are also able to produce spores in submerged culture (Glazebrook *et al.* 1990; Kendrick and Ensign 1983).

Morphology and structure formation vary from species to species, based on strain-specific genetic make-up that is yet poorly understood (Jakimowicz and van Wezel 2012). Many genes and physiological mechanisms are involved in the development of a particular morphological type (Kossen 2000). A survey of the submerged growth of over 100 reference species identified a continuum of morphological types, ranging from large macroscopic mycelial pellets several millimeters in diameter to small fragmented particles (Tresner *et al.* 1967). The different types of mycelia have been classified as pellets (compact masses of over around 1 mm in diameter), clumps (less compact masses between 0.6 - 1 mm in diameter), branched hyphae and non-branched hyphae (Pamboukian *et al.* 2002). *Streptomyces* species can be further subdivided into those which sporulate in liquid culture (*S. albus, S. griseus, S. roseosporus*), and those that do not (Glazebrook *et al.* 1990; Kendrick and Ensign 1983; van Wezel *et al.* 2009). When grown under different conditions, growth rate and morphology change depending on the composition of the growth medium, pH, temperature, mixing intensity, dissolved oxygen concentration and inoculum (Tough and Prosser 1996; Cui *et al.* 1998). In a sense, mycelial morphology is the classic example of 'nature versus nurture' - an observed morphology emerges from the combination of genetic and environmental factors in a fermentation.

The filamentous nature of streptomycetes, resulting in highly viscous broths, unfavorable

pellet formation and slow growth, strongly affects the rheology of liquid cultures, which makes fermentation difficult (van Wezel *et al.* 2009). Large clumps are mainly physiologically active around the edge of the pellet, with oxygen and nutrient depletion in the centre. Increased broth mixing may improve transport, but results in shearing off of pellet tips and lysis. Shear force may also rupture the pellet as a whole, especially if the pellet is already hollow due to oxygen or substrate limitations (Meyerhoff *et al.* 1995). In addition, downstream processing of fermentation broths is complex and costly (van Wezel *et al.* 2006). The understanding and control of morphology is therefore key for optimization of industrial fermentations. The relationship between growth and morphology, on the one hand, and biomass accumulation and productivity on the other, is complicated, and optimal morphology varies from product to product.

Studies on erythromycin production by *Saccharospolyspora erythraea* showed a strong correlation between mycelium fragment diameter (defined as the minimum diameter of a sphere that can bound a *hyphal fragment*, or pellet) and productivity, with a critical pellet diameter of 88 μm, below which production was drastically reduced (Wardell *et al.* 2002). Variants with decreased branching frequency showed increased hyphal strength, larger mycelial fragments, and increased antibiotic production. In *Streptomyces,* regulation of the secondary metabolism is complex, necessitating directed systems-level engineering approaches for strain improvement (van Wezel and McDowall 2011). One of the most direct ways of tackling the morphological problems was achieved by overexpression of the SsgA protein, which results in fragmentation of mycelial clumps (Kawamoto *et al.* 1997; van Wezel *et al.* 2000a). SsgA and its paralogue SsgB are required for the activation of cell division in streptomycetes, with SsgB recruiting the cell division scaffold protein FtsZ (Keijser *et al.* 2003; Willemse *et al.* 2011), and the enhanced expression of SsgA improving growth rates in batch fermentations of *S. coelicolor* and *Streptomyces lividans,* and resulting in a two-fold increase in yield of enzyme production with a higher production rate (van Wezel *et al.* 2006). Secretion capacity is also directly related to the activity of SsgA (Noens *et al.* 2007). This highlights the potential of genetic engineering approaches based on understanding of the biological processes that govern morphology and production. The effects of enhanced division on antibiotic production are less predictable (van Wezel *et al.* 2000b), and better insight into this relationship is needed.

Morphological modeling is a valuable tool to suggest potential strain improvements and predict optimal fermentation conditions. Present models largely investigate the influence of environmental factors on morphology, while modeling with a strong focus on genetics may be powerful (Kossen 2000), but has not been attempted. Several models for growth

of filamentous organisms (both fungal and actinomycete) have been proposed, including single-pellet models that focus on microscopic morphology and model three-dimensional tip elongation and branching. An initial model was based on diffusion-reaction of a hypothetical intracellular growth-limiting component (Yang *et al.* 1992a); this model was later extended to include the diffusion of limiting substrates and fragmentation due to shear forces (Meyerhoff *et al.* 1995). Basing growth on a tip extension rate depending on oxygen concentration, a similar model combined microscopic morphology with analysis of solute profiles along the pellet radius and the fractal dimension (Lejeune and Baron 1997). Macroscopic (fermentation) models focus instead on the effects of mass transport on growth and production in a reactor, providing *e.g.* an unstructured approach for modeling growth of mycelial pellets in submerged cultures. These models integrate growth kinetics at hyphal scale with the physical mechanisms of mass-transfer processes in pellets and the fermentor (van Suijdam *et al.* 1982). Modeling of microbial kinetics may also be based on structured models that describe rates by means of selected cell components rather than by the undifferentiated biomass (Nielsen and Villadsen 1992). Fermentation-scale models are typically combined with a population balance, in which the behavior and effect of pellet populations in cultivations is studied, *e.g.* predicting changes in the distribution of pellet sizes within a population growing in a fermentor (Tough and Prosser 1996). Fermentation population models have also been coupled with structured models, with a particular focus on morphological forms, with various growth and production rates in different hyphal elements. In an early example of structured modeling, hyphae of *Aspergillus awamori* were divided into five differentiation states with different growth and metabolite synthesis rates (Megee *et al.* 1970). This approach was extended to include fragmentation and compared to experimental data for submerged growth of *Geotrichum candidum*, *Streptomyces hygroscopicus*, and *Penicillium chrysogenum* (Nielsen 1993). Population-based structural models were used to study the production of among others penicillin (Birol *et al.* 2002) or streptomycin (Liu *et al.* 2005). While these models keep track of the proportions of hyphal elements in a fermentor, they do not incorporate changes to the developing pellet during the fermentation process. Each structural element represents a fraction of the clump, without providing insight into the three-dimensional pellet morphology. Despite the strong increase in computational power and available modeling software, little has been done in recent years to improve and expand these models.

In this work growth of a mycelial pellet of *Streptomyces* is modeled, combining three-dimensional morphological pellet formation with a structured approach. We propose a combined morphological and structured model of a single-pellet, with a three-dimensional

computational framework including oxygen (or other solute) diffusion and reaction in pellets, hyphal growth, branching and shearing, cross-wall formation and fragmentation, as well as collision detection during development. Biological information regarding the processes of differentiation and branching in liquid cultures of the model organism *S. coelicolor* has been implemented. The current modeling platform allows for study of the relationship between enzyme or antibiotic production and morphology and structure.

MATHEMATICAL MODEL DESCRIPTION

Fermentations involve many interacting factors of biological, chemical and physical nature. The microorganism itself, and its genetic make-up, are the backbone of the process, but process conditions (nutrients, oxygen, heat, mixing) also play a crucial role in controlling microbial growth, hyphal/pellet morphology and productivity. Mathematical models should incorporate these variables, so as to provide a *test drive for the fermentation process* and to pre-assess the effect of different variables on productivity. Although all cells in a hyphal element share a common cytoplasm with multiple nuclei, significant cellular and functional differentiation within the mycelial pellet exists (Megee *et al.* 1970). Earlier studies indicate that secondary metabolite production in filamentous organisms is associated with this morphological differentiation, which favors a structured approach to modeling (Giudici *et al.* 2004; Manteca *et al.* 2008). In creating a structured model, hyphae may be divided into three compartments: (i) apical, (ii) subapical, and (iii) hyphal compartment, each type indicating a different stage of cellular differentiation (Figure 1a).

At the start of growth, a spore germinates to form a new apical compartment (A_{new}). Oxygen and substrate are assimilated within the apical compartment for growth and apical extension (Gray *et al.* 1990). The apical compartment A extends until a maximum apical length is reached. As apical extension continues, some of compartment A is converted into subapical compartment B. Compartment B has an intracellular composition very similar to compartment A. However, oxygen and substrate consumption in compartment B results not in growth, but rather in the formation of new branches (A_{new}). Within mycelial pellets, where substrate levels are depleted, compartment B transforms into the hyphal compartment H. Based on the observation that pellet and clump formation are important determinants for yield, it is the hyphal compartment that is taken to be responsible for secondary metabolite production (Manteca *et al.* 2008). The various metamorphosis reactions described are shown in Figure 1b.

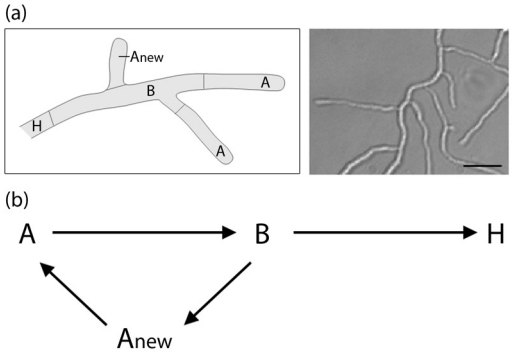

Figure 1. *Graphical representations of hyphal growth.*

(a) Left: Hyphal element with different compartments: apical (A), subapical (B), newly-formed apical as a result of branching (Anew) and hyphal (H). Right: light microscopy image of S. coelicolor hyphae for comparison. Scale bar, 3 µm. (b) Metamorphosis reactions between different hyphal compartments: apical (A), subapical (B), newly-formed apical as a result of branching (Anew) and hyphal (H).

Growth

To describe three-dimensional growth of the mycelium, a hyphal tip growth and branching model (Yang *et al.* 1992a) was adapted, with the assumptions that hyphae are cylindrical, have constant diameter *d* and density ρ_x and grow by apical extension. Three-dimensional collision detection is employed to prevent overlapping hyphae. The orientation of the growing tip is characterized by angles θ and φ in spherical coordinates that change stochastically as a function of time. During growth, an apical compartment extends until the maximum apical length ($L_{A,max}$) is reached, which may occur before the formation of a cross-wall near the tip. Tip extension is exponential until $L_{A,max}$ is reached, after which apical extension continues, but rather than extending compartment A, a new compartment B is added. In this case, the net result of tip extension is actually the formation of subapical cells from apical cells.

Growth rate is based on local oxygen concentration according to Monod kinetics (with maximum specific growth rate μ_{max} and half-saturation coefficient K_O). The total growth rate in a shell with thickness *dr* situated at distance *r* from the pellet centre is calculated as the sum of extension rates α of all tips in that shell. The total growth rate is correlated with the oxygen consumption rate by a yield coefficient Y_{OX}.

$$\mu(r)C_{X,A}(r) = \frac{1}{V}\left(\frac{\pi d^4}{4}\right)\cdot\frac{C_O(r)}{K_O + C_O(r)}\cdot\sum\alpha_{i,\max(A)} \qquad (1)$$

Although *Streptomyces* grow by apical extension, the model assumption is that once the apical compartment has reached its maximum length, growth results in formation of subapical compartment (eq. 2).

$$\mu(r)C_{X,B}(r) = \frac{1}{V}\left(\frac{\pi d^4}{4}\right)\cdot\frac{C_O(r)}{K_O + C_O(r)}\cdot\sum\alpha_{i,\max(B)} \quad (2)$$

Ageing cells become increasingly vacuolated and have a completely different metabolism than actively growing apical cells (Zangirolami *et al.* 1996). Differentiation is the process of conversion of subapical cells B to hyphal cells H once a certain arbitrary differentiation age (A_{diff}) has been reached. The assumption is made that at this time point, growth results in formation of hyphal compartment (eq. 3), reflecting the natural differentiation observed, but still poorly understood, within *Streptomyces sp.* Hyphal cells do not grow or branch, but are responsible for secondary metabolite production. The amount of hyphal cells in a pellet can be taken as indicative of the level of secondary metabolite production.

$$\mu(r)C_{X,H}(r) = \frac{1}{V}\left(\frac{\pi d^4}{4}\right)\cdot\frac{C_O(r)}{K_O + C_O(r)}\cdot\sum\alpha_{i,\max(H)} \quad (3)$$

Because of the hyphal differentiation assumed in the model, apical, subapical and hyphal compartments may have different oxygen consumption rates. However, because it is not known whether this is a valid assumption, a single yield coefficient is taken for all compartments. Upon fitting the model to experimental data, different yield coefficients may be obtained.

Branching

New branches form by the extension of new tips A_{new} from the subapical compartment B. These tips grow in the plane perpendicular to the parent segments. Initially, a new coordinate system is set up with the parent branches defining the x-y plane, and a z-vector drawn perpendicular to the plane. The direction of the new branch growth in this plane is chosen stochastically from a uniform distribution. Once the branch endpoint has been chosen within the new coordinate system, this point is placed back within the original coordinate system. In *Streptomyces*, branching depends on the essential protein DivIVA, which localizes at tips and new branch sites, recruiting or activating cell wall synthesis enzymes (Flärdh 2003; Hempel *et al.* 2008). In the model, branching occurs according to the local oxygen concentration in the pellet: probability of branching tapers off towards the inside of the

pellet, where the oxygen concentration is diminished. As branching rates have not been measured within pellets, the correlation of branching and oxygen concentration is a model assumption made to decrease levels in the crowded inner core of a pellet. Distance between branches results from the branching probability and a chosen branching interval (b_{int}). As in growth, collision detection is employed to prevent overlapping hyphae during branching.

Cross-wall Formation

The current model relies on the assumption that cross-walls form near branches (Reichl *et al.* 1990). Once cross-wall formation has been initiated, a cross-wall will form directly before or after a branch. Subsequent cross-walls on the branch will form at a multiple (random uniform distribution) of the specified interval (c_{int}) from the first cross-wall. Cross-wall formation occurs at a chosen time interval. Multiple cross-walls may simultaneously form on a given branch during a cross-wall formation event, as evidenced in live-imaging experiments (Jyothikumar *et al.* 2008). The number of cross-walls formed on a given hyphae is dependent on the number of branches on the hyphae. However, if the choice of new cross-wall position is at another branch point or location of an existing cross-wall, the cross-wall is not formed.

Fragmentation

Stirring in the fermentor creates shear forces that enforce fragmentation of the pellets. Similarly to the model of Meyerhoff, a biomass density parameter (m^3 biomass/m^3 total volume) was chosen above which hyphae are not affected by shear because they stabilize each other within the pellet. A respective threshold radius (r_{thres}) is chosen based on this density, and a breaking probability (P_{break}) is chosen at a certain distance to this radius from the tip r_{tip}. The expression for the probability of breaking, assuming shear force parameter λ_{shear} is given by equation (4).

$$P_{break} = 100.0 - 100.0 \cdot \exp\left[-\lambda_{shear} \cdot \frac{\left(r_{tip} - r_{thres} \right)}{r_{thres}} \right] \tag{4}$$

Breaking is assumed to occur at cross-wall locations, where the hyphal wall is reported to be weaker (Krabben and Nielsen 1998), and this is supported by the strong effect of the cell-division activator protein SsgA on fragmentation (Traag and van Wezel 2008).

Collision Detection

The computational framework includes collision detection between the hyphal branches,

which has not been incorporated in any previous model for micro-scale pellet formation. Collision detection is required to build a realistic model, as it avoids overlap of growing and branching hyphae in a spatially constrained environment. Moreover, the implemented collision detection algorithm ensures that the resulting pellet volume densities do not surpass 100% filled volume near the pellet centre. Diffusion of oxygen and substrates into the pellet can then be based on real rather than hypothetical pellet cell volume density. Further, data on the location of *e.g.* the cell division and secretion machineries along the hyphae can be implemented in the model.

In the collision detection algorithm, the space domain is partitioned into cubes and all segments of the mycelium are placed in the space cube corresponding to their location. Collision is checked between a new hyphal segment and other segments in the same and neighboring space cubes. A collision is detected if any points on the segments are closer than the distance of two hyphal radii from each other. The algorithm from (Ericson 2005) was used for determining the distance between two segments. Once a near collision has been detected, tip growth or branching does not take place in the given time step. In the following time step, should a growth or branching angle be stochastically chosen which does not result in collision, extension of the mycelium at the given location can take place. This corresponds to observations during live imaging of hyphal growth which revealed that when two hyphal tips are found close to each other, one may exert apical dominance over the other and arrest the latter's growth for a period of time ((Jyothikumar *et al.* 2008) and our unpublished data).

Oxygen Diffusion

Oxygen is taken to be the limiting substrate, based on previous studies which have shown that oxygen can become mass transfer limited within mycelial pellets (Michel *et al.* 1992). The one-solute assumption is made here for the simplicity of the case study and more solutes can easily be taken into account. When a pellet reaches a certain critical size, oxygen limitation within the centre occurs, resulting in lysis. This critical size is a function of the pellet biomass density, the dissolved oxygen concentration in the bulk liquid and the hyphal respiration rate (Cui *et al.* 1998).

Initially, a fully three-dimensional (3D) model for the oxygen diffusion and reaction within the pellet was developed. Oxygen concentrations in concentric shells obtained with the three-dimensional model were subsequently compared with the radial (one-dimensional, 1D) oxygen profile obtained assuming spherical symmetry (Lejeune and Baron 1997). Obviously, the 3D model was computationally much more intensive than the 1D counterpart,

but nevertheless resulted in a very similar oxygen concentration profile. Therefore, the simplified 1D radial symmetry was further assumed for each pellet, with oxygen transport occurring by molecular diffusion. Alteration in local oxygen concentration is assumed to be slow compared to growth, and hence a differential equation with stationary coupling of oxygen diffusion and reaction rates can be written in radial coordinates *r* (eq. 5).

$$D_{O2,eff}\frac{1}{r^2}\frac{d}{dr}\left(r^2\frac{dC_O}{dr}\right)=\frac{\mu(r)}{Y_{XO}}C_X(r)=OUR \tag{5}$$

The expression for oxygen uptake rate (*OUR*) can be rewritten to take into account the extension of the apical, subapical or hyphal compartment at different points in the branch lifetime (eqs. 6-8). The apical compartment is extended if the branch length is less than the maximum apical compartment length ($L_{branch} < L_{A,max}$). The subapical compartment is extended thereafter until the branch reaches differentiation age (A_{diff}), at which point the hyphal compartment is extended. Until data is obtained to prove otherwise, the yield coefficients of biomass on oxygen $Y_{XO,A}$, $Y_{XO,B}$, $Y_{XO,H}$ are assumed to be the same in all compartments.

$$OUR=\frac{\mu(r)}{Y_{XO,A}}C_{X,A}(r) \qquad \text{if } L_{branch} < L_{A,\max} \tag{6}$$

$$OUR=\frac{\mu(r)}{Y_{XO,B}}C_{X,B}(r) \qquad \text{if } A_{branch} < A_{diff} \tag{7}$$

$$OUR=\frac{\mu(r)}{Y_{XO,H}}C_{X,H}(r) \qquad \text{otherwise.} \tag{8}$$

Within the pellet, the effective diffusion coefficient D_{eff} was computed proportional to the pellet porosity (ε). The boundary conditions were (1) constant oxygen concentration in the bulk phase and (2) zero oxygen flux (symmetry condition) at the center of the pellet.

Parameter Values and Simulation

The computational model was implemented in MATLAB (MATLAB 2008b, Mathworks, Natick, MA, www.mathworks.com) and visualization of pellets was performed using the freeware Persistance of Vision Raytracer software (Pov-Ray, www.povray.org). The 1D diffusion-reaction solution was approximated using the finite differences method. Parameter values for a typical simulation run are given in Table 1. Parameters for variation in tip angle direction are based on measurements performed in growth chambers (Yang *et al*. 1992b). Branching and cross-wall intervals are parameters that are strain dependent; differences in the intervals result in significant morphological variation. The yield of biomass on oxygen was

based on literature, with a value of 1.2 kg kg^{-1} assumed for all compartments (Meyerhoff *et al.* 1995). The model may later be fitted to experimental data to determine whether different yield coefficients exist for each compartment type. The shearing probability was adjusted to result in realistic breakage.

Table 1. *Values of model parameters used in a typical simulation run for pellet morphology.*

Parameter	Unit	Value	Source
r	µm	0.25	*S. coelicolor* average radius
ρ_x	kg dw m^{-3}	100	Assumed (Lejeune and Baron 1997)
α_{max}	µm · h^{-1}	5	Conservative estimate
dθ	°	12	(Yang *et al.* 1992b)
dφ	°	12	(Yang *et al.* 1992b)
b_{int}	branch μm^{-1}	1/2	Estimated
c_{int}	cross-wall μm^{-1}	1/10	Estimated
D_{O2}	m2 s^{-1}	2.25×10^{-9} (at 30°C)	Diffusion coefficient of O_2 in water
K_{O2}	kg m^{-3}	1.0×10^{-4}	(Meyerhoff *et al.* 1995)
Y_{XO}	kg kg^{-1}	1.2	(Meyerhoff *et al.* 1995)
$C_{b,O2}$	kg m^{-3}	0.009	(Lejeune and Baron 1997)
λ_{shear}	-	0.5	(Meyerhoff *et al.* 1995)

MODEL OUTPUT

The results of a simulation can be assessed by visualizing the mycelium morphology development (growth, branching and cross-wall formation) or numerical analysis of several quantitative measures. These measures include: the hyphal growth unit (HGU), fractions of different mycelial types over time or space, number of tips for a given morphology, number of cross-walls formed, biomass density, number of fragmentation events, etc. Here, we will limit the discussion to visualization, the hyphal growth unit and component fractions.

Visualization of Pellet Development

Modern software enables first-rate visualization of biological information, such as the localization of cell division proteins within developing hyphae. Morphological differentiation of streptomycetes is closely integrated with fundamental growth and cell-cycle processes (Flärdh and Buttner 2009). Implementation of knowledge on components that control morphogenesis (such as cell division components) or product formation (*e.g.* biosynthesis and secretion of natural products) is required to allow for building a more realistic model. A

3-d rendering of a simulated portion of a growing mycelium is given in Figure 2. The DivIVA protein (marked as green) drives tip growth and branching and is therefore always present at apical sites (Hempel *et al.* 2008). Cross-walls, where cell division proteins localize, are given in red. The potential of modern visualization software to enable realistic rendering of hyphal growth and pellet formation is demonstrated. Protein localizations were derived from the *in vivo* localizations of GFP-tagged proteins. The model can be readily extended with novel biological data and insights, such as the localization of antibiotic and protein secretion machineries depending on growth or the function of novel morphoproteins.

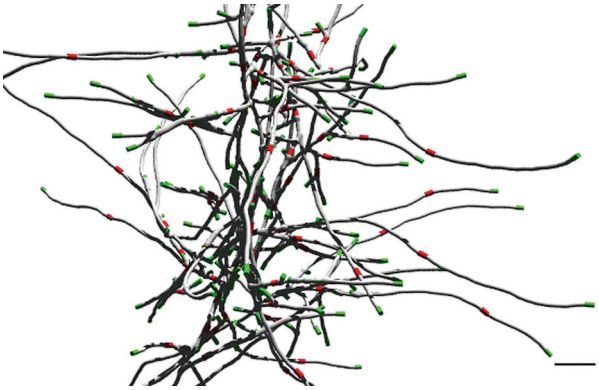

Figure 2. *Simulation of early mycelial pellet formation with DivIVA localizing at hyphal tips (green) and cross-walls (red) forming at roughly 10 µm intervals. Scale bar, 5 µm.*

Hyphal Growth Unit

The ratio between the size of the mycelium and the number of tips is a characteristic morphological variable called the hyphal growth unit of a simulated pellet (Caldwell and Trinci 1973). Although originally defined as the total mycelium length divided by the number of tips, it may also be based on the total mycelium volume or mass (Nielsen 1993). In this study, HGU is calculated according to the original definition based on the total mycelium length. If the HGU is constant, both tip extension rate and branching frequency are proportional to the specific growth rate of the biomass. The HGU also provides an idea of the mycelium morphology: a large value indicates long hyphal threads with few branch points, whereas a small value indicates a dense hyphal structure with many branch points (Nielsen and Villadsen 1992). The hyphal growth unit provides a quick assessment of morphological type; a change of parameters which results in an increase in the HGU may provide a wider or more fragmented morphology with enhanced mass transfer capability and better performance in the fermentor.

Ratio of Compartment Types

Given that secondary metabolite production in filamentous organisms is associated with morphological differentiation in the mycelium, it is interesting to compare the ratio of different compartment types over time for a given morphology. Recent structured models correlate the amount of antibiotic production in a fermentation to the amount of subapical or hyphal compartments, where secondary metabolite formation is expected to take place (Paul and Thomas 1996; Birol *et al.* 2002; Giudici *et al.* 2004; Liu *et al.* 2005). The ratio of component types can be followed over pellet development, or alternatively, represented as a function of pellet radius. Classification of the mycelium into components with different metabolic activity and function may provide more understanding of the relationship between morphology and biomass accumulation and productivity.

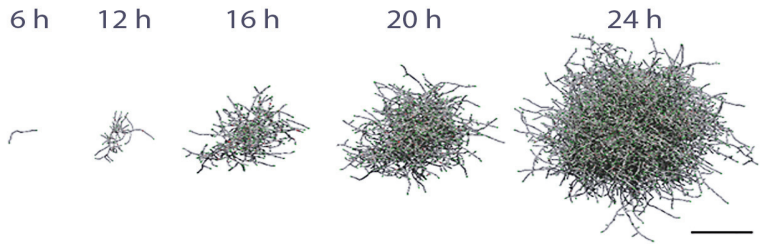

Figure 3. *Two-dimensional projection of a 3D simulated pellet. Images based on the three-dimensional model presented as Supplemental Video. Parameters as given in Table 1. Growth time indicated. Scale bar, 100 µm.*

CASE STUDY

A case study was performed to demonstrate the model's ability to accurately show differences in *Streptomyces* strain morphologies and incorporate molecular information. Depending on model parameters the model represents the different morphological variants (pellets, mycelial mats or hyphal fragments). Quantitative model output parameters, such as the hyphal growth unit and fractions of different component types are discussed. To visualize growth, an example of mycelium development over time is given (Figure 3 and Supplemental Video).

Starting from a single unbranched mycelium, a full quasi-spherical pellet with high inner cellular density and a loose outer layer of outgrowing filaments develops after one day. Different modeled morphological types were simulated and compared to real mycelial clumps with the described morphologies (Figure 4).

The biomass density profiles (kg biomass/m^3 of pellet volume) for the pellet and mycelial mat morphologies are given in Figure 5, showing the larger density of the pellet morphology. Pellet growth was simulated using the parameters given in Table 1; mycelial mat formation was simulated by increasing the distance between branches (from one branch every 2 µm to one every 20 µm); fragments were created when the pellet scenario was simulated taking

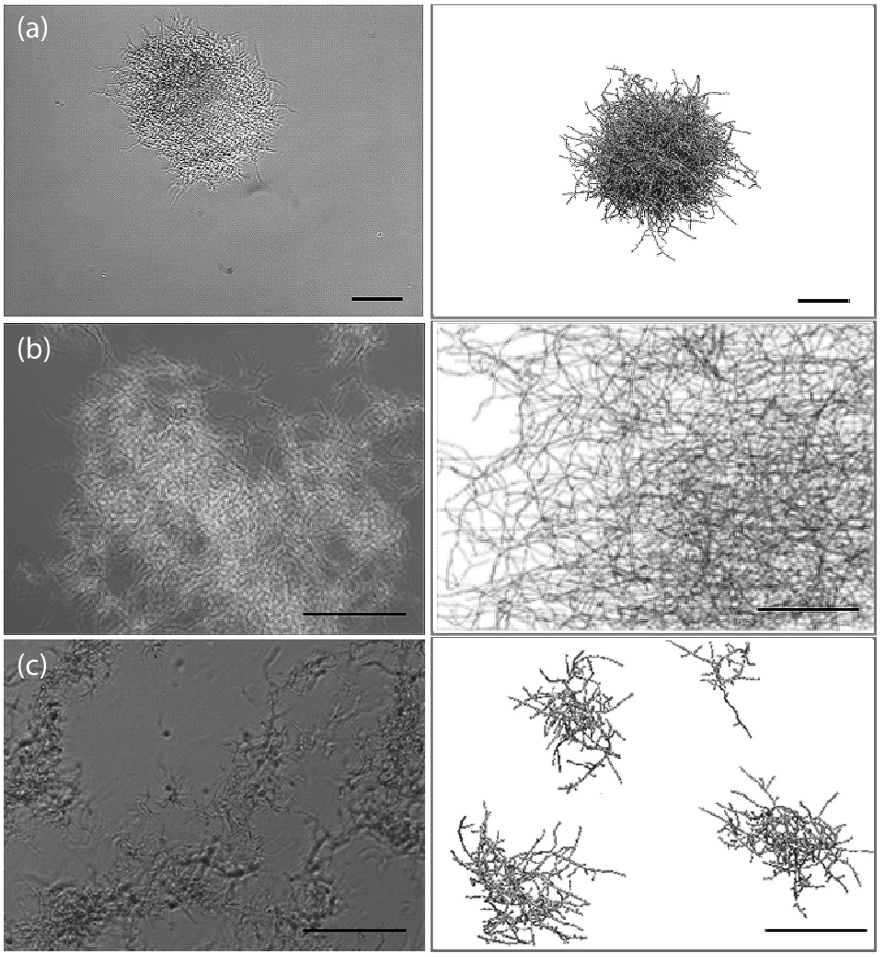

Figure 4. *Qualitative comparison of real (left) and simulated (right) mycelial morphologies. Shake flask cultures were grown in TSBS/YEME medium at 30 °C for 20 hrs. (a) characteristic pellet produced by S. coelicolor M145 (wild-type strain); (b) mycelial mat produced by S. lividans variant MR (GPvW, unpublished); (c) fragmented growth of S. coelicolor GSA2 (overexpressing ssgA; (van Wezel et al. 2000a)). For simulation parameters see Table 1. In case (b) branching interval was set to 1 branch/20 µm. In case (c) broken mycelial fragments are shown from a case where shear is taken into consideration. All the bars: 50 µm.*

shear into consideration. Formation of fragments (Figure 3c) is representative of strains such as the *S. coelicolor* GSA2 strain over-expressing SsgA (van Wezel *et al.* 2000a), which shows increased sensitivity to shear and a pronounced tendency to fragment (van Wezel *et al.* 2006). Mycelial mat formation occurs naturally in other stains, such as *S. lividans* variant MR (GPvW, unpublished). Changing a single parameter value may have a major impact on the predicted morphology. By performing parameter sensitivity analysis studies and investigating the results, optimal production strains can be designed.

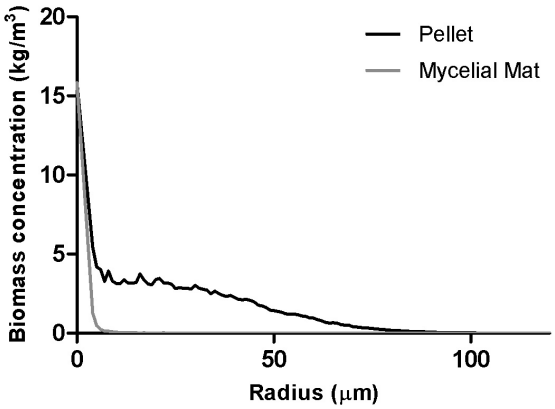

Figure 5. *Biomass density profiles (kg biomass/m3 of pellet volume) for the pellet and mycelial mat morphologies showing increased density at the pellet/mat core and the larger density of the pellet morphology.*

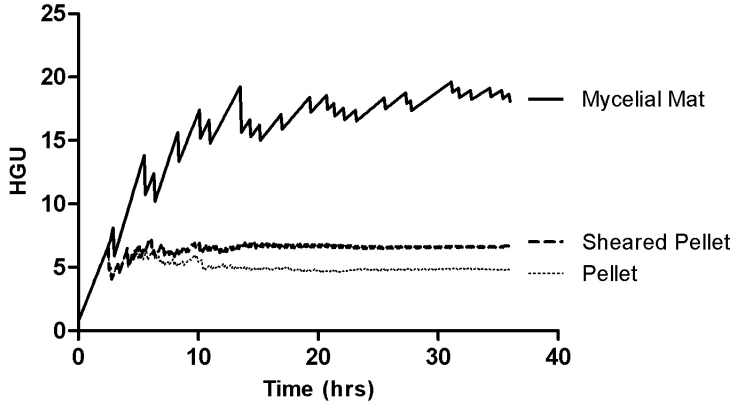

Figure 6. *Hyphal growth unit (HGU) values for simulated dense pellet, mycelial mat and sheared pellet morphologies over time.*

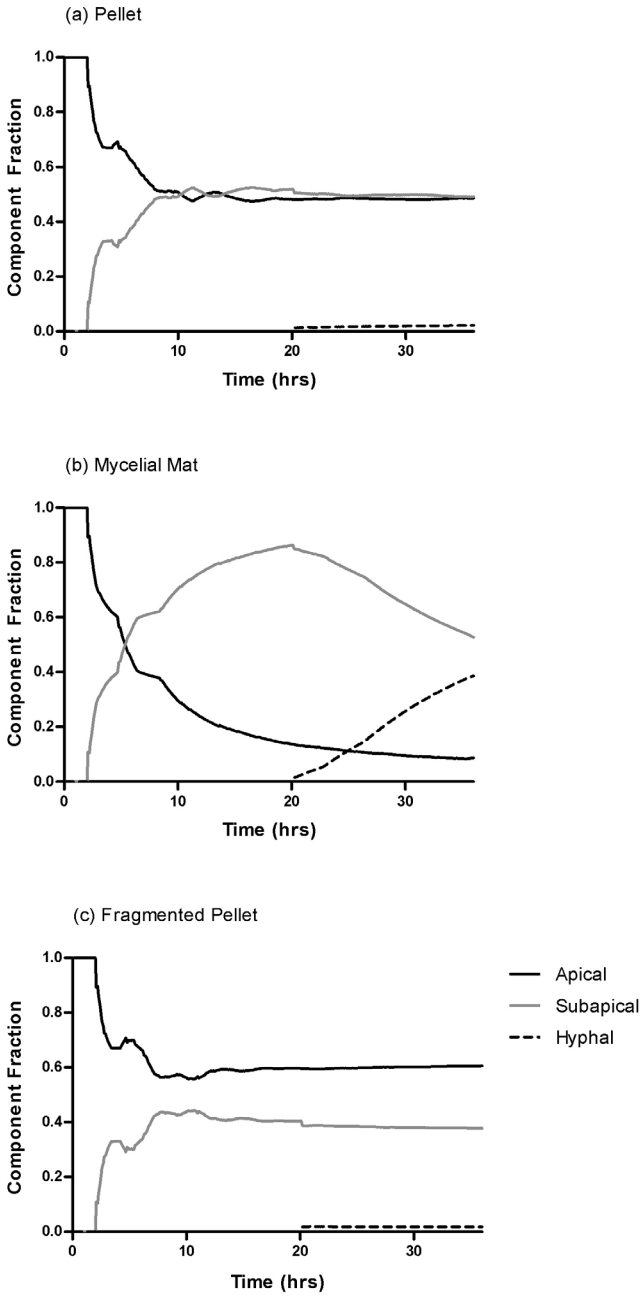

Figure 7. *Comparison of component fractions (apical, subapical and hyphal) in simulated mycelial morphologies: (A) pellet, (B) mycelial mat, (C) fragmented pellet, plotted over time.*

The HGU values were determined for the different simulated morphologies over 36 hours of growth (Figure 6), with higher HGU values indicating more open morphological structures. As expected, the dense pellet HGU is much smaller than that of the mycelial mat morphology. Fragmentation results in an increase in the HGU. Interestingly, for the pellet and sheared pellet (fragmented) morphologies, HGU levels off at roughly 12 hours, while it continues increasing for the mycelial mat morphology. This indicates that in the mat, the mass of the mycelium increases more by extension of existing branches than by addition of new ones.

Component fractions for the three simulations were compared (Figure 7). In the pellet (Figure 7a), dense growth of branches results in almost equal distribution of apical and sub apical component at 36 hours; ageing of cells, however, has begun. The hyphal fraction will extend steadily as oxygen and space limitations within the pellet limit growth and addition of new branches. In the mycelial mat (Figure 7b), because of the reduced frequency of branching, at 36 hours, the mycelium already consists of 40% hyphal fraction and only 10% apical component. Conversely, fragmented growth (Figure 7c) results in a high apical fraction, due to the presence of a large new population of apical pieces.

In the above examples, the exact fraction values are not of importance. Rather, the plots serve to illustrate the potential of structural modeling, where the mycelium is considered to be a differentiating species, consisting of cells with different metabolic function. Such modeling can have an important role in the strategic genetic and morphological design of *Streptomyces* for industrial fermentations. As was demonstrated previously (Liu *et al.* 2005), fermentation trials can be used to modify the described morphogenesis reactions between structural components (Fig. 1b) such that the fractions of components directly correlate to production of metabolites.

The distribution of component fractions can also be plotted over hyphal radius at different time points (Figure 8). The hyphal component is situated within the pellet centre because as the pellet ages, subapical compartment transforms into hyphal compartment. It is evident that oxygen limitation within the pellet results in decreased formation of branches, with an equal distribution of apical and subapical compartments. Where the oxygen level is higher, fraction of subapical component decreases because branching rate is higher and more apical compartments are being formed. The exterior of the pellet consists entirely of new, apical compartments. When coupled with confocal microscopy (Manteca *et al.* 2008) and microsensor measurements of oxygen concentration (Hille *et al.* 2005), such modeling can provide insight into processes that occur within pellets during fermentations.

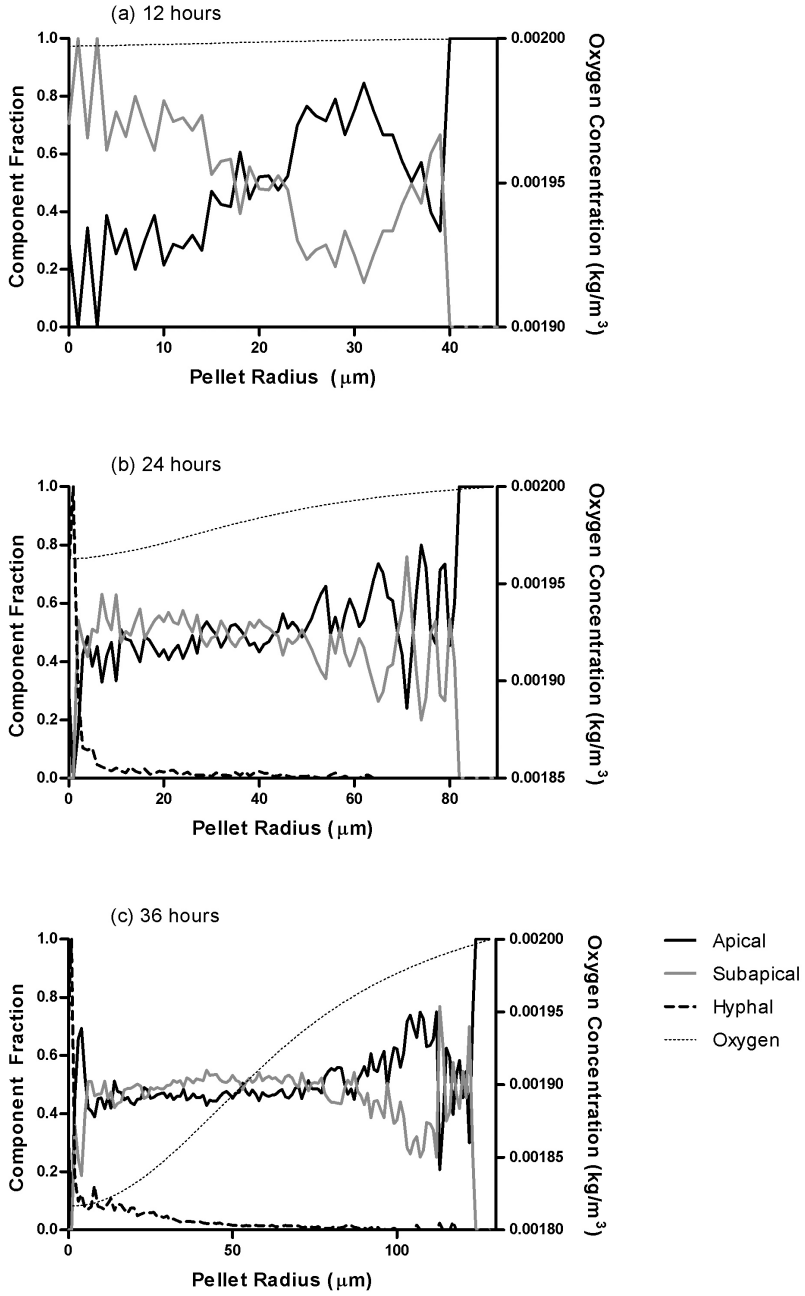

Figure 8. *Fractions of apical, subapical and hyphal components versus pellet radius in a simulated dense pellet after (a) 12, (b) 24, and (c) 36 hours of growth. Oxygen concentration along the radius indicates how branching frequency is affected by oxygen level. The hyphal compartment is located within the pellet core.*

CONCLUSIONS AND PERSPECTIVES

The presented model integrates for the first time three-dimensional morphological visualization with structured modeling. It thereby provides a realistic, single-pellet, three-dimensional framework to study the relationship between enzyme or antibiotic production and morphology and structure. Simulations can be analyzed via visualization of mycelium development (growth, branching and cross-wall formation) or analysis of numerical measures, such as the hyphal growth unit (HGU) or fractions of different mycelial types over time or space. The output thus provides both a visual and numerical assessment of morphological type; for example, a change of parameters which results in an increase in the HGU may provide a wider or more fragmented morphology with enhanced mass transfer capability. Classification of the mycelium into compartments with different metabolic activity and function can provide better understanding of the relationship between morphology and biomass accumulation and productivity. The purpose of this type of modeling is to replace the conventional 'black-box' approach to morphological engineering with a directed rational design and evolution approach in order to better understand how growth rate and morphology affect secretion and yield. Literature describes key regulators that govern pivotal processes during growth in submerged culture, such as Crp for germination (Piette *et al.* 2005), DivIVA for tip growth and branching (Hempel *et al.* 2008) and SsgA for fragmentation (Kawamoto *et al.* 1997; van Wezel *et al.* 2000a), but further insight into these regulatory mechanisms is needed. Optimal morphology should facilitate fermentations from an engineering perspective as well as result in sufficient production of the desired metabolite product.

ACKNOWLEDGEMENTS

We are grateful to Jozef Anné for discussions. This research is supported by a VICI grant (10379) of the Netherlands Applied Research Council (STW) to GPvW, and by a VIDI grant (864.06.003) from the Netherlands Organization for Scientific Research (NWO) to CP.

NOMENCLATURE

A_{branch}	branch age (h)
A_{diff}	differentiation age (h)
b_{int}	branch formation interval (m^{-1})
c_{int}	cross-wall formation interval (m^{-1})
C_O	oxygen concentration in fermentation broth (kg/m^3)
C_X	concentration of biomass (kg/m^3)
$C_{X,A}$	concentration of biomass, apical ($kg\ m^{-3}$)
$C_{X,B}$	concentration of biomass, subapical ($kg\ m^{-3}$)
$C_{X,H}$	concentration of biomass, hyphal ($kg\ m^{-3}$)
d	hyphal diameter (m)
dt	time step (h)
$D_{O2,eff}$	effective diffusion coefficient for oxygen ($m^2\ h^{-1}$)
HGU	hyphal growth unit
K_O	microbial saturation coefficient for oxygen ($kg\ m^{-3}$)
$L_{A,max}$	maximum length of apical compartment (m)
OUR	oxygen uptake rate ($kg\ m^{-3}\ h^{-1}$)
P_{branch}	probability of branching ($\%\ h^{-1}$)
P_{break}	probability of breaking ($\%\ h^{-1}$)
r	radius of pellet (m)
r_{tip}	distance from pellet centre to tip (m)
r_{thres}	threshold radius (m)
V	hyphal segment volume (m^3)
Y_{XO}	yield of biomass on oxygen ($kg\ kg^{-1}$)
$Y_{XO,A}$	yield of biomass on oxygen, apical ($kg\ kg^{-1}$)
$Y_{XO,B}$	yield of biomass on oxygen, subapical ($kg\ kg^{-1}$)
$Y_{XO,H}$	yield of biomass on oxygen, hyphal ($kg\ kg^{-1}$)

Greek symbols

$\alpha_{i,max}$	maximum linear apical extension rate of branch ($m\ h^{-1}$)
$\alpha_{i,max(A)}$	maximum linear extension rate of branch , apical compartment ($m\ h^{-1}$)
$\alpha_{i,max(B)}$	maximum linear extension rate of branch , subapical compartment ($m\ h^{-1}$)
$\alpha_{i,max(H)}$	maximum linear extension rate of branch , hyphal compartment ($m\ h^{-1}$)
λ_{shear}	shear force parameter

μ	maximum specific hyphal growth rate (h^{-1})
ρ_x	density of hyphae (kg dw m^{-3})
θ	polar angle in spherical coordinates
ϕ	cone angle in spherical coordinates

Supplemental Material - Supplemental Video

Modeling of a *Streptomyces* pellet formed over time in submerged culture. The model represents 24 h of growth, with pellet diameter in the final frame roughly equal to 200 µm. Simulation parameters are given in the text in Table 1. The pellet was rendered using the Persistance of Vision Raytracer software (Pov-Ray, www.povray.org) and images were stitched together using QuickTime (www.apple.com/nl/quicktime/download).

Chapter 6

Dynamic Biological Visualization - 3D Modeling using WebGL

INTRODUCTION

During the initial implementation the *Streptomyces* morphological model presented in Chapter 6, the rational choice of tool for the task at hand was MATLAB®. A powerful, high-level, yet easy to use programming language, MATLAB is commonly used by scientists and engineers alike for technical computing. Using an object-oriented approach, the *Streptomyces* mycelium was modeled as a collection of branches, which in turn were modeled as a collection of points with various properties. Properties included whether a point was the start of a new branch or a cross wall location, and its compartment type (apical, subapical or hyphal). Point positions (x, y, z coordinates in 3D space) and properties (denoted in binary notation) were stored within matrices. During the simulation, the processes of growth, branching, cross wall formation, as well as fragmentation, were looped through sequentially, resulting in change of the morphology, and consequently, change in local oxygen concentration. The assumption was that continued growth and branching would deplete oxygen within a pellet, while increasing pellet density, affecting diffusion. Decreased local oxygen concentration would in turn affect growth and branching, resulting in a feed-forward, feed-back mechanism of pellet formation, as well as differentiation, which is known to correlate to productivity. Simulation results were matrices of branch points, reflecting the morphology resulting from a particular set of input parameters.

Matlab functionality allows plotting of two- or three-dimensional plots for data visualization. In this way, if the points of each branch in the mycelium were connected by lines, a simple visual representation of the mycelium could be obtained. To improve upon this still rather crude output, the freely available Persistance of Vision Ray-Tracing software (www.povray.org) was used to create more visually realistic images of simulated pellets (see Chapter 6). Pov-Ray uses ray tracing for image generation, which is a technique that involves tracing the path from a light source through pixels in an image plane and simulating the effects that this light beam would have as it encounters the virtual objects in its path. Although a high degree of visual realism could be achieved, Pov-Ray suffers from lack of dynamics, and individually rendered images need to be stitched together to generate a movie or simulation. Although the Pov-Ray output allowed us to demonstrate that model results provided a realistic portrait of mycelial morphology, this form of visualization was time-consuming and not intuitive.

To develop an interactive version of the model, and drawing inspiration from the Bio-digital Human project (https://www.biodigitalhuman.com/home/) and the Open Worm Browser (http://browser.openworm.org/), part of the code was converted to Javascript so

as to generate a web-based 3D version of the model of *Streptomyces* pellet growth and morphological development. The idea was to create a dynamic model in the browser, where a user can see a pellet grow while adjusting parameters and immediately see the effect of parameter changes on pellet morphology, and ultimately, production.

Use of the Web as a software deployment platform has only recently become possible with the emergence of the HTML5 (http://www.w3.org/TR/html5) and WebGL (http://www.khronos.org/webgl) standards. HTML5 complements capabilities of the existing HTML standard in order to enable support of the latest multimedia, such as the embedding of audio and video directly into web pages, effectively to help in the transformation of the browser into a programming environment (Anttonen, Salminen *et al.* 2011). To give an example, the canvas element, a 2D graphics API (application programming interface) for defining shapes and bitmaps rendered directly in the web browser, is a new feature of HTML5, while WebGL enables visualization of Graphics Processing Unit (GPU) hardware-accelerated 3D graphics in the browser without additional software, plug-ins or extensions. With the help of THREE.js, a lightweight, cross-browser Javascript library, a simplified version of the model could be reprogrammed as a WebGL 3D computer graphics element, able to run in the browser.

Programming of the model in Javascript involved re-thinking the way that the model is structured and coded. Javascript, or JS, is an interpreted language, originally implemented for web browsers to enable user interaction and change of document content via client-side control of the browser. The power, or rather difficulty of Javascipt, lies in the fact that it is weakly (or loosely) typed, meaning that variables do not have a type (ie. int or char), and can hold any object, without restrictions. In order to maintain the hierarchical structure of the model (a mycelium or pellet containing branches, which in turn contain points), an object-oriented approach was used in Javascript, which involved creating different functions for each hierarchical level, with corresponding properties.

During initialization of the page, a THREE.js scene is constructed, including the mycel (short for mycelium) object itself, consisting of branches, with associated branchunits (lines), as well as a camera, light source, and renderer. Application interaction is possible by using the mouse to rotate the pellet during growth and to zoom using the mouse wheel. One javascript function file contains all the variables involved, to be called from the other files as needed. A graphical user-interface (GUI) is provided with, for the moment, four variables: branching interval, tip growth rate, and tip growth angles phi and theta.

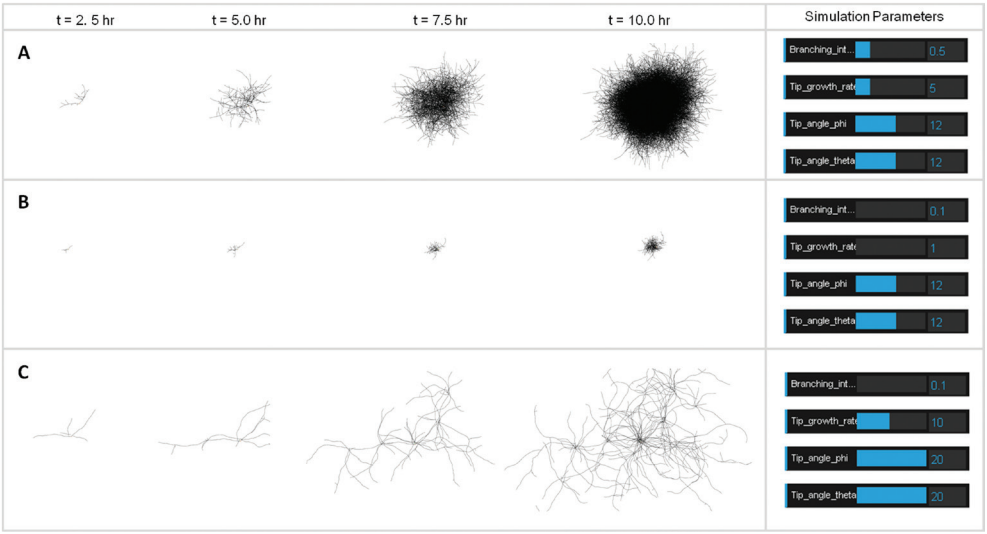

Figure 1. *WebGL simulated morphologies. (A) Dense pellet formation. (B) A very small pellet results when the tip growth rate is decreased. In this simulation, branching interval was also set to 1 branch per 10 µm, but due to the very slow growth rate, the effect this has on morphology is not evident. (C) A mycelial mat structure results from a low branching interval and high growth rate. Tip angle variation was also increased in this simulation, resulting in hyphae which curl more during growth. Parameters are provided in the graphic user interface boxes to the right.*

Adjusting the variables results in the development of various morphologies. A comparison between three different simulation runs with different parameter initializations is shown in Figure 1. The default parameters result in a dense pellet morphology (Figure 1A), while decreasing the growth rate demonstrates that in adverse conditions, small pellets may develop (Figure 1B). Increasing the tip growth rate as well as the interval between branches results in a mycelial mat morphology (Figure 1C). The simulations are a good illustration of the large difference in morphology that can result when only a few parameters are adjusted. Moreover, improving upon the MATLAB model, parameters can be changed during the simulation, illustrating how an influx of nutrients, or a change in fermentation parameters can potentially affect morphology. Figure 2 provides a screenshot from a simulation run during which parameters were changed dynamically. The resulting pellet is dense on the inside, but with a more open outgrowth of external branches.

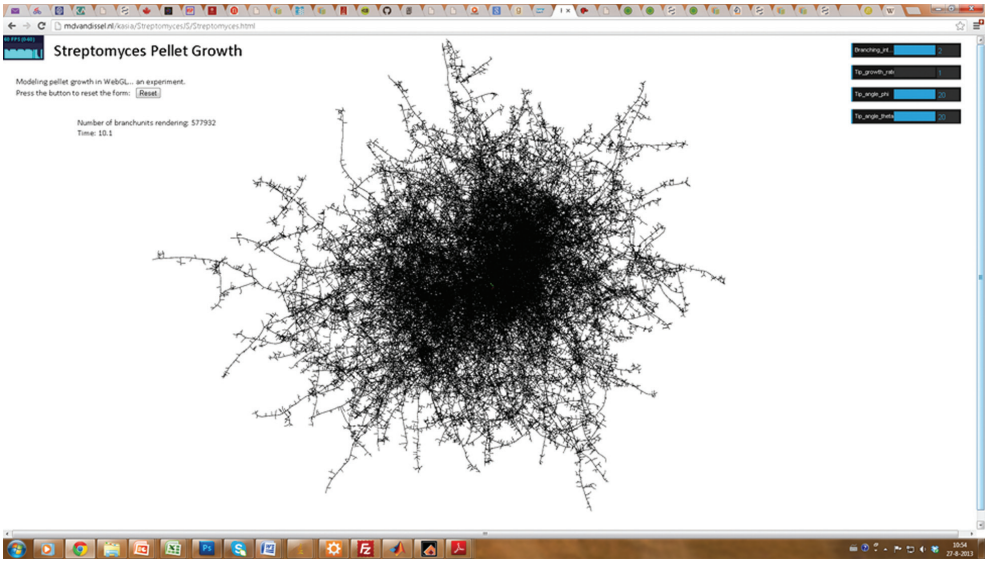

Figure 2. *Screenshot from simulation run, demonstrating the effect of parameter changes on morphology. An initially fast tip growth rate, and average branching interval resulted in rapid growth of the pellet. Branching interval was then decreased, resulting in larger distances between branches, and enabling extension of long branches outside of the pellet core. Near the end of the simulation, tip growth rate was set at a minimum, while branching interval was increased, resulting in short distances between the new branches emerging on the long outreaching hyphae.*

FUTURE PERSPECTIVES

At the moment the WebGL simulation is a simplified version of what was previously coded in and achieved with Matlab and PovRay. The basis, however, is there. With some additional steps, the code can be improved and extended to provide a more realistic and useful morphological simulation.

Firstly, it is necessary to implement the oxygen diffusion algorithms to model oxygen diffusion and consumption by the growing pellet. Solving equations in the browser is something that is now possible to achieve in WebGL by using the graphics processor to simultaneously solve sets of parallel equations (Janik 2012). This is currently only possible for sets of linear equations, but developers are working on creating non-linear equation solvers for the browser. Secondly, collision detection should be implemented to prevent hyphae from overlapping within the centre of the pellet. Because of the large interest in the use of WebGL to create 3D games in the browser, numerous algorithms exist to implement collision detection. Thirdly, it would be beneficial to implement a pellet render function once growth

has completed to model the lines as three dimensional objects. Since immediate modeling of the hyphae as three-dimensional cylinders or tubes is very taxing on the browser, lines were chosen to visually represent the mycelium and give a realistic approximation of the morphology, albeit only at lower zoom levels. With the help of a pellet render function, during zooming and morphological analysis of the pellet, a user would be able to better visualize and analyze the pellet packing and calculate the void fractions corresponding to various modeling scenarios.

As the web technology for in-browser modeling improves, the power and speed of the simulation will also increase, facilitating model expansion and improvement. Adding and implementing new experimental data from fermentation trials based on different strains and morphologies, as well as gene expression data relating to morphogenesis, such as the effect of ssgA overexpression (van Wezel, Krabben *et al.* 2006), will increase the biological relevance of the model and may lead to new insights. In the future, such a dynamic, easily-accessible, 3D-modeling approach may prove to be valuable for strain improvement, with modeling effectively a test-drive for the fermentation process to pre-assess the effect of variables on productivity (Celler *et al*. 2012). At present, it demonstrates the application of WebGL, a new web technology for three-dimensional modeling in the browser, for visualization and modeling of *Streptomyces* pellet growth. The tool can be used for teaching purposes to showcase the mathematical beauty and complexity of *Streptomyces sp.*, and the intricacies of branching growth and morphogenesis in liquid cultures.

Chapter 7

Functional Analysis of Novel Coiled-Coil Proteins in *Streptomyces coelicolor* and their Role in the Control of Growth and Morphogenesis

Katherine Celler, Joost Willemse and Gilles P. van Wezel

Manuscript in preparation.

ABSTRACT

In the morphologically complex streptomycetes, reproduction occurs via specialized aerial hyphae that produce chains of unigenomic spores, involving an unusually complex process of coordinated cell division and DNA segregation. Cytoskeletal elements play an important structural role in this process, and mutants of *Streptomyces coelicolor* lacking the cytoskeletal genes *filP*, *mreB* or *scy* show various defects in the integrity and shape of aerial hyphae and spores. Here we show that the tandem gene sets SCO2259-2260 and SCO3285-3286, which encode hitherto unstudied proteins containing coiled-coil motifs, play an important role in facilitating sporulation-specific cell division and morphogenesis. SCO2259 and SCO3285 localize in large evenly-spaced foci in young aerial hyphae, while SCO3286 forms long filaments inside immature spores. Scanning and transmission electron microscopy revealed aberrant and branching spore chains in SCO2259 and SCO3286 mutants, while SCO3285 mutants demonstrated chains with misaligned spores. Notably, null mutants lacking the flotillin-domain protein SCO3286 demonstrated enhanced frequency of spore chain formation, with many short and branching spore chains. Deletion of both SCO3286 and SCO3285 inhibited sporulation, with a small number of spores that were highly sensitive to heat treatment. Our results highlight the intricate role of cytoskeletal genes in the *Streptomyces* developmental program.

INTRODUCTION

For bacteria, maintaining the proper cell shape during growth and division is important for survival of progeny. Cytoskeletal elements play an important role in coordinating these processes, with actin-homologs MreB and Mbl working to maintain shape during growth of rod-shaped bacteria (Jones *et al.* 2001; Carballido-Lopez and Errington 2003; Kruse, *et al.* 2005), and tubulin-homolog FtsZ forming the scaffold for the contractile ring (the Z-ring) during cell fission (Bi and Lutkenhaus 1991). In addition, an abundance of coiled-coil rich proteins exists in other bacteria to enable a great diversity of cellular architectures - such as spiral (Specht *et al.* 2011), crescent (Ausmees *et al.* 2003), or filamentous (Bagchi *et al.* 2008). For a detailed account of the bacterial cytoskeleton, the reader is referred to Chapter 2 of this thesis.

Perhaps due to their complex morphogenesis and multicellular lifestyle, the streptomycetes are particularly rich in cytoskeletal and coiled-coil proteins proposed to be cytoskeletal in nature (Letek *et al*. 2012). In addition to MreB and Mbl (Mazza *et al.* 2006; Heichlinger *et al.* 2011), and FtsZ (McCormick *et al.* 1994; Schwedock *et al.* 1997), sequence analysis has identified more than ten putative coiled-coil cytoskeletal proteins encoded for in streptomycete genomes, most of which have yet to be characterized (Table 1).

Table 1. *Confirmed and putative cytoskeletal proteins in Streptomyces.*

Protein	Annotation[1]	Reference
SCO2082, FtsZ	Cell division protein; homolog of tubulin	(McCormick *et al.* 1994; Schwedock *et al.* 1997)
SCO2611, MreB	Rod-shape determining protein; homolog of actin	(Mazza *et al.* 2006)
SCO2451, Mbl	Rod-shape determining protein; homolog of actin	(Heichlinger *et al.* 2011)
SCO1407	Hypothetical protein	
SCO2259, ScyB	Multi-domain regulatory protein	
SCO2260, ScyC	Putative membrane protein	
SCO3285, ScyD	Large glycine/alanine-rich protein	
SCO3286, ScyE	Putative secreted protein	
SCO3542	Putative transferase	
SCO5396, FilP	Filament-forming protein	(Bagchi *et al.* 2008)
SCO5397, Scy	*Streptomyces* cytoskeletal element	(Walshaw *et al.* 2010; Holmes *et al*. 2013

[1] Annotations adapted from StrepDB, the Streptomyces Annotation Server (http://strepdb.streptomyces.org.uk/).

Proteins rich in coiled-coil motifs are capable of self-assembly into filaments *in vitro*, forming flexible filaments which are resistant to strain and have strong mechanical properties, necessary to maintain cell integrity (Herrmann and Aebi 2004).

Unlike rod-shaped bacteria, which grow by lateral cell-wall extension, *Streptomyces* hyphae grow apically, with new material deposited at hyphal tips. Critical for control of apical growth is coiled-coil protein DivIVA (Flärdh 2003; Flärdh 2010). DivIVA is a homolog of MinE, and in *Bacillus subtilis* controls the localization of the cell division inhibitors MinCD, contributing to septum positioning (Edwards and Errington 1997). That DivIVA orchestrates cell-wall synthesis in the streptomycetes suggests that its role has changed during evolution, along with the different mode of growth (Claessen *et al.*, *submitted*). Its depletion or overproduction results in aberrant branching and altered hyphal characteristics. In *M. tuberculosis*, interaction between DivIVA and penicillin-binding protein PBP3, supports the role of DivIVA as a polarity marker that recruits the cell-wall machinery during polarized growth (Mukherjee *et al.* 2009). Recent results show that DivIVA is part of a larger tip-organizing center in the streptomycetes, colocalizing with several other proteins and complexes. These include, among others, the coiled-coil rich cytoskeletal proteins FilP (Bagchi *et al.* 2008) and Scy (Walshaw *et al.* 2010), as well as the cell-wall remodeling protein SsgA (Noens *et al.* 2005).

Rich in coiled-coil domains, FilP is important for the stability of the hyphae and for correct DNA segregation (Bagchi *et al.* 2008; Fuchino *et al.* 2013). Atomic force microscopy (AFM) demonstrated that *filP*-deletion mutants have weaker hyphae than the wild-type strain. In vitro, FilP forms a cis-interconnected network, demonstrating the mechanistic basis for its control of rigidity (Fuchino *et al.* 2013). Encoded by a gene immediately upstream of *filP*, Streptomyces cytoskeletal protein Scy was recently proposed to control polarized growth in existing hyphal tips, as well as to promote new tip formation during branching (Holmes *et al.* 2013). Deletion of *scy* affects polarized growth and as a consequence also hyphal geometry, resulting in irregular hyphal width, short hyphal length and aberrant branching.

The cytoskeletal machinery also plays an important role in control of cell division. In most bacteria, the precise localization of the division septum at mid-cell involves the action of negative control systems such as the Min system, which prevents Z-ring assembly at the cell poles (Raskin and de Boer 1997; Marston *et al.* 1998) and nucleoid occlusion that prevents the formation of the Z-ring over non-segregated chromosomes (Wu and Errington 2004). FtsZ is the first to localize to the future division site, and subsequently initiates the recruitments of the other divisome proteins to construct the cell division Z-ring. Cell division in the streptomycetes occurs via a completely different mechanism, perhaps explained by

the lack of a mid-cell reference point in the multinucleoid hyphae. During growth of the vegetative mycelium, crosswalls form at irregular intervals to separate the syncytial cells into compartments. For more details on the mechanism of crosswall formation, the reader is referred to Chapter 4. Nutrient depletion then triggers the formation of the reproductive aerial myelium. During sporulation-specific cell division, FtsZ first forms long filaments in aerial hyphae, followed by focal points, and then ladders (Schwedock *et al.* 1997; Grantcharova *et al.* 2005; Willemse and van Wezel 2009). Eventually, following a complex process of coordinated cell division and DNA segregation (McCormick 2009; Jakimowicz and van Wezel 2012), cytokinesis results in the formation of long chains of unicellular spores.

Aerial septation in *Streptomyces coelicolor* was the first demonstrated case of positively-controlled cell division, with FtsZ recruited by the membrane-associated divisome component SsgB, and SsgB in turn recruited by SsgA (Willemse *et al.* 2011). SsgA and SsgB are members of the SsgA-like protein family (SALPs), which occur exclusively in the morphologically complex actinomycetes (Traag and van Wezel 2008). Ensuring the viability and integrity of these spores is critical for survival of progeny and it is little wonder that the cytoskeleton plays an important role in this respect. In fact, actin homologs MreB and Mbl, which support rod-shaped growth in *E. coli* and *B. subtilis* are essential for the integrity of the spore wall in *Streptomyces*. In addition, other members of the family of SsgA-like proteins (SsgC-G) function to control the build-up of septal peptidoglycan during sporulation and finally also its autolytic degradation during spore maturation (Noens *et al.* 2005).

Here we characterize two sets of novel cytoskeleton-related proteins in S. coelicolor, which we have termed Streptomyces cytoskeletal element ScyB (SCO2259) and ScyC (SCO2260) as well as ScyD (SCO3285) and ScyE (SCO3286), demonstrating their role in sporulation specific cell division.

RESULTS

As a first step towards the characterization of the genes with proposed, but as yet unknown, cytoskeletal functions (Table 1), cosmid-insertion mutants were obtained, and SsgA-, SsgB- and FtsZ-eGFP localization analyzed in the mutants. A basic analysis of membranes and cell wall, as well as live-dead staining analysis was performed using stains FM5-95, wheat germ agglutinate (WGA) and propidium iodide (PI) with SYTO 82, respectively. FM5-95 is an analog of FM4-64, which labels the plasma membrane, preferentially associating with membranes enriches in negatively charged phospholipids such as phosphatidylglycerol (PG) and cardiolipin (CL) (Sun and Margolin 1998; Pogliano *et al.* 1999; Grantcharova *et al*. 2003);

and WGA labels N-acetylglucosamine and N-acetylneuraminic acid (sialic acid) residues, which are found in newly-forming cell wall (Wright 1984; Schwedock *et al.* 1997). PI and SYTO 82 are routinely used in live-dead staining experiments (Fernandez and Sanchez 2001); PI is a non-cell-permeating nucleid acid stain which therefore stains dead cells and SYTO 82 is a green fluorescent stain which labels nucleic acids in all cells - both those with damaged and non-damaged membranes. Based on these initial experiments, we decided to focus on genes SCO2259, SCO2260 and SCO3285 and additionally SCO3286, which is co-transcribed with SCO3285, for further analysis; these mutants demonstrated promising phenotypes with increased FtsZ-ladder formation.

Using COILS, a program which identifies coiled-coils in protein sequences (Lupas, *et al.* 1991), the location and abundance of the coiled-coil motifs in the selected genes were determined (Figure 1). Domains predicted with more than 50% certainty are shown, and their size denoted by the bar length indicated.

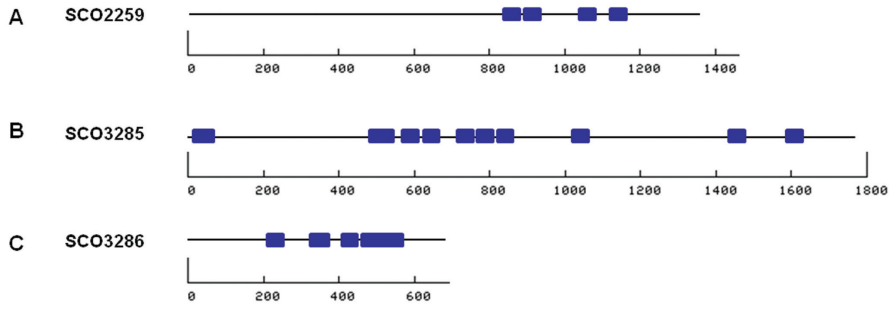

Figure 1. *Predicted coiled-coil domains in ScyB (SCO2259), ScyD (SCO3285) and ScyE (SCO3286). Location and size of motifs predicted with more than 50% certainty are indicated, based on output from the COILS Server from the ExPASy Bioinformatics Resource Portal (Lupas et al. 1991). ScyC (SCO2260) does not contain coiled-coil motifs.*

SCO2259 encodes for a large protein with one certain and several predicted coiled-coil domains. SCO2260 does not contain coiled-coil domains, but is potentially a site-2 protease (S2P) class of metalloproteases (MEROPS family M50) which cleaves transmembrane domains of substrate proteins, regulating intramembrane proteolysis of diverse signal transduction mechanisms. It may therefore have an influence on cellular differentiation and lipid metabolism, as prokaryotic S2P/M50 homologs have been shown to regulate stress responses, sporulation, cell division and differentiation (Marchler-Bauer *et al.* 2013). In *E. coli*, the S2P homolog RseP is involved in the sigmaE pathway of extracytoplasmic stress responses (Akiyama *et al*. 2004), and in *B. subtilis*, the S2P homolog SpoIVFB is involved

in the pro-σ^K pathway of spore formation (Lu *et al*. 1995). SCO3285 and SCO3286 show perfect co-occurrence, strongly suggesting a functional relationship, though they do not occur in all streptomycetes. The proteins encoded for by these genes are rich in coiled-coil domains. SCO3285 codes for a very large protein (>1700 amino acids in length), with a conserved ATPase domain which is putatively involved in DNA repair, while SCO3286 codes for a flottilin-domain protein. The genes have highly similar orthologues in *Pseudomonas* and other distant microbes.

Considering the coiled-coil domains of SCO2259, SCO3285 and SCO3286 and the role of the proteins in morphogenesis (see below), we tentatively designated them ScyB (SCO2259), ScyC (SCO2260), ScyD (SCO3285) and ScyE (SCO3286).

Transcriptional analysis by promoter probing

To roughly localize the promoters of the genes and assess their strength *in vivo*, we used the *redD* promoter-probe system (van Wezel *et al.* 2000c). For this purpose, DNA fragments containing the upstream region of all genes were cloned into promoter-probe vector pIJ2587, so as to place it in front of the promoterless *redD* gene. The resulting constructs were introduced in *S. coelicolor* A3(2) M512 (Floriano and Bibb 1996), which lacks the pathway-specific transcriptional activator genes *redD* and *actII-ORF4* for the biosynthesis of the pigmented antibiotics undecylprodigiosin and actinorhodin, respectively. Cloning of a DNA fragment with promoter activity in pIJ2587 allows transcription of *redD*, resulting in production of the red-pigmented and nondiffusible undecylprodigiosin (Red), which can easily be assessed visually or spectrophotometrically. Transformants were grown on R2YE plates supplemented with thiostrepton for 5 days. Production of the red-pigmented undecylprodigiosin (Red) was strongly stimulated by the *scyE* promoter and weakly by the *scyB* and *scyD* promoters (Figure 2). This indicates that all genes have their own promoter, although on the basis of gene organization we cannot rule out that *scyD* may be transcribed at least in part from P_{scyE}.

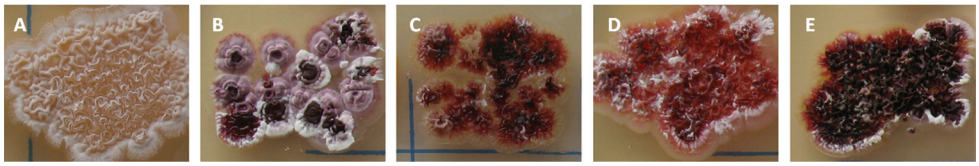

Figure 2. *Initial localization of promoters in the scyB, scyC, scyD and scyE upstream regions by promoter probing. S. coelicolor M512 harbouring (A) empty vector pIJ2587; (B) pGWS1111 (scyB upstream region); (C) pGWS1112 (scyC upstream region); (D) pGWS1113 (scyD upstream region); and (E) pGWS1114 (scyE upstream region). All upstream regions stimulated transcription of redD, as visualized by the red-pigmented patches of the respective transformants. Plates were grown on R2YE plates with thiostrepton as selective marker.*

Construction of in-frame deletion mutants

To construct in-frame deletion mutants, we replaced the entire coding region of each gene of interest by the apramycin cassette (*aacC4*) flanked by *loxP* sequences. For each experiment five transformants exhibiting the desired double-crossover phenotype ($Apra^R$ $Thio^S$) were selected and verified by PCR as described in the *Materials and Methods*. Following removal of the *aacC4* cassette by the Cre recombinase, deletion mutants were obtained for *scyB* (M145 ΔSCO2259), *scyD* (M145 ΔSCO3285) and *scyE* (M145 ΔSCO3286). In addition, the *scyDE* double mutant was constructed. Considering that the genes located downstream of gene pairs are divergently transcribed, polar effects due to insertional gene replacements were not anticipated.

Despite many attempts, we were unable to obtain an IFD double recombinant of SCO2260. A cryo-scanning electron microscopy (cryo-SEM) analysis of the cosmid insertion mutant did not reveal appreciable differences from the wild-type phenotype and the results described in this chapter therefore do not include this mutant. Further study is necessary to properly characterize this gene.

Characterization of the mutants

Mutants were plated on an SFM agar plates for 5 days at 30 ºC with the parental strain M145. The *scyD* null mutant had a lighter grey appearance than the parent, *scyB* and *scyE* mutants showed darker grey pigmentation, while the *scyDE* double mutant had a white appearance. The observed enhanced and reduced pigmentation likely indicates disturbance in the production of the grey-pigmented spores. The mutants did not show appreciable differences in development when grown on minimal medium agar plates supplemented with mannitol or on R2YE agar plates (not shown).

Fluorescence microscopy (FM) analysis revealed that, though similar in phenotype to wild-type, *scyB* and *scyE* null mutants produced branching spore chains and some aberrant spores (Figure 3A-E). Most spore chains of the *scyD* mutant had spores which were not completely aligned within chains, and spore chains occasionally branched. The most obvious phenotypic change, however, was observed in the *scyDE* double mutant, which sporulated far less abundantly than the parental strain M145. The few spore chains that were found had large spores (up to three to four times the length of wild-type spores) within spore chains of regular-sized spores. Box-plot statistical analysis indicated that, on average, spores of the *scyB*, *scyD* and *scyE* null mutants had a length similar to that of wild-type spores, with average lengths of 0.78 ± 0.07 µm, 0.85 ± 0.07 µm and 0.74 ± 0.12 µm, respectively, compared to a wild-type average length of 0.85 ± 0.11 µm, while the *scyDE*

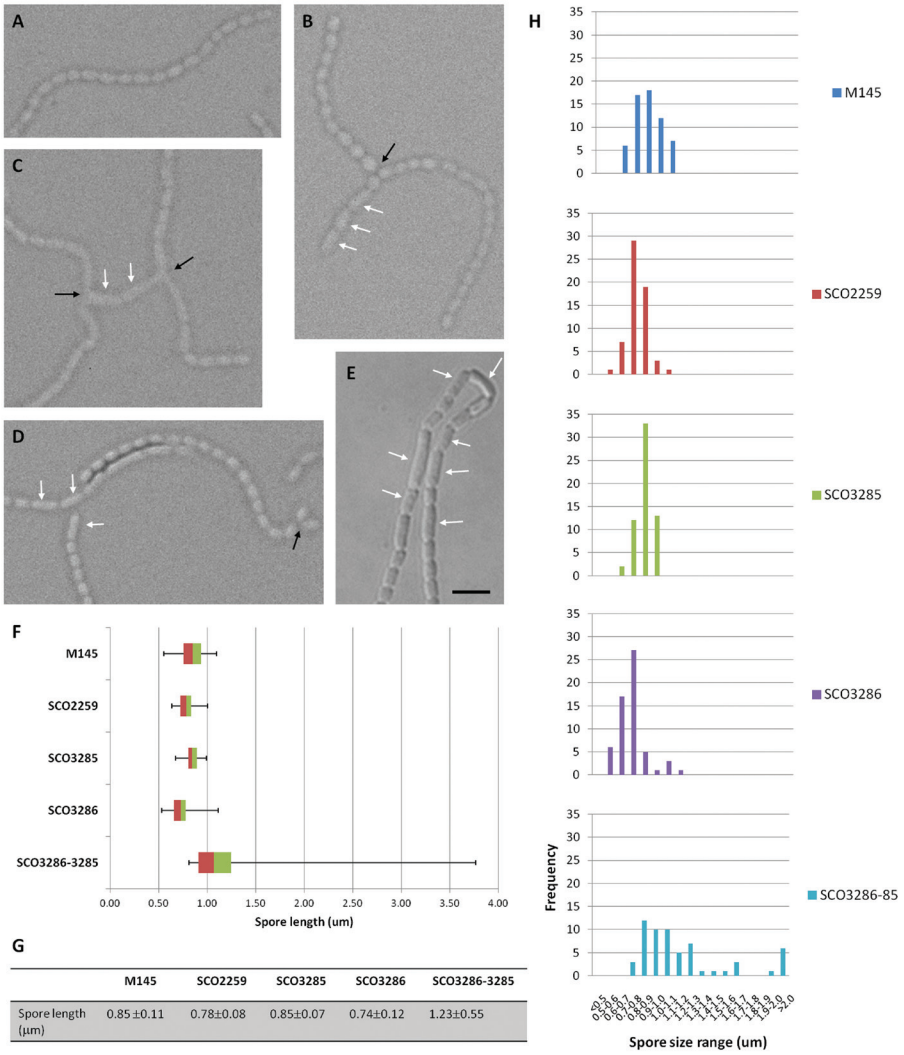

G

	M145	SCO2259	SCO3285	SCO3286	SCO3286-3285
Spore length (µm)	0.85±0.11	0.78±0.08	0.85±0.07	0.74±0.12	1.23±0.55

Figure 3. *Variation in spore size and chain length between mutants and wild type. Phase contrast micrographs of S. coelicolor M145 (parent; A) and its scyB (B), scyD (C), scyE (D) and scyDE null mutants. White arrows indicate aberrant spores in the deletion mutants, which appear to be delayed in formation and sometimes two or multiple times the size of wild type spores. Black arrows indicate branching spore chains. (F) Box plot of the spore length distribution in chains spores. Average spore length is given in (G). Spores of mutants scyB and scyE were on average slightly shorter, while spores of the scyDE double mutant were on average longer, sometimes up to two or three times the length of wild-type spores. Values are based on 60 spores measured by phase contrast microscopy. (H) Distributions of the spore lengths. Note that the size distribution of the scyDE double mutant is much broader than for the other strains. Scale bar, 2 µm, all images.*

double mutant had significantly larger spores, with greater variation, namely 1.23 ± 0.55 µm (Figure 3F). Distributions of the measurements indicate that the single mutants have narrow distributions, similar to that of the wild-type, while the double mutant *scyDE* has a very wide distribution, and irregular spore sizes. The large spores within the spore chains skew the distribution towards on average larger spore sizes than found in the wild-type strain.

Staining with FM5-95, WGA and DAPI was used to determine if the cell membrane, cell wall and DNA localization, respectively, was affected in the mutants (Figure 4). In particular, the *scyD* null mutant appeared different, with some membrane and wall material found at the external edges of forming spores. In the *scyDE* mutant, membrane and cell-wall staining within forming spore chains revealed that not all septa were at the same stage of completion. Staining with DAPI did not reveal significant differences in DNA segregation and condensation between mutants and the parental strain.

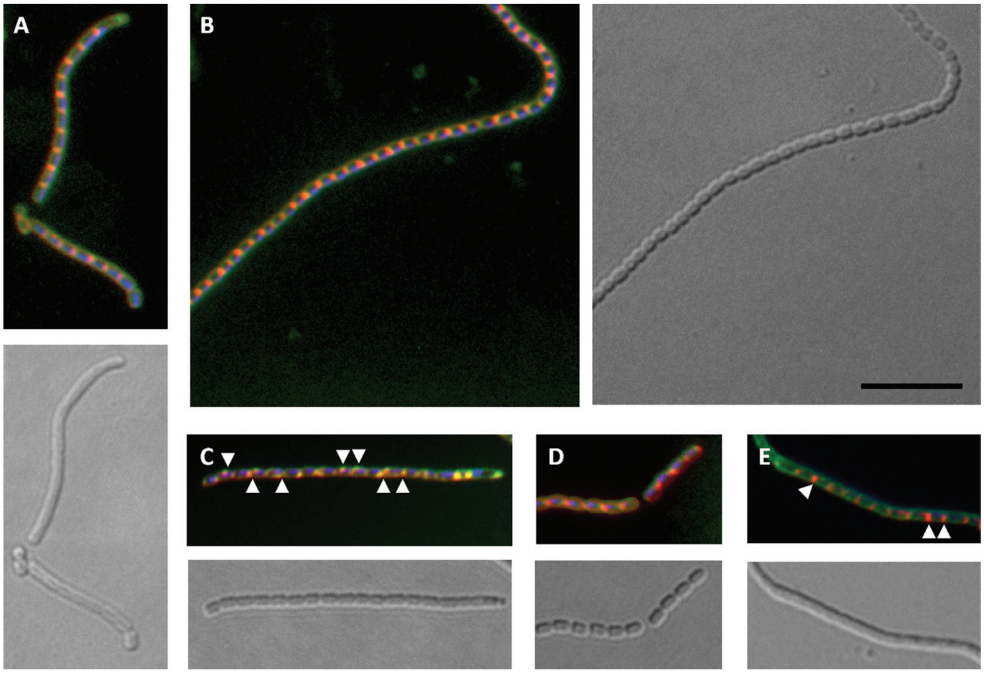

Figure 4. *Membrane (FM5-95; red), cell wall (WGA; green) and DNA (DAPI; blue) staining of sporogenic aerial hyphae of S. coelicolor M145 (parent; A) and its scyB (B), scyD (C), scyE (D) and scyDE mutants. Overlays of the three channels are shown, as well as a light image. The scyB mutant appeared similar to wild type. In scyD null mutants, some membrane and cell wall mislocalization was seen, with some staining of the edges of the spore exterior (arrows). The scyDE mutant showed enhanced membrane staining between spores within a chain (arrows), suggesting that spore maturation was at different stages of completion in those chains. Scale bar, 5 µm.*

Cryo-SEM revealed that *scyB* and *scyD* mutants develop similarly to the wild-type strain, although some spores were slightly irregular and not perfectly aligned within spore chains (Figure 5). The *scyE* null mutant was strongly affected in sporulation, however, with a multitude of short spore chains. Non-sporulating aerial hyphae were scarce, though all samples were grown for the same amount of time. In the *scyDE* double mutant spore chains were scarce. Those which were found appeared irregular, containing small and large spores.

Transmission electron microscopy (TEM) provided further detail of spore morphology (Figure 6). The *scyB* null mutant appeared most similar to wild-type, though branching spore chains were occasionally encountered (Figure 6B). The spore wall of the *scyD* null mutant appeared lighter than that of the wild type or of the other mutants (Figure 6C), but examining other micrographs indicated that this may be an artifact of fixation. TEM of the *scyE* mutant revealed that spores are slightly shorter and rounder (Figure 6D). The *scyDE* mutant occasionally produced larger spores, though most spore chains were regular (Figure 6E).

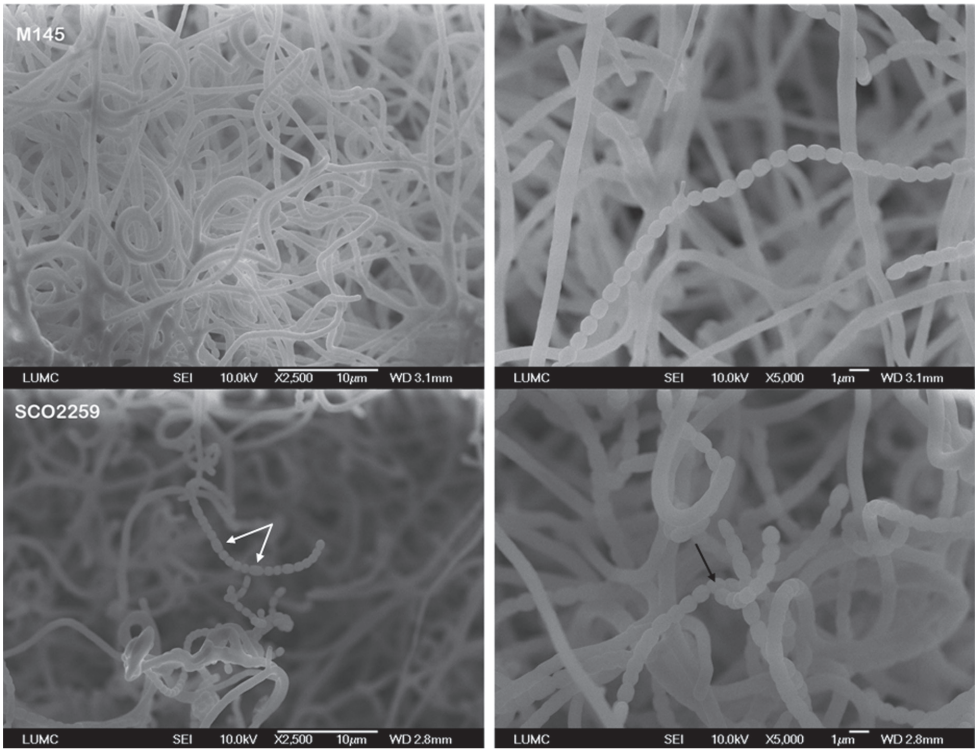

(Figure 5. continued on overleaf)

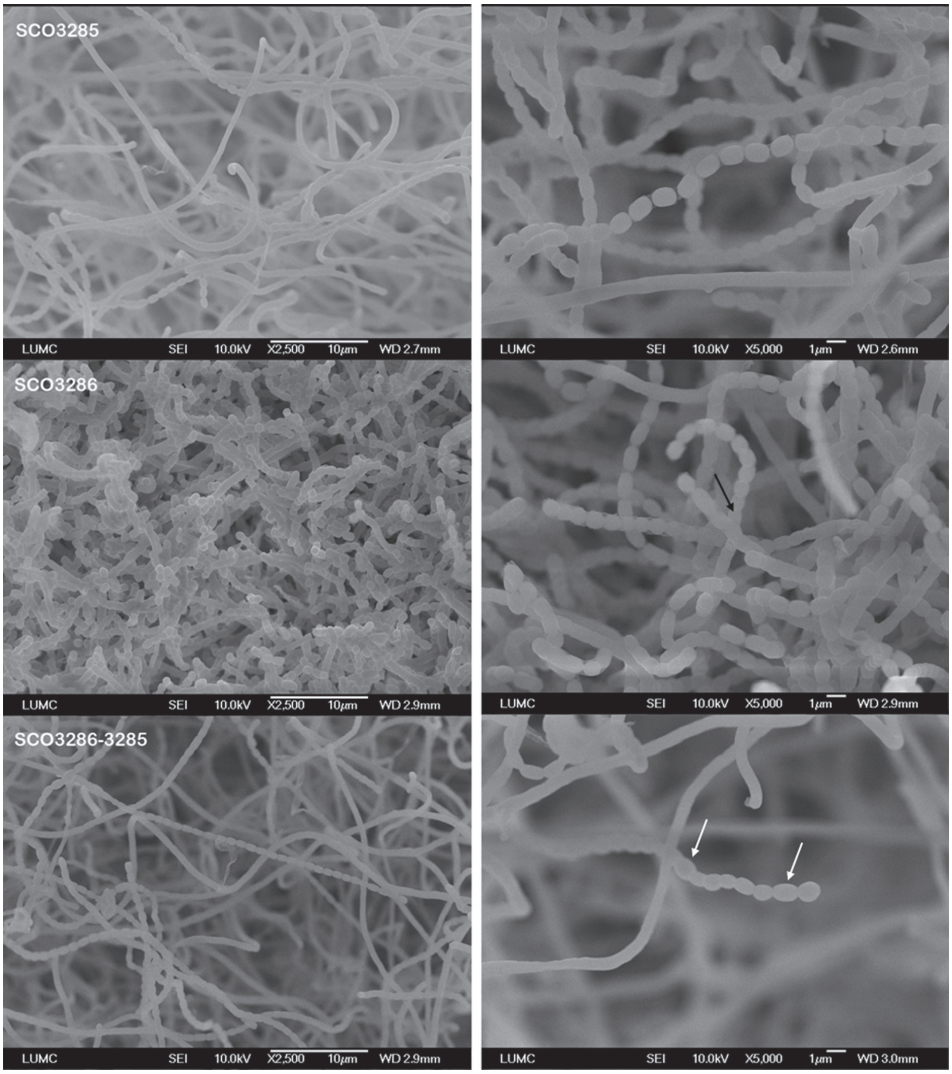

Figure 5. *Cryo-scanning electron micrographs of the scyB, scyD and scyE mutants and scyDE double mutant. The scyB mutant produced spores with up to twice the length of wild-type spores (white arrows), and branching spore chains (black arrow). The scyE mutant formed short spore chains, with certain spores appearing to branch (black arrow). The scyDE double mutant had few irregular spore chains (white arrows).*

Figure 6. *(Right) Transmission electron micrographs of the wild-type strain (A) and its scyB (B), scyD (C), scyE (D) and scyDE (E) null mutants. Black arrows indicate where spore chains appear to branch. The spore wall of the scyD null mutant was more electron-lucent than that of other samples, which is likely an artifact of fixation . Similar staining was seen in previous experiments for the wild-type strain. Spores of the scyE deletion mutant appear shorter and rounder than those of the wild type or the other mutants, while in the scyDE double mutant both longer (left) and normal (right) were found. Scale bar, 1 µm.*

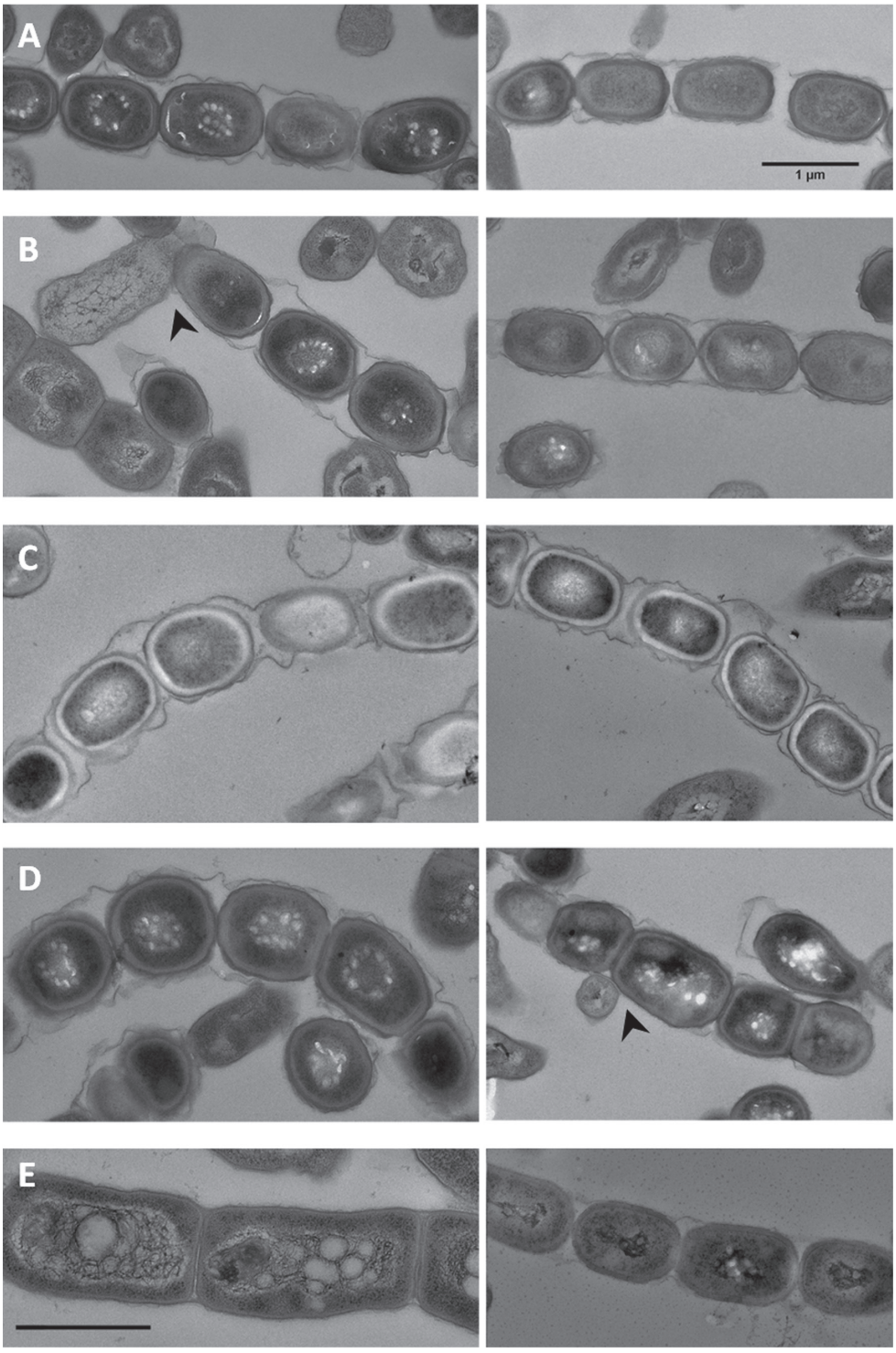
A
1 µm
B
C
D
E

To further investigate the effect of these mutations on sporulation and spore integrity, spore viability was determined by live-dead staining using PI and SYTO, and spores were tested for resistance to heat treatment and SDS buffer (see *Materials and Methods*). Wild-type spores are resistant to exposure at moderately high temperature as well as to treatment with SDS, which has, in fact, been reported to activate germination (Grund and Ensign 1982). In contrast, spores with compromised integrity show decreased survival rates upon heat and detergent treatment (Mazza *et al.* 2006; Willemse *et al.* 2012). Spores of the *scyB*, *scyD* and *scyE* null mutants were as viable in terms of colony forming units as those of the parental strain, but demonstrated decreased heat resistance (Figure 7). Treatment with SDS activated germination of these mutants, as in the wild-type (not shown). Only 75% of the untreated spores of the *scyDE* double mutant were viable, however, and these were very sensitive to heat and SDS. While 99% of wild-type spores were viable, and roughly 98% and 66% survived 10 or 20 minutes, respectively, of heat treatment, 10 minutes of heat treatment at 60 ºC was sufficient to kill all spores of the *scyDE* double mutant. Only roughly 60% of *scyDE* double mutant spores survived one hour of incubation at room temperature in 5% SDS.

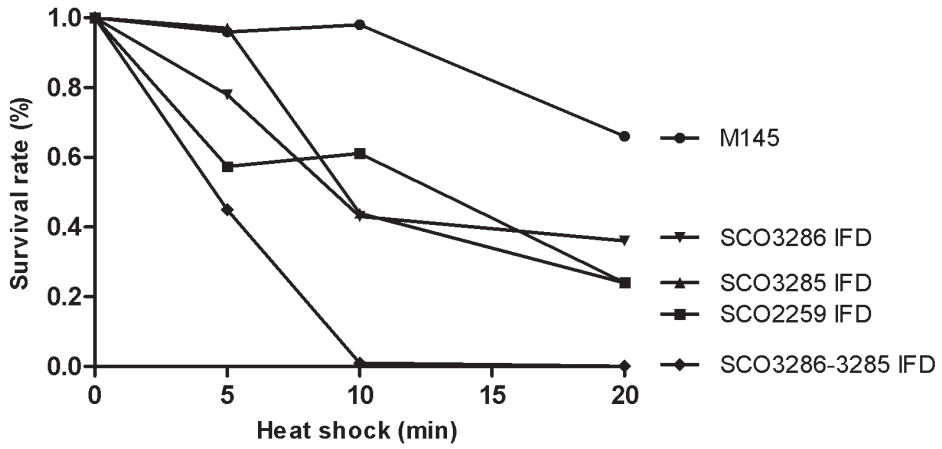

Figure 7. *Spore survival rate upon heat shock at 60 °C. The single deletion mutants show reduced resistance to treatment, compared to the wild-type, demonstrating affected spore integrity. In particular, the SCO3286-3285 (scyDE) double mutant was greatly affected, and no colony forming units remained after 10 minutes of heat treatment. IFD, in-frame deletion mutant.*

Protein localization and genetic complementation of mutants

To investigate the localization of the proteins, low copy-number vectors were constructed that harbor the respective genes and their upstream region followed by the gene for eGFP, so as to express C-terminal eGFP fusions from the natural promoters. In this way, plasmids pGWS1105 (for ScyB-eGFP), pGWS1106 (for ScyD-eGFP) and PGWS1107 (for ScyE-eGFP) were created, and introduced in the respective null mutants, as well as in the parental strain M145. Fluorescence microscopy indicated that ScyB-eGFP localized in large, sometimes somewhat oblong focal points along early aerial hyphae (Figure 8). With a similar pattern, ScyD-eGFP localized in large foci regularly positioned along aerial hyphae, appearing before the start of sporulation. ScyE-eGFP localized predominantly to the cell wall of aerial hyphae, at a somewhat later stage than ScyD, appearing before the completion of spore constriction. Portions of hyphae in which localization was observed demonstrated complete envelopment by filament-like structures. In an attempt to analyze the localization of ScyD and ScyE simultaneously, similar fusions as for eGFP were created using the red-fluorescent mCherry, but in this case the fluorescence of the chimeric proteins was too weak and the studies therefore not feasible.

The *scyB* and *scyE* null mutants could be fully restored to wild-type sporulation by the respective chimeric proteins, as shown by cryo-SEM (Figure 9). A light grey phenotype of the *scyD* null mutant containing pGWS1106 on plate (not shown) indicated a potential reduction of WhiE spore pigment; cryo-SEM, however, indicated the presence of spore chains similar to those of the wild-type (Figure 9). To see if complementation could be achieved with copies of the wild-type genes, constructs pGWS1108, pGWS1109 and pGWS1110 were created, which contain wild-type *scyB*, *scyD*, and *scyE* and upstream regions, respectively. Work is underway to assess if these constructs restore wild-type growth and development to the mutants.

Localization of FtsZ-eGFP in the mutants

Vector pFK41 (Grantcharova *et al.* 2005), which is an integrative vector that expresses FtsZ-eGFP from the *ftsZ* promoter region, was used to assess FtsZ localization in the mutants (Figure 10). While the parental strains showed typical spectacular Z-rings, aberrant Z-rings were observed in the mutants. In aerial hyphae of *scyB* and *scyE* mutants, ladders were evenly spaced, but not all were at the same stage of formation. Sometimes FtsZ localized partially at one side of a hyphae (red arrows in Figure 10), corresponding to the aberrant spore chains seen in SEM and TEM, in which not all spores within a chain were at the same stage of completion. In all mutants, upon spore formation, FtsZ localized to the spore wall

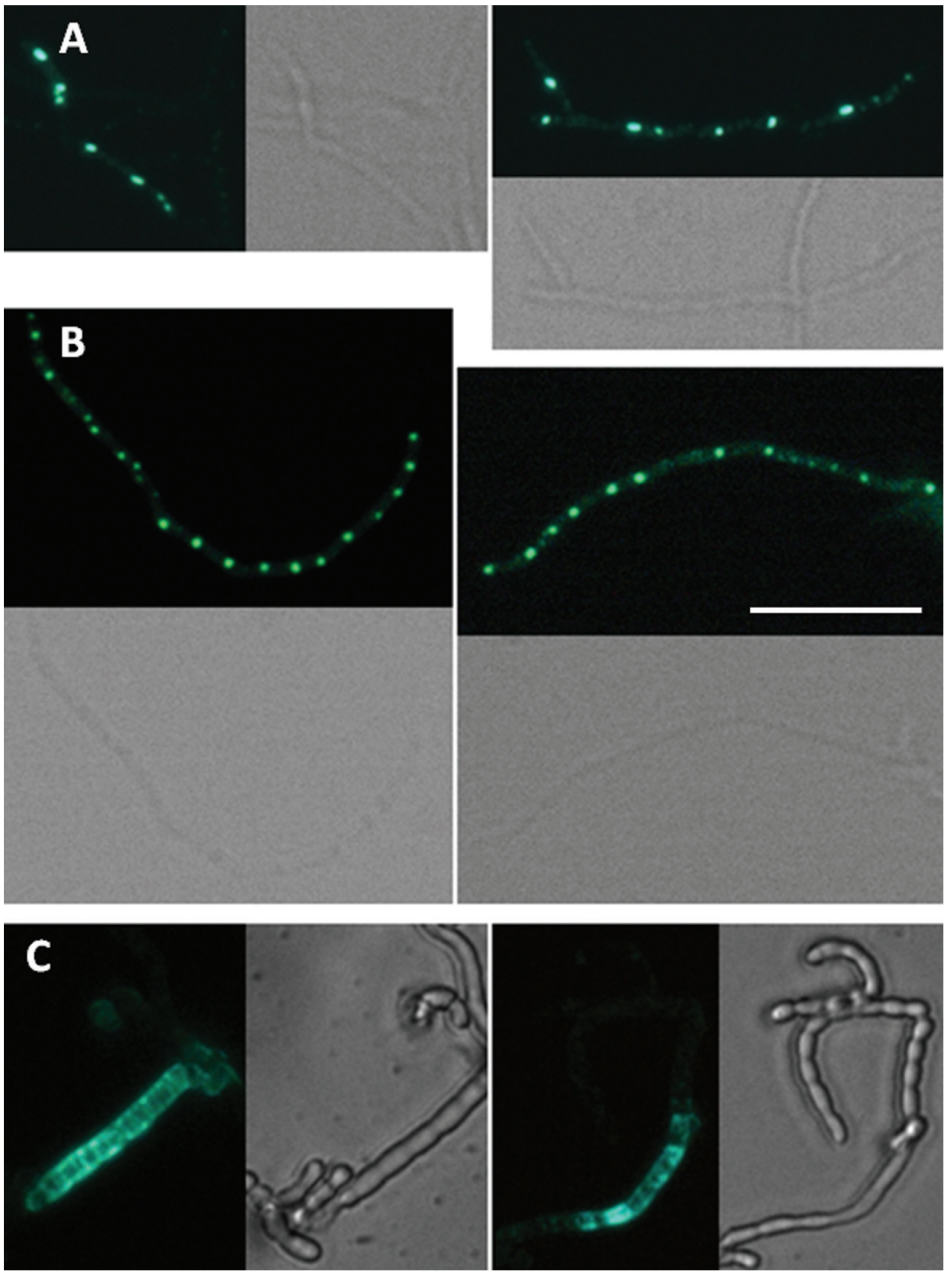

Figure 8. *Localization of ScyB and ScyD and ScyE. (A) In the scyB null mutant harboring pGWS1105, ScyB-eGFP localized in large (often oblong) foci in young aerial hyphae. (B) In the scyD null mutant harboring pGWS1106, ScyD-eGFP formed large foci at roughly 1 µm intervals. (C) In the scyE null mutant harboring pGWS1107, ScyE-eGFP formed filaments, which apparently enveloped the spores. Scale bar, 5 um, all images.*

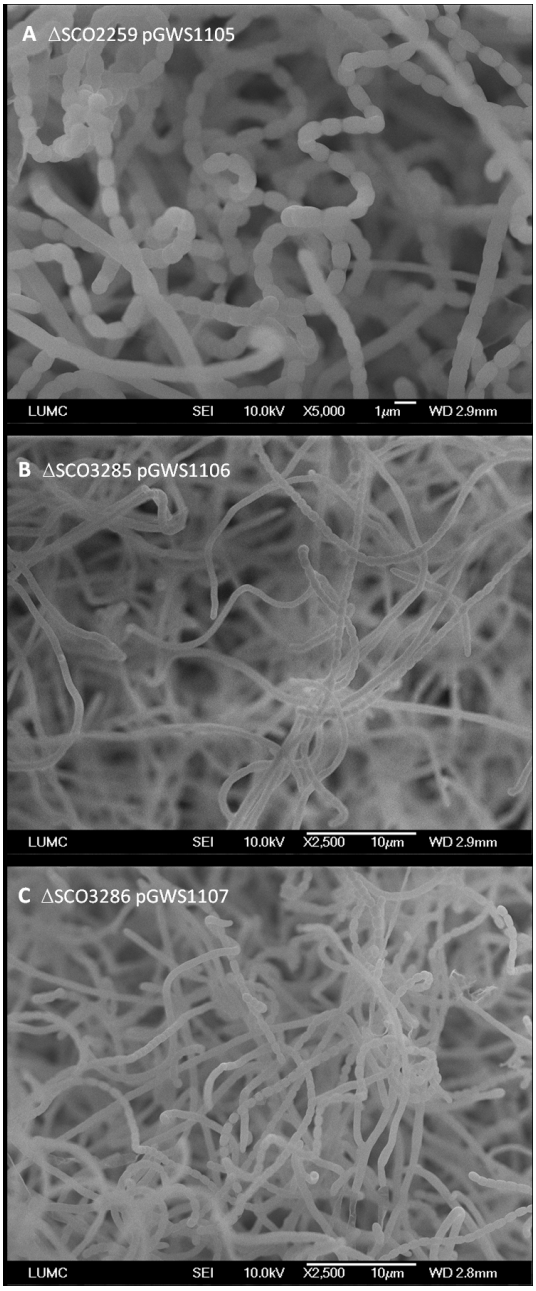

Figure 8. *Cryo-scanning electron micrographs of scyB (SCO2259) (A), scyD (SCO3285) (B), and scyE (SCO3286) (C) deletion mutants complemented with pGWS1105 (expressing ScyB-eGFP), pGWS1106 (expressing ScyD-eGFP) and pGWS1107 (expressing ScyE-eGFP), respectively. Mutants could be restored to wild-type sporulation by the respective chimeric proteins.*

(white arrows in Figure 10), which is not seen in wild type. In the *scyDE* double mutants, FtsZ localized diffusely, or formed filaments around aerial hyphae. Sometimes FtsZ ladders were seen, but these were irregular, seemingly occurring by change of the filamentous localization into more condensed localization. Again, when spores were formed, FtsZ localized to the spore wall.

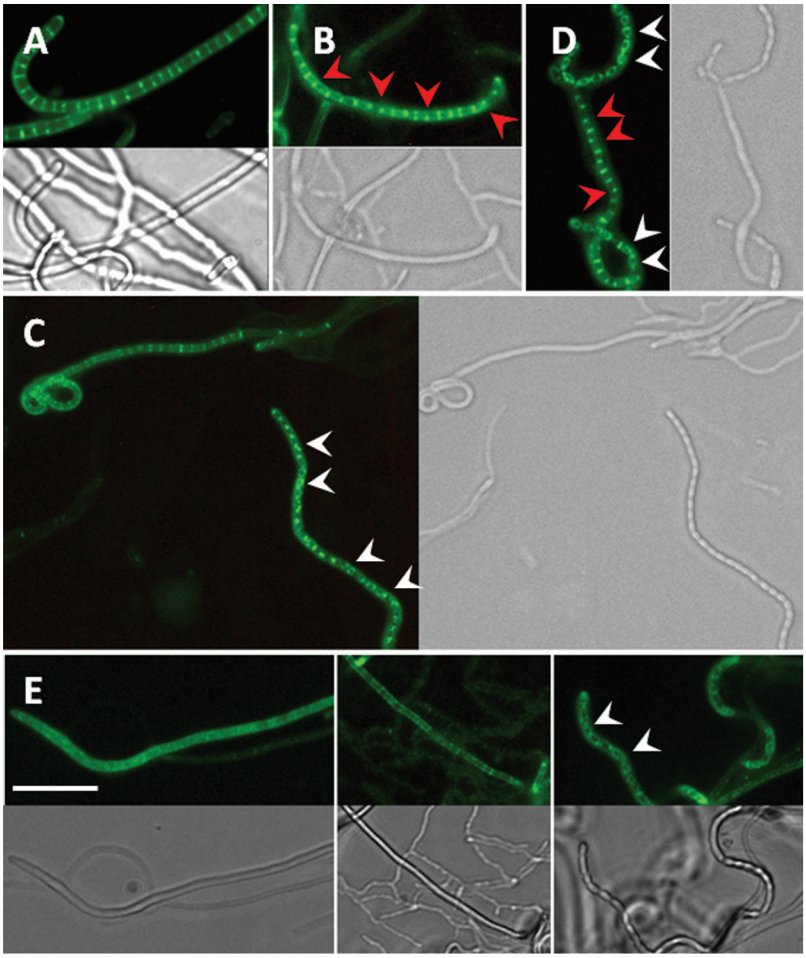

Figure 10. *Localization of FtsZ in the mutants. FtsZ-eGFP localization in (A) M145 pKF41, and its scyB (B), scyD (C), scyE (D) and scyDE null mutants. For the latter, three panels are presented showing FtsZ localization in young (left), pre-sporulation (middle) and sporulating (right) aerial hyphae. Partially formed FtsZ ladders indicated with red arrows; FtsZ localization to the spore wall indicated with white arrows. Scale bar, 5 µm, all images.*

DISCUSSION

Multiple cell division during sporulation of streptomycetes requires the coordination of septum-site localization and cell division with DNA replication and segregation (Flärdh and Buttner 2009; Jakimowicz and van Wezel 2012). This complicated process involves synchronized chromosome segregation and condensation by ParA and ParB (Ruban-Ośmiałowska, *et al.* 2006), as well as activation of sporulation-specific cell division by SsgA and SsgB (Willemse *et al.* 2011). In addition, the *whi* genes, so called because of the lack of pigmentation of the mutant colonies (Chater 1972), ensure the correct timing of developmental FtsZ production (Willemse *et al*. 2012). Ultimately, the process of division culminates in the formation of spectacular FtsZ-ladders and subsequently the division of aerial hyphae into unigenomic spores. Yet even if all the above morphological checkpoints are correctly passed, if spore integrity cannot be ensured, neither can the survival of progeny. Multiple cytoskeletal elements play a role at this point of the lifecyle, working to ensure that spores are resistant to desiccation and mechanical stress, able to lie dormant for years before germinating again in favorable conditions.

Structural support in cells is often provided by proteins with coiled-coil motifs, which are capable of self-assembly into filaments *in vitro*, forming a strong, yet flexible, mechanical basis for maintaining cell integrity. It is perhaps little wonder, given the complexity of the *Streptomyces* development program, that streptomycete genomes encode for numerous coiled-coil proteins, most with as yet unknown function. Those characterized (DivIVA, FilP and Scy) function during hyphal growth, ensuring strength of extending apical tips and forming part of a larger tip-organizing complex in *Streptomyces* (Flärdh 2010; Fuchino *et al.* 2013; Holmes *et al.* 2013). During development, several other cytoskeletal elements come in to play. Actin-homologs MreB and Mbl, which in rod-shaped bacteria are essential to maintain shape during growth, are not essential for vegetative growth in *Streptomyces coelicolor*, but rather for spore integrity (Mazza *et al.* 2006; Heichlinger *et al.* 2011), while the SsgA-like proteins SsgC-G are essential for the build-up and degradation of septal peptidoglycan (Noens *et al.* 2005). Mutations in these genes result in aberrant spore formation.

Here we show that coiled-coil rich proteins ScyB, ScyD and ScyE play an important role during spore formation in *Streptomyces* reproductive cell division. Deletion of *scyB* resulted in minor defects in sporulation; some uneven spore chain formation, and occasional large or branching spores. Containing one, and possibly more (up to four) coiled-coil domains, it is likely that this protein provides structural support during sporulation, while perhaps carrying out additional functions with its N-terminal domain. Deletion of *scyD* affected

deposition of new cell-wall material during sporulation. New wall material did not localize evenly to spore ends, and as a result, spore chains of *scyD* null mutants did not align correctly (end-to-end) within spore chains, but rather formed zig-zagging chains. Nevertheless, chromosome segregation and septation occurred synchronously, and spore viability was not compromised in the mutant. A major phenotypic difference was seen upon deletion of *scyE*, which encodes a flotillin homolog; null mutants showed dramatically enhanced sporulation, seen most clearly in TEM micrographs, and the creation of multiple spore chains of small, round spores. Flotillins are a divergent membrane protein family associated with lipid rafts in eukaryotes and characterized by the SPFH (Stomatin, Prohibitin, Flotillin and HflK/C) domain of unknown function and extended heptad repeat regions (Hinderhofer *et al*. 2009). A study on dynamin and flotillin homologues in *B. subtilis* demonstrated that dynamin orthologue DynA plays a role in cell division, colocalizing with FtsZ and affecting Z-ring formation, while flotillin seems to generate a local environment favoring membrane curvature and perhaps help to recruit cell division proteins to the division site (Dempwolff *et al.* 2012). Interestingly, almost perfect co-occurrence could be seen between ScyE and another flottilin-domain protein in *Streptomyces*, SCO3607 (STRING, database of known and predicted protein interactions, www.string-db.org). When SCO3607 was disturbed in *Streptomyces albus*, enhanced sporulation was observed (our unpublished results), suggesting that flotillin lipid-raft markers perhaps create regions where division is preferred, preventing its occurrence elsewhere. Absence of these domains results in accelerated spore maturation, abundance of cell division events and over-sporulation.

Interestingly, the simultaneous deletion of *scyDE* resulted in a white phenotype, explained by a dramatic decrease in cell division. It is therefore likely that these genes work in concert to enable the onset of reproductive cell division. In their absence, division still occurs, but much less frequently, and spores are often two, three or even four times the length of wild-type spores - though then with the requisite number or chromosomes, indicating that chromosome replication and segregation is not disturbed.

Localization of ScyB, ScyD and ScyE was performed using a low copy-number vector harboring each gene and its upstream region followed by the gene for eGFP, so as to express C-terminal eGFP fusions from the natural promoters. ScyB-eGFP localized in localized in large, sometimes somewhat oblong focal points along early aerial hyphae. With a similar pattern, ScyD-eGFP localized in bright fluorescent foci at roughly 1 µm intervals in early aerial hyphae, while the ScyE-eGFP fluorescent fusion localized to forming spore chains, enveloping them in filament-like structures.

Attempts at colocalization of proteins using mCherry fusions were not successful, due

to the low fluorescence. Work is underway to localize the combination of genes behind the strong *scyE* promoter and with an mCherry fusion at the C-terminus. Other technologies include immunoelectron microscopy for localization studies, and FRET-FLIM for in vivo colocalization and interaction studies. This should aid us in gaining further insight into the function and localization of the proteins and their interaction partners.

Summarizing, our work demonstrates that the coiled-coil proteins ScyB, ScyD and ScyE play a role in controlling morphogenesis, and in particular ensure correct sporulation-specific cell division. At this stage, it is yet unclear how they exert their functions. Considering that the proteins contain hallmarks of cytoskeletal proteins, such as the presence of coiled-coil domains and the effect of gene disruption on the integrity of the hyphae, we anticipate that they play a cytostructural role during the later stages of development. It is important to note that ScyD and ScyE are widespread in bacteria, including many that do not sporulate (such as Pseudomonas), strongly suggesting that they have a conserved function in the bacterial cell cycle that likely extends beyond the control of sporulation. Further studies should shed more light on whether indeed they form IF-like cytostructural elements, what their interactions partners are and how precisely they contribute to the control of morphogenesis in *Streptomyces*.

MATERIALS AND METHODS

Bacterial strains and media

The bacterial strains described in this work are listed in Table 2. *E. coli* K-12 strains JM109 (Sambrook *et al.* 1989) and ET12567 (MacNeil *et al.* 1992) were used for plasmid propagation, and were grown and transformed by standard procedures (Sambrook *et al.* 1989). *Streptomyces coelicolor* A3(2) was the parent for all mutant strains described in this work. All media and routine *Streptomyces* techniques are described in the *Streptomyces* manual (Kieser *et al.* 2000). Soy Flour Mannitol (SFM) medium was used for making spore suspensions and R2YE agar plates for regenerating protoplasts and, after the addition of appropriate antibiotic, for selecting recombinants. Phenotypic characterization of mutants was done on SFM, R2YE and on minimal medium agar plates with mannitol (MMman) as the sole carbon source (Kieser *et al.* 2000). For fluorescence microscopy, samples from liquid cultures were spotted onto a glass microscope slide before microscopy analysis. Images of vegetative hyphae from solid growth samples were collected from samples that had been inoculated at the acute-angle junction of coverslips inserted at a 30° angle in SFM agar plates.

Table 2. *Bacterial strains used in this study.*

Bacterial Strain	Genotype	Reference
S. coelicolor A3(2), M145	SCP1$^-$ SCP2$^-$	(Kieser *et al.* 2000)
S. coelicolor M512	M145 Δ*redD*Δ*actII-ORF4*	(Floriano *et al.* 1996)
	M145 SCO2259::*Tn5062, Apr*^{R}	This work.
	M145 SCO2260::*Tn5062, Apr*^{R}	This work.
	M145 SCO3285::*Tn5062, Apr*^{R}	This work.
	M145 ΔSCO2259	This work.
	M145 ΔSCO3285	This work.
	M145 ΔSCO3286	This work.
	M145 ΔSCO3286-3285	This work.
E. coli JM109	See reference.	(Sambrook *et al.* 1989)
E. coli ET12567	See reference.	(MacNeil *et al.* 1992)

Plasmids, constructs and oligonucleotides

All plasmids and constructs are summarized in Table 3. The shuttle vectors pHJL401 (Larson and Hershberger 1986) and pSET152 (Bierman *et al.* 1992) were used for cloning in *Streptomyces*, which both have the pUC ori for high-copy number replication in *E. coli* and the SCP2* ori on pHJL401 (around five copies per chromosome) and the *attp* sequence, allowing

integration at the attachment site of bacteriophage φC31, on pSET152 for maintenance in *S. coelicolor*. PCRs were done with Pfu polymerase (Stratagene), in the presence of 10% (v/v) DMSO. The oligonucleotides are listed in Table S1.

Insertion mutants were made using the Tn5062 transposon single-gene insertion knock-out cosmids (Fernandez-Martinez *et al.* 2011). For insertional inactivation of genes, transposon single-gene insert knock-out cosmids were used. For this, *E. coli* ET12567 containing puZ8002 was used for conjugation-mediated introduction of the relevant cosmids into pre-germinated spores of *S. coelicolor* M145. SCO2259 was removed by replacement with a recombinant cosmid harboring transposant 1G2.2.A05, SCO2260 by 1G2.2.C08, and SCO3285 by E39.2.C08.

The strategy for creating in-frame knock-out mutants is based on the unstable multi-copy vector pWHM3 (Vara *et al.* 1989). For each knock-out construct, roughly 1.5 kb of up- and downstream region of the respective genes were amplified by PCR from *S. coelicolor* genomic DNA and inserted into the instable multi-copy shuttle vector pWHM3 as described (van Wezel *et al.* 2005). For the exact location of the oligonucleotides, see Table S1. Fragments were inserted into pWHM3, and the engineered XbaI site was used for insertion of the apramycin resistance cassette *aacC4* flanked by *loxP* sites between the upstream and downstream flanking regions. The presence of the *loxP* recognition sites allows the efficient removal of the apramycin resistance cassette following the introduction of a plasmid pUWLcre expressing the Cre recombinase. We constructed the knock-out plamids pGWS1101, pGWS1102 and pGWS1103 for the single gene replacement of SCO2259, SCO3285 and SCO3286, respectively. Plasmid pGWS1104 was used for the double replacement of SCO3286-3285. To analyze correctness of the mutants, PCRs were done on mycelium from liquid-grown cultures, with oligonucleotide pairs as given in Table S1.

Table 3. *Plasmids and constructs*

Plasmid	Description	Reference
pHJL401	*Streptomyces/E.coli* shuttle vector (5-10 and roughly 100 copies per genome, respectively)	(Larson and Hershberger 1986)
pSET152	*Streptomyces/E. coli* shuttle vector (integrative in *Streptomyces*, high copy number in *E. coli*)	(Bierman *et al*. 1992)
pWHM3	Cloning vector, *colE1* replicos, psG4 replicon, Tsr^R, Amp^R	(Vara *et al*. 1989)
pUWLcre	pUWLoriT derivative with *cre(a)* gene under *ermE** promoter	(Fedoryshyn *et al.* 2008)
pIJ2587	Promoter probe vector containing promoterless *redD* gene	(van Wezel *et al.* 2000c)
pKF41	pSET152-derived integrative vector expressing FtsZ-eGFP	(Grantcharova *et al.* 2005)
pGWS1101	pWHM3 containing flanking regions of *S. coelicolor* SCO2259 with *apraloxP_*	This work.
pGWS1102	pWHM3 containing flanking regions of *S. coelicolor* SCO3285 with *apraloxP_*	This work.
pGWS1103	pWHM3 containing flanking regions of *S. coelicolor* SCO3286 with *apraloxP_*	This work.
pGWS1104	pWHM3 containing left-flanking regions of *S. coelicolor* SCO3286 and right-flanking regions of with *S. coelicolor* SCO3285 *apraloxP_*	This work.
pGWS1105	pHJL401 harboring SCO2259 behind its own promoter and fused to eGFP	This work.
pGWS1106	pHJL401 harboring SCO3285 behind its own promoter and fused to eGFP	This work.
pGWS1107	pHJL401 harboring SCO3286 behind its own promoter and fused to eGFP	This work.
pGWS1108	pHJL401 harboring SCO2259 behind its own promoter	This work.
pGWS1109	pHJL401 harboring SCO3285 behind its own promoter	This work.
pGWS1110	pHJL401 harboring SCO3286 behind its own promoter	This work.
pGWS1111	pIJ2587 with SCO2259 promoter region (−587/+707 relative to the start of SCO2259)	This work.
pGWS1112	pIJ2587 with SCO2260 promoter region (−566/+658 relative to the start of SCO2260)	This work.
pGWS1113	pIJ2587 with SCO3285 promoter region (−300/+212 relative to the start of SCO3285)	This work.
pGWS1114	pIJ2587 with SCO3286 promoter region (−300/+763 relative to the start of SCO3286)	This work.

Heat and SDS sensitivity tests

To determine heat resistance of spores, spore suspensions were diluted to 10^4 spores/mL in 20% glycerol and incubated at 60 ºC for 5, 10 and 20 minutes. To test SDS sensitivity, SDS (5% w/v end concentration) or water (control) was added to spore suspensions and incubated at room temperature for 1 hr. After heat or SDS treatment, the suspensions were diluted and plated on SFM agar, followed by incubation for 2 days at 30 ºC. Survival rate was calculated as the ratio of colony forming units (cfu) with and without heat or SDS treatment.

Microscopy

Electron microscopy

For morphological studies of surface-grown aerial hyphae and spores of *S. coelicolor* M145 and its mutant derivatives by cryo-scanning electron (cryo-SEM), specimens were quickly frozen in liquid nitrogen slush and transferred directly to the cryo-transfer attachment of the microscope. Specimens were subsequently sputter-coated with a 2 nm layer of gold and examined using a JEOL JSM6700F scanning electron microscope.

Samples for the analysis of cross-sections of hyphae and spores via transmission electron microscopy (TEM) were prepared as follows. Slices of mycelium were cut from agar plates and placed in a fixative containing 1.5% (wt/vol) glutaraldehyde in 0.1 M cacodylate buffer (pH 7.4; 360 mosmol) at room temperature for 20 h. Post-fixation was performed in 1% (wt/vol) osmium tetroxide in phosphate buffer (pH 7.3; 330 mosmol) at room temperature for 2 h. After rinsing, samples were dehydrated in a graded series of ethanol, and then incubated in a graded series of epoxy resin LX-112 (Ladd Research Industries, Burlington, Vt.) in propylene oxide. The sample blocks were then placed in capsules filled with epoxy resin and polymerized at 60°C for 72 h. Ultrathin sections (70 nm) were cut on an ultramicrotome (Reichert OM U3), collected on copper grids, stained with uranyl acetate and lead hydroxide, and examined in a Philips EM410 transmission electron microscope.

Fluorescence microscopy

Fluorescence and corresponding light micrographs were obtained with a Zeiss Axioscope A1 upright fluorescence microscope (with an Axiocam Mrc5 camera at a resolution of 37.5 nm/pixel), with, for the green channel, 470- to 490-nm excitation and 515 long-pass detection; and for the red channel, 530- to 550-nm excitation and 590 long-pass detection. The green fluorescent images were created using 470/40-nm bandpass excitation and 525/50 bandpass detection; for the red channel, 550/25-nm bandpass excitation and 605/70 bandpass detection were used. For staining of the cell wall (peptidoglycan), we used TRITC-

WGA; for membrane staining, we used FM5-95 (both obtained from Molecular Probes). All images were background-corrected, setting the signal outside the hyphae to 0 to obtain a sufficiently dark background. These corrections were made using Adobe Photoshop CS5.

Computer analyses

DNA and protein databank searches were performed using the BLAST server of the National Center for Biotechnology Information at the National Institute of Health, Bethesda, MD, USA (http://www.ncbi.nlm.nih.gov) and the *S. coelicolor* genome page services (http://strepdb.streptomyces.org.uk/). Protein interactions were determined using the STRING database of known and predicted protein interactions (www.string-db.org).

Supplemental Material

Table S1. *Oligonucleotides used in this study.*

Name	5'-3' sequence	Purpose and restriction sites
2259_LF-1500	gtcagaattcggccgccgccctgctgccggacagc	Cloning, EcoRI
2259_LR+9	gtcagaagttatccatcacctctagagccggtcacgggggttttgtcc	Cloning, XbaI
2259_RF-9	gtcagaagttatcgcgcatctctagactcgtctgacgcctgccacacg	Cloning, XbaI
2259_RR+1500	gtcaaagcttcgccgacgagctgctggagcggttc	Cloning, HindIII
2260_LF-1169	gtcagaattctcagcggcggatgccgtgtcgt	Cloning, EcoRI
2260_LR+9	gtcagaagttatccatcacctctagaggtggacatggaactccctg	Cloning, XbaI
2260_RF-9	gtcagaagttatcgcgcatctctagaggcggatgaggccgctcagc	Cloning, XbaI
2260_RR+1500	gtcaaagcttgccagcaccgtcgcacccgcccgg	Cloning, HindIII
3285_LF-1500	gtcagaattcagcacgtgcgcaccaatgaggcgc	Cloning, EcoRI
3285_LR+9	gtcagaagttatccatcacctctagaggtggccatgagcggttcg	Cloning, XbaI
3285_RF-9	gtcagaagttatcgcgcatctctagagagcggtgagcgcggggccg	Cloning, XbaI
3285_RR+1500	gtcaaagcttggcgacagccgtccgctccccttcc	Cloning, HindIII
3286_LF-1500	gtcagaattctaggaggggccacgacccggtag	Cloning, EcoRI
3286_LR+9	gtcagaagttatccatcacctctagagacttccatggcatacgtcc	Cloning, XbaI
3286_RF-9	gtcagaagttatcgcgcatctctagaagggtctgaccggccatcacc	Cloning, XbaI
3286_RR+1500	gtcaaagcttcaggaggcggcgagcgcccggtag	Cloning, HindIII
2259_IFD_fw_+263	tgctcggcgaagccggtccaggt	PCR confirmation
2259_IFD_rev_-260	tcctggtgctgatgccgttgcag	PCR confirmation
2260_IFD_fw_+653	agggcttcgaagtgccgggtctc	PCR confirmation
2260_IFD_rev_-646	ccggcaagctcgtcgtcgactgc	PCR confirmation
3285_IFD_fw_+240	acgtgcagaacctgacggtctcg	PCR confirmation
3285_IFD_rev_-470	agcacgtcgcggactggacgctg	PCR confirmation
3286_IFD_fw_+541	tgcatcgaccgatccgaccagtg	PCR confirmation
3286_IFD_rev_-500	agcggtgcaggtccgcgaactcc	PCR confirmation
p2259_fw_eco_new	gtcagaattcgccgtgcacacgacggcgaacag	2259 own promoter, EcoRI
SCO2259SacI-rev	cacggtaccggcgcggttgagctccccggc	2259 pt 1 rv, KpnI, SacI
2259_pt.2_fw_Eco	gtcagaattctccacgcggagctgctcagc	2259 pt 2 fw, EcoRI
SCO2259MluI-rev	gccggtaccctgccacgcgtccagctcc	2259 pt 2 rv, KpnI, MluI
SCO2259MluI-fw	cgctctagagctggacgcgtggcagaaccc	2259 pt 3 fw, XbaI, MluI
2259_comp_rv_Hind_Bam	gtcaaagcttggatcctcagacgagggcgacggcctcc	2259 pt 3 rv (+Stop), HindIII, BamHI
2259_rev_XbaHind	aagctttctagagacgagggcgacggcctcctgc	2259 pt 3 rv GFP fusion, HindIII, XbaI
p2260_fw_eco_new	gtcagaattcagcgcgtcgtcgagcacgac	2260 own promoter, EcoRI
2260_comp_rv_Hind_Bam	gtcaaagcttggatcctcatccgcccggcgtgcacagc	2260 rv (+Stop), HindIII, BamHI
2260_rev_XbaHind_new	gtcaaagctttctagatccgcccggcgtgcacagcgg	2260 rv GFP fusion, HindIII, XbaI
3285_comp_fw_EcoRI	gtcagaattcacggctcgtcgagcttcaccgacg	3285 own promoter, EcoRI

3285_p1rv_BglII	aagcttagcgcgtcgtagatctcggtcc	3285 pt 1 rv, HindIII, BglII
3285_pt2fw_BglII	gaattccggaccgagatctacgacgcgct	3285 pt 2 fw, EcoRI, BglII
3285_p2_rev_PstI	aagcttgaactcgtcgaggcgcagctgcag	3285 pt 2 rv, HindIII, PstI
3285_p3_fw_PstI	gaattcatcaccggaggccggctgcagct	3285 pt 3 fw, EcoRI, PstI
3285_comp_rv_Hind_Bam	gtcaaagcttggatcctcaccgctccgttccgccggcc	3285 pt 3 rv (+Stop), HindIII, BamHI
3285_p3_rev_XbaHind	aagctttctagaccgctccgttccgccggccgcgt	3285 pt 3 rv GFP fusion, HindIII, XbaI
3286_comp_fw_EcoRI	gtcagaattccggacgatgacgacgaagacgacg	3286 own promoter, EcoRI
3286_comp_rv_Hind_Bam	gtcaaagcttggatcctcagaccctggccgtgccgttcagg	3286 rv (+Stop), HindIII, BamHI
3286_rev_XbaHind	gtcaaagctttctagagaccctggccgtgccgttcagg	3286 rv GFP fusion, HindIII, XbaI

Chapter 8

General Discussion and Conclusions

GENERAL DISCUSSION

Examining *Streptomyces* under the microscope, irrespective of scale, reveals a beautiful organism. From spore, to individual hyphae, to colony - in liquid broth or on solid media - the fractal-like symmetry of branching growth, colourful hues of secreted products, and fluorescent flashes of dynamically localizing proteins are all signs of the intricacies of *Streptomyces* biology. These microbes have an extraordinary ability to adapt to a diversity of ecosystems and thrive alongside a variety of competing and coexisting organisms. To do so, they have evolved a complex multicellular lifecycle, including several steps of morphological differentiation, with development tightly linked to antibiotic production (van Wezel and McDowall 2011; McCormick and Flärdh 2012).

Although the streptomycetes produce numerous commercially-important secondary metabolites, enzymes, and other secreted products (Hopwood 2007; Horinouchi 2007), the relationship between growth and morphology, on the one hand, and biomass accumulation and productivity, on the other, is complicated and poorly understood. In liquid cultures, *Streptomyces* grow by a balance of tip extension, branching, and fragmentation, creating an extensive mycelial network. Within this mycelium, programmed cell death in certain hyphal parts (and not others) occurs to provide nutrients to the growing organism (Manteca *et al*. 2008); this stage of development is linked with antibiotic production. A major scientific challenge lies in understanding how growth parameters are controlled in response to nutritional conditions, and how this affects the efficiency of production and secretion of proteins and antibiotics. Studies have demonstrated that morphology is key, but morphology varies from species to species. Besides genetics and physiological parameters, environmental triggers and growth conditions also play a large role in determining how a mycelium will grow. In effect, antibiotic and enzyme production results from a combination of species-specific genetic make-up and the environment (natural or laboratory) in which the organism is found. The work presented in this thesis aims to arrive at a better understanding of *Streptomyces* morphogenesis and development, and how these processes link to productivity.

To better understand how protein secretion relates to growth, we performed localization studies on the twin-arginine transport, or Tat, protein export machinery. Live imaging of fluorescent fusions revealed that the three subunits (TatA, TatB, and TatC) of the Tat complex translocate dynamically throughout hyphae before colocalizing, often roughly 2 µm behind the tip. To facilitate quantitative analysis of focal trajectories, we therefore developed a single particle tracking package specially suited for application to diffusion-limited foci in

long *Streptomyces* hyphae. We tested the package against other algorithms by participating in the IEEE International Symposium on Biomedical Imaging (ISBI) 2012 Single Particle Tracking Challenge (http://bioimageanalysis.org/track/). Although no algorithm performed best for all competition data sets, the superior performance of some algorithms over others appeared to stem mainly from careful parameter tuning and making the best possible use of prior knowledge about the data. The outcome of the challenge and an analysis of participating algorithms has been submitted for publication (Chenouard *et al. submitted*).

We applied our particle tracking package to better understand the dynamics of TatA, the most abundant subunit of the Tat machinery, and found that TatA undergoes different motion regimes during localization, with small units, likely consisting of tetramers, oligomerizing during the localization sequence before colocalizing with TatBC to form a functional translocation complex (Chapter 3). Use of the tracking package enabled quantitative analysis of the localization dynamics, which previously could only be described qualitatively. Analysis of other dynamically localizing proteins (for example, the cell division protein SsgA) in this manner should provide more insight their function in time and space during hyphal growth.

Work on this thesis coincided with the opening of the Netherlands Centre for Electron Nanoscopy (NeCEN) in 2012. It was my good fortunate to be the first to use the new 300 keV Titan microscope to study of *Streptomyces* ultrastructure at an unprecedented resolution. In the past years, the possibility to image biological samples at high keV has been revolutionizing the field of bacterial cell biology. 3D reconstructions, or tomograms, of tilt series images collected provide an inside-view of cryo-fixed cells at nanometer resolution, avoiding the artifacts of chemical fixatives. Building on this technology, we developed cryo-correlative light and electron tomography (cryo-CLET) for use in *Streptomyces*. Cryo-CLET enables labeling and identification of cellular structures at low resolution with cryo-fluorescent light microscopy, and then imaging at NeCEN to obtain a high resolution tomogram at the location of interest.

This very powerful and novel combination of technologies allowed us to discover a vast intracellular membrane system within hyphae, and establish that in fact the DNA and membranes are mutually exclusive (Chapter 4). As the Min and NOC control systems, which act to ensure that division occurs at mid-cell in rod-shaped bacteria, are missing in *Streptomyces sp*., it was until now not clear how and where crosswall formation is initiated and completed in the multinucleoid hyphae. The work published in this thesis shows that most likely intracellular membranes fulfill this role, and mediate division-site selection and nucleoid occlusion in the vegetative mycelium. During growth and development, membranes, consisting of a heterogeneous distribution of lipids, dynamically localize to the

division site, creating a large cell-delimiting barrier to ensure that septum formation can occur without damage to the chromosomes. Additionally, cross-membranes fully colocalize with - and are dependent on - the division scaffold protein FtsZ, demonstrating that a subtle interplay exists between membrane and cell wall formation during the initiation of cell division.

This study illustrates the power of cryo-electron tomography and correlative techniques for elucidating the ultrastructural details of cell-cycle processes. Excitingly, we are only at the tip of the iceberg in terms of what can be discovered with these technologies. Improvement in cryo-light resolution, as well as fluorescence signal enhancement of reporters (such as eGFP) under cryo-conditions should achieve a long-term goal, namely the localization of protein complexes directly in high resolution images, and on native samples. Development of live-fluorescent imaging - prior to plunge freezing of samples for tomography - will make possible the capture of dynamic events as they are taking place. With these technologies, high resolution structural information can be gained about cell-cycle processes, creating macromolecular landscapes of the unperturbed cell.

Cryo-electron tomography has recently been applied to the study of cytoskeletal elements in bacteria (Briegel *et al.* 2006; Ingerson-Mahar *et al.* 2010; Pilhofer *et al*. 2011; Swulius *et al.* 2011). Control of bacterial shape is the task of the cytoskeleton, and numerous structural proteins cooperate to ensure that the elaborate shapes of bacteria are maintained throughout growth and division. In *Streptomyces coelicolor*, coiled-coil rich proteins DivIVA (Flärdh 2003), FilP (Bagchi *et al.* 2008; Fuchino *et al.* 2013) and Scy (Walshaw *et al.* 2010; Holmes *et al.* 2012) have been characterized, and their function in controlling polarized growth and hyphal integrity described. Cytoskeletal proteins and their interaction partners, however, not only play a role in establishing cell shape - they also have roles in cell division (FtsZ and the SsgA-like proteins), growth (MreB in rod-shaped bacteria; DivIVA in *Streptomyces*), DNA partitioning (ParA) and motility (in motile bacteria). Study of the cytoskeleton is a dynamic field, with new discoveries made by high resolution light and electron microscopy techniques rapidly changing the way we perceive bacteria (reviewed in Chapter 2).

Perhaps due to their complicated mycelial lifestyle and developmental program, *Streptomyces sp*. encode for many more coiled-coil rich proteins. In this work, I focused on novel genes for coiled-coil and associated proteins: SCO2259 and the adjacent gene SCO2260 as well as SCO3285 and SCO3286 (Chapter 7). SCO2259 and SCO3285 encode large proteins with coiled-coil motifs, while SCO3286 encodes for a flotillin domain protein, associated with lipid raft formation in eukaryotes. In *B. subtilis* flotillins seem to generate

a local environment favoring membrane curvature, perhaps helping to recruit cell division proteins to the division site (Dempwolff *et al.* 2012). We were therefore particularly interested in studying the putative function of SCO3286 in membrane formation. Deletion of SCO2259 and SCO3285 affected spore chain formation; in the SCO2259 mutant some spores were branching, while in the SCO3285 mutant, new cell wall material was not deposited correctly, resulting in spores not correctly aligned within chains, but rather forming zig-zags. A large phenotypic difference was observed when SCO3286, was deleted. This mutant demonstrated a dramatic increase of sporulation, with many short spore chains and few non-sporulating aerial hyphae at a time where wild-type cells only produce aerial hyphae. A similar phenotype was obtained when a different flotillin homolog, SCO3607, was disturbed in *Streptomyces albus*, suggesting that flotillins either induce sporulation where they localize or play an important role in the negative control of sporulation. Interestingly, the double mutant of SCO3286 and SCO3285 demonstrated difficulty sporulating. Localization studies of these proteins using fluorescent eGFP fusions revealed that SCO3285 localizes in young aerial hyphae and that SCO3286 forms long filaments around forming spores. These genes appear therefore to cooperate to ensure that sporulation-specific cell division can take place correctly. Our results highlight the importance of the *Streptomyces* developmental program, where many large coiled-coil rich proteins contribute to ensure that strong, viable spores are reliably formed for the survival of progeny.

To integrate the multi-scale information obtained during this work, and arrive at a better understanding of *Streptomyces* morphogenesis and development, a structured morphological model was created. The model can be applied as a framework for rational design of *Streptomyces sp.* for production purposes (Chapter 5). Since secondary metabolite production in filamentous organisms is associated with morphological differentiation (Giudici *et al.* 2004; Manteca *et al.* 2008), a structured approach, in which hyphae are divided into compartments indicating different stages of cellular differentiation, was favored. With this approach, a particular morphology (dictated by branching and cross wall formation frequency, as well as fragmentation), has a particular ''structure'' or compartmentalization. A fraction of the pellet is able to actively produce antibiotic (the hyphal compartment), a fraction to branch (the subapical compartment), and a fraction to grow (the apical compartment). Pellet composition (based on these compartment fractions) can be correlated with information gained in fermentation trials, relating morphology to productivity. The structured morphological modeling approach is a step towards rational strain improvement and process design.

Drawing inspiration from the Google Chrome Experiments (http://www.chromeexperiments.com) and the new trend of using the web as a platform for software applications, an

interactive version of the model was created in Javascript for HTML5 browser-based viewing and manipulation (Chapter 6). Basic model processes of growth and branching were coded and visualized using WebGL, a new web technology which enables visualization of Graphics Processing Unit (GPU) hardware-accelerated 3D graphics on the browser without additional software, plug-ins or extensions. Although the combination of HTML5 and WebGL is not yet suitable for scientific computing, further development should enable the shift from binary application-based modeling to dynamically delivered web application-based modeling (Taivalsaari *et al.* 2011). A proof-of-concept model was therefore coded to determine the capabilities and limitations of online modeling. Based on the promising results, future plans are to extend the model to include additional graphical user interface (GUI) parameters and experimental data to increase the biological relevance of the model. By adjusting the parameters, a user should be able to affect morphology and follow the 3D growth of a pellet over time. Such an interactive in-browser modeling framework could be a valuable tool to enhance visualization of morphological changes and their effect on natural product formation.

The work presented in this thesis is diverse and multidisciplinary in nature, combining molecular biology, light and electron microscopy, and computational modeling techniques to better approach the questions at hand. Not only are these multi-disciplinary techniques - but also multi-dimensional, spanning the whole scale of experimental observation, from whole mycelial colony, down to individual genes and their expression. Such a combined approach is fundamental for improving understanding of *Streptomyces* biology.

Each of the research directions pursued leave many questions unanswered. In the case of the cytoskeletal proteins, it will be interesting to study more proteins with flotillin domains (there are six encoded for in *Streptomyces coelicolor*) to better understand the role of lipid rafts in control of growth and development. The particle tracking package can be applied to live imaging studies of other dynamically localizing proteins (such as the aforementioned SsgA) to better understand how and where they localize during growth and morphogenesis. A major contribution of this thesis was the work done at NeCEN and the discoveries made regarding the role of intracellular membranes in *Streptomyces* vegetative division. This work must undoubtedly continue and mutants with altered lipid composition, or affected in cell division (*ssgA*- overexpressing strains or the *ftsZ* deletion strain) imaged to better understand the mechanisms behind membrane formation and localization. As more information is gained, extension of the modeling framework will be of value to provide a real test drive for the fermentation process and to pre-assess the effect of different variables on productivity.

NEDERLANDSE SAMENVATTING

Als je *Streptomyces* bacteriën onder de microscoop bekijkt, zie je op elke schaal een schitterend organisme. Van spore tot individuele hyfe tot kolonie - in vloeibare culture of op vaste voedingsbodems - de fractal-achtige symmetrie van zich vertakkende hyfen, kleurrijke tinten van de natuurstoffen die worden geproduceerd of het fluorescente flitsen van dynamische eiwitten zijn allemaal uitingen van grote biologische complexiteit. Streptomyceten ondergaan een complexe levenscyclus en zijn een zeldzaam complexe en multicellulaire bacterie. Daarbij wordt de morfologische ontwikkeling gekoppeld aan de productie van antibiotica (van Wezel and McDowall 2011; McCormick and Flärdh 2012). Streptomyceten kom je overal tegen, onder meer doordat ze zich zeer makkelijk aanpassen een breed scala van ecosystemen, waarbij ze groeien op nagenoeg alle biopolymeren die in de natuur voorkomen (zoals cellulose, chitine of agar) en overleven in een omgeving die vele concurrerende en symbiotische micro-organismen bevat.

Hoewel streptomyceten een groot aantal secundaire metabolieten, enzymen en andere producten maken (Hopwood 2007; Horinouchi 2007), is de relatie tussen aan de ene kant groei en morfologie en aan de andere kant biomassa- en productvorming, ingewikkeld en nog slecht begrepen. Het mycelium groeit door verlenging en vertakking van de myceliumdraden of hyfen, waardoor een complex dradennetwerk gevormd wordt. Celdood gevolgd door afbraak van het oude mycelium voorziet de kolonie op vaste ondergrond - zoals in de grond of in Petrischalen - van voedsel voor de groei van het luchtmycelium (Manteca *et al.* 2008). Tijdens deze fase van de levenscyclus worden doorgaans ook de antibiotica geproduceerd. In vloeibare cultures (zoals de fermentor) resulteert groei en vertakking veelal in de vorming van dichte klonten of pellets, die traag groeien en tevens slecht nutriënten en zuurstof opnemen, waardoor de binnenkant van de pellet al snel afsterft. Dit is ongunstig voor de industriële productie. Fragmentatie van de mycelia door verhoogde celdeling resulteert in snellere groei (van Wezel *et al.* 2006), maar dat heeft vaak weer een negatieve invloed op de antibioticumproductie. Het verkrijgen van beter inzicht in hoe streptomyceten groeien afhankelijk van de nutriënten en hoe de groei op zijn beurt weer de productie en secretie van eiwitten en antibiotica beïnvloedt is dan ook van groot belang voor industriële toepassingen. De controle en productie van antibiotica en enzymen hangt sterk af van de genetische samenstelling van een organisme en de omgeving waarin het zich bevindt. Het onderzoek beschreven in dit proefschrift richt zich op het begrijpen van de morfogenese en ontwikkeling van *Streptomyces*, en hoe deze processen gekoppeld zijn aan productie.

Om meer inzicht te krijgen in de relatie tussen eiwitexport en de groei, is het twin-

arginine transport (Tat) eiwit transport systeem gelokaliseerd tijdens de groei. Live-imaging experimenten van fluorescente fusie-eiwitten liet zien dat de drie subeenheden (TatA, TatB, and TatC) van het Tat complex zich op dynamische wijze door de hyfen verplaatsen voordat ze samenkomen en één complex vormen, doorgaans zo'n 2 µm achter een groeiende tip. Om de afgelegde trajecten van deze eiwitten kwantitatief te kunnen analyseren, is een single particle tracking package ontwikkeld om fluorescente moleculen te volgen in de hyfen van *Streptomyces*. Met dit algoritme hebben we tevens deelgenomen aan de IEEE International Symposium on Biomedical Imaging (ISBI) 2012 Single Particle Tracking Challenge (http://bioimageanalysis.org/track/). Hoewel geen enkel algoritme optimaal was voor alle datasets, waren het vooral de pakketten die gebruik maakten van zorgvuldige parameter tuning en het beste de data doorgrondden die de beste resultaten verkregen. De resultaten van deze boeiende competitie en een analyse van alle deelnemende algoritmes is ingediend voor publicatie (Chenouard *et al. submitted*).

Ons algoritme hebben we vervolgens toegepast om de dynamische localisatie van TatA te analyseren. TatA komt verreweg het hoogst tot expressie en is daarom het makkelijkst te volgen. Dit liet zien dat tetrameren van TatA oligomeriseren voordat ze met TatBC colokaliseren om zo een functioneel exportcomplex te vormen (Hoofdstuk 3). Met de ontwikkelde software konden we op een kwantitatieve manier de dynamische localisatie van het Tat complex analyseren, wat eerder alleen kwalitatief kon. Analyse van de dynamische localisatie van andere eiwitten (bijvoorbeeld het celdelingseiwit SsgA welke zich zeer dynamisch gedraagt in de cel) zal ook voor die eiwitten belangrijke nieuwe inzichten opleveren over hun functie.

Mijn promotieonderzoek viel samen met de opening van de Nederlands Centrum voor Electron Nanoscopie (NeCEN) in 2012. Ik had daarbij het geluk om als eerste de nieuwe 300 keV Titan microscoop te mogen gebruiken om de ultrastructuur van *Streptomyces* te bestuderen op zeer hoge resolutie. De mogelijkheid om biologische monsters op hoge keV te bestuderen heeft een revolutie in de bacteriële celbiologie teweeg gebracht. 3D reconstructies, zogenaamde tomogrammen, van series van EM beelden opgenomen tijdens het kantelen van het specimen met alleen cryofixatie, geven een uniek beeld van de fascinerende wereld in de cel, zonder de artefacten die typisch het gevolg zijn van chemische fixatie. Om nog meer inzicht te krijgen hebben we cryo-correlatieve licht- en electronen tomografie (cryo-CLET) ontwikkeld. Cryo-CLET maakt het mogelijk om fluorescentiemicroscopie te combineren met electronenmicroscopie, zodat we celstructuren specifiek kunnen identificeren op lagere resolutie en dit vervolgens kunnen correleren met een beeld op hoge resolutie van exact hetzelfde sample. Dit was tot voor kort niet mogelijk, zodat het onduidelijk bleef wat er nu

precies op hoge resolutie EM beelden te zien was.

Op deze manier hebben we een spectaculair intracellulair membraansysteem ontdekt in de hyfen en laten zien dat er nooit overlap is tussen deze membranen en het chromosomale DNA en dat celdelingsstrukturen gevormd worden in deze beschermende 'cross-membranen' (Hoofdstuk 4). Het is waarschijnlijk dat dit het systeem is wat in streptomyceten voorkomt dat het groeiende septum het DNA kan beschadigen. Dit wordt ook wel nucleoid occlusion (NOC) genoemd. Andere controlesystemen zorgen ervoor dat het septum (celdelingsstruktuur) op exact de juiste plek en op de juiste tijd wordt gevormd. De controlesystemen die in andere bacteriën zijn gevonden komen niet voor in *Streptomyces* en het was lang onduidelijk hoe de controle van celdeling in deze bacterie werkt. Dit proefschrift laat zien dat het membranen zijn die zeer waarschijnlijk de taak van NOC uitvoeren in het vegetatieve groeistadium. Bovendien colokaliseren cross-membranen met - en zijn afhankelijk van - het celdelingseiwit FtsZ, het eiwit welke de daadwerkelijke celdelingsring vormt (Bi and Lutkenhaus 1991). Er bestaat dus een subtiele wisselwerking tussen membranen en celwandopbouw tijdens celdeling in *Streptomyces*.

Het hier boven beschreven werk laat de kracht van cryo-electronentomografie en correlatieve technieken zien. Deze methoden brengen ultrastructurele details van cellulaire processen aan het licht. De uitdaging is nu om de technologie verder te ontwikkelen, bijvoorbeeld door verbetering van cryo-licht resolutie, of door de fluorescente signaal van reporters (zoals eGFP) in diepgevroren toestand te versterken. Het ultieme doel is daarbij om individuele eiwitten te kunnen identificeren in hoge resolutie tomogrammen. Ontwikkeling van live-fluorescentiemicroscopie - om het juiste beeld te kunnen selecteren voordat de samples ingevroren worden voor tomografie - zal het vastleggen van dynamische processen mogelijk maken. Zo zullen we structurele informatie op hoge resolutie kunnen verkrijgen, waardoor als het ware een macromoleculair landschap zal kunnen worden getekend van de levende cel.

Cryo-electron tomografie werd in de laatste jaren ook toegepast tijdens onderzoek van het bacteriële cytoskelet (Briegel *et al.* 2006; Ingerson-Mahar *et al.* 2010; Pilhofer *et al.* 2011; Swulius *et al.* 2011). Controle van de morfologie van de cel is de taak van het cytoskelet, waarbij een groot aantal structurele elementen samenwerkt om de cellen in de juiste vorm te houden. In *Streptomyces coelicolor* spelen onder meer DivIVA (Flärdh 2003), FilP (Bagchi *et al.* 2008; Fuchino *et al.* 2013) en Scy (Walshaw *et al.* 2010; Holmes *et al.* 2012) hierbij een belangrijke rol. Het cytoskelet speelt tevens een doorslaggevende rol bij de celdeling (FtsZ en de SsgA-achtige eiwitten), de DNA segregatie (ParA) en beweging in die bacteriën die zich actief bewegen. Hoge resolutie electronenmicroscopie levert daarbij belangrijke informatie

op over de structurele en functionele aspecten van het bacteriële cytoskelet (Hoofdstuk 2).

Streptomyceten hebben een complex cytoskelet, hetgeen vermoedelijk relateert aan de complexe levenscyclus. In dit proefschrift zijn vier mogelijk cytoskeletgenen geanalyseerd die nog niet eerder bestudeerd zijn: SCO2259 en SCO2260, alsmede SCO3285 en SCO3286 (Hoofdstuk 7). SCO2259 en SCO3285 coderen voor grote eiwitten met zogenaamde coiled-coil motieven, terwijl SCO3286 codeert voor een eiwit met een flotillin domein. In eukaryoten zijn flotillins van belang voor de vorming van zogenaamde lipid rafts. In Bacillus subtilis zorgen flotillins plaatselijk voor kromming van de membraan, hetgeen hoogstwaarschijnlijk een rol speelt bij het recruteren van celdelingseiwitten naar de juiste plek voor de celdeling (Dempwolff *et al.* 2012). Dit maakt de rol van SCO3286 dus met name interessant vanuit het perspectief van de controle van celdeling. Mutanten van SCO2259 en SCO3285 vertonen problemen met de sporulatie, waarbij in SCO2259 mutanten sommige sporen vertakken, terwijl in de SCO3285 mutant de sporen in de sporenketens een zigzagpatroon vertonen, vermoedelijk als gevolg van problemen met celwandsynthese. De grootste afwijking wordt veroorzaakt door het uitschakelen van SCO3286. Mutanten van SCO3286 produceren veel meer maar ook kortere sporenketens. Uitschakelen van een gen voor een ander flotillin domein eiwit, SCO3607, liet een vergelijkbaar fenotype zien. Gebaseerd op deze waarnemingen lijken eiwitten met een flotillindomein een belangrijke rol te spelen bij de sporulatie. Samen met de al eerder geïdentificeerde cytoskeletelementen toont dit aan hoe complex het ontwikkelingsprogramma van *Streptomyces* is, waarbij vele vaak grote eiwitten met meerdere coiled-coil domeinen een belangrijke rol spelen bij de controle van sporulatie en celdeling (Celler *et al.* 2013).

Om de multidimensionale informatie verkregen uit de verschillende benaderingen uit dit proefschrift te integreren en zo tot een betere begrip van *Streptomyces* morfogenese en ontwikkeling te komen, is een model gemaakt waarin de structuur-morfologie informatie is geïntegreerd (Hoofdstuk 5). Het model kan als een raamwerk voor rationeel ontwerp van *Streptomyces* bacteriën worden beschouwd, met als ultieme doel om zo stammen te ontwerpen die beter geschikt zijn voor de industriële productie. Omdat de productie van secundaire metabolieten in filamenteuze micro-organismen gekoppeld is aan groei, morfologie en ontwikkeling (Giudici *et al.* 2004; Manteca *et al.* 2008) is een structurele benadering gekozen voor modelering. In een structureel model kunnen hyfen theoretisch verdeeld worden in compartimenten waarin verschillende stadia van ontwikkeling tegelijk voorkomen. Met deze benadering heeft een bepaalde morfologie (die ontstaat als gevolg van groei, vertakking en fragmentatie) een bepaalde ''struktuur'' of compartimentvorming. Een fractie van de pellet kan zo antibiotica produceren (het 'hyphal' compartiment), een

andere fractie kan vertakken (het 'subapical' compartiment), en weer een andere kan groeien (het 'apical' compartiment). De samenstelling, die gebaseerd is op de verhouding tussen de verschillende compartimenten op een gegeven moment, kan vervolgens gecorreleerd worden aan gegevens van werkelijke fermentaties. Door deze wisselwerking tussen modeleren enerzijds en informatie uit de praktijk anderzijds, krijgen we meer inzicht in de relatie tussen morfologie en productiviteit. Zo'n model is daarmee een belangrijke stap in de richting van rationeel procesontwerp.

Geïnspireerd door de Google Chrome Experiments (http://www.chromeexperiments.com) en de nieuwe trend om het worldwide web als platform voor software applicaties te gebruiken, is een interactieve versie van het model geschreven met behulp van Javascript (Hoofdstuk 6). Modelprocessen van groei en vertakking zijn daarbij gecodeerd en gevisualiseerd middels WebGL, een nieuwe technologie die visualisatie mogelijk maakt van Graphics Processing Units (GPU) met 3D graphics direct in de browser, zonder dat daar andere software bij nodig is. Hoewel de combinatie van HTML5 en WebGL nog niet geschikt is voor wetenschappelijke berekeningen, is de verwachting dat in de komende jaren de huidige binaire applicatie-gebaseerde modellen vervangen zullen gaan worden door dynamische modellen die gebaseerd zijn op web applicaties (Taivalsaari *et al.* 2011). Om dit alvast uit te proberen is daarom een conceptstudie uitgevoerd en dit model zal nu uitgebreid kunnen worden met bijvoorbeeld een graphical user interface (GUI), om zo de biologische relevantie en gebruiksvriendelijkheid te verhogen. Door aanpassing van de parameters zal de gebruiker direct de morfologie in silico kunnen aanpassen en zien hoe dit de driedimensionale pellet beïnvloedt. Middels zo'n interactief in-browser model kunnen we het effect van de morfologie op productie beter zichtbaar maken en begrijpen.

Het onderzoek dat in dit proefschrift staat beschreven is divers en multidisciplinair en ontstaan uit een combinatie van moleculaire biologie, microscopie en in silico modellen, waardoor het gehele spectrum van de experimentele waarneming zo'n beetje is beslagen. Deze benadering stelt ons in staat om de complexe biologie van streptomyceten beter te begrijpen. Voor elk van de verschillende onderzoekslijnen zijn er ook weer diverse belangrijke vragen in de plaats gekomen die zullen moeten worden beantwoord en daarmee vormt dit onderzoek ook weer de basis voor nieuwe richtingen van onderzoek in de toekomst. Wat betreft het cytoskelet zal het interessant zijn om de rol van eiwitten met flotillindomeinen te bestuderen en daarmee ook de rol van zogenaamde lipid rafts, met name in relatie tot de controle van groei en ontwikkeling. Middels de hier ontwikkelde particle tracking software zullen gegevens uit de live imaging van verschillende dynamische eiwitten kunnen worden vertaald naar biologische processen, om zo meer inzicht in de

localisatie van de eiwitten te verkrijgen. Een belangrijke bijdrage van dit proefschrift aan het onderzoeksveld is mijns inziens de ontwikkeling en toepassing van cryo-CLET en de daaruit voorvloeiende ontdekking van intracellulaire membranen in *Streptomyces* en hun rol bij de celdeling. Dit werk zal hopelijk tot inspiratie dienen voor nieuw onderzoek, waarbij onder meer nieuwe stammen met veranderde lipidesamenstelling of die verstoord zijn in de celdeling, ons verder zullen helpen om de rol van membranen bij de controle van celdeling en DNA segregatie te begrijpen. Tot slot zullen alle data met betrekking tot de groei, morfologie en productiviteit van streptomyceten kunnen blijven worden geïntegreerd in een model wat zo steeds beter de werkelijkheid zal benaderen. Dit kan dan vervolgens als een realistisch theoretisch testsysteem dienen voor de fermentatie-industrie, zodat *black box* benaderingen uiteindelijk vervangen kunnen worden door rationeel design.

References

REFERENCES

Adams, D.W., Errington, J. (2009) Bacterial cell division: assembly, maintenance and disassembly of the Z-ring. *Nat Rev Microbiol* **7**:642-53.

Addinall, S.G., Lutkenhaus, J. (1996) FtsZ-spirals and -arcs determine the shape of the invaginating septa in some mutants of *Escherichia coli*. *Mol Microbiol* **22**:231-237.

Akiyama, Y., Kanehara, K., Ito, K. (2004) RseP (YaeL), an *Escherichia coli* RIP protease, cleaves transmembrane sequences. *EMBO J* **23**(22):4434-4442.

Alberts, B., Johnson, A., Lewis, J., Raff, M., Roberts, K., Walter, P. (2002) Molecular Biology of the Cell, 4 ed. Garland Science, New York.

Alexandre, S., Colé, G., Coutard, S., Monnier, C., Norris, V., Margolin, W., Yu, X., Valleton, J.M. (2002) Interaction of FtsZ protein with a DPPE Langmuir film. *Colloids Surf., B* **23**(4):391-395.

Alexeeva, S., Gadella, Jr., T.W., Verheul, J., Verhoeven, G.S., den Blaauwen, T. (2010) Direct interactions of early and late assembling division proteins in *Escherichia coli* cells resolved by FRET. *Mol Microbiol* **77**:384-398.

Anttonen, M., Salminen, A., Mikkonen, T., Taivalsaari, A. (2011) Transforming the web into a real application platform: new technologies, emerging trends and missing pieces. *ACM Symposium on Applied Computing*, ACM, New York.

Arechaga, I., Miroux, B., Karrasch, S., Huijbregts, R., de Kruijff, B., Runswick, M.J., Walker, J.E. (2000) Characterisation of new intracellular membranes in *Escherichia coli* accompanying large scale over-production of the b subunit of F(1)F(o) ATP synthase. *FEBS Lett* **482**(3):215-219.

Ausmees, N., Kuhn, J.R., Jacobs-Wagner, C. (2003) The bacterial cytoskeleton: an intermediate filament-like function in cell shape. *Cell* **115**:705-13.

Bagchi, S., Tomenius, H., Belova, L.M., N. Ausmees, N. (2008) Intermediate filament-like proteins in bacteria and a cytoskeletal function in *Streptomyces*. *Mol Microbiol* **70**:1037-50.

Banga, I., Szent-György, A. (1942) Preparation and properties of myosin A and B. *Stud. Inst. Med. Chem. Univ. Szeged.* **I**:5-15.

Banigan, E.J., Gelbart, M.A., Gitai, Z., Wingreen, N.S., Liu, A.J. (2011) Filament depolymerization can explain chromosome pulling during bacterial mitosis. *PLoS Comput Biol* **7**:e1002145.

Barak, I., Muchová, K. (2013) The role of lipid domains in bacterial cell processes. *Int J Mol Sci* **14**(2):4050-4065.

Barak, I., Muchová, K., Wilkinson, A.J., O'Toole, P.J., Pavlendová, A. (2008) Lipid spirals in *Bacillus subtilis* and their role in cell division. *Mol Microbiol* **68**(5):1315-1327.

Barak, I., Wilkinson, A.J. (2007) Division site recognition in *Escherichia coli* and *Bacillus subtilis*. *FEMS Microbiol Rev* **31**(3):311-326.

Bennett, J.A., Yarnall, J., Cadwallader, A.B., Kuennen, R., Bidey, P., Stadelmaier, B., McCormick, J.R. (2009) Medium-dependent phenotypes of *Streptomyces coelicolor* with mutations in *ftsI* or *ftsW*. *J Bacteriol* **191**(2):661-664.

Bernander, R., Ettema, T.J. (2010) FtsZ-less cell division in archaea and bacteria. *Curr Opin Microbiol* **13**:747-52.

Bernhardt, T.G., de Boer, P.A. (2005) SlmA, a nucleoid-associated, FtsZ binding protein required for blocking septal ring assembly over Chromosomes in *E. coli*. *Mol Cell* **18**:555-64.

Bi, E.F., Lutkenhaus, J. (1991) FtsZ ring structure associated with division in *Escherichia coli*. *Nature* **354**:161-4.

Bierman, M., R. Logan, O'Brien, K., Seno, E.T., Nagaraja Rao, R., Schoner, B.E. (1992) Plasmid cloning vectors for the conjugal transfer of DNA from *Escherichia coli* to *Streptomyces spp*. *Gene* **116**(1):43-49.

Birol, G., Ündey, C., Parulekar, S.J., Çinar, A. (2002) A morphologically structured model for penicillin production. *Biotechnol Bioeng* **77**(5):538-552.

Brady, S.T. (1985) A novel brain ATPase with properties expected for the fast axonal transport motor. *Nature* **317**:73-5.

Briegel, A., Chen, S., Koster, A.J., Plitzko, J.M., Schwartz, C.L., Jensen, G.J. (2010) Correlated light and electron cryo-microscopy. *Methods Enzymol* **481**:317-41.

Briegel, A., Dias, D.P., Li, Z., Jensen, R.B., Frangakis, A.S., Jensen, G.J. (2006) Multiple large filament bundles observed in *Caulobacter crescentus* by electron cryotomography. *Mol Microbiol* **62**:5-14.

Cabeen, M.T., Jacobs-Wagner, C. (2005) Bacterial cell shape. *Nat Rev Microbiol* **3**:601-10.

Cabeen, M.T., Jacobs-Wagner, C. (2010) The bacterial cytoskeleton. *Annu Rev Genet* **44**:365-92.

Caldwell, I.Y., Trinci, A.P. (1973) The growth unit of the mould *Geotrichum candidum*. *Arch Mikrobiol* **88**(1):1-10.

Capoulade, J., Wachsmuth, M., Hufnagel, L., Knop, M. (2011) Quantitative fluorescence imaging of protein diffusion and interaction in living cells. *Nat Biotechnol* **29**:835-839.

Carballido-Lopez, R., Errington, J. (2003) The bacterial cytoskeleton: in vivo dynamics of the actin-like protein Mbl of *Bacillus subtilis*. *Dev Cell* **4**(1):19-28.

Celler, K., Koning, R.I., Koster, A.J., van Wezel, G.P. (2013) Multidimensional view of the bacterial cytoskeleton, *J Bacteriol* **195**:1627-1636.

Celler, K., Picioreanu, C., van Loosdrecht, M.C., van Wezel, G.P. (2012) Structured morphological modeling as a framework for rational strain design of Streptomyces species. *Anthonie van Leeuwenhoek* **102**:409-423.

Charbon, G., Cabeen, M.T., Jacobs-Wagner, C. (2009) Bacterial intermediate filaments: in vivo assembly, organization, and dynamics of crescentin. *Genes Dev* **23**:1131-44.

Chater, K.F. (1972) A morphological and genetic mapping study of white colony mutants of *Streptomyces coelicolor*. *J Gen Microbiol* **72**(1):9-28.

Chater, K.F., Losick, R. (1997) Mycelial life style of *Streptomyces coelicolor* A3(2) and its relatives. In: Shapiro JA, Dworkin M (eds) Bacteria as multicellular organisms. Oxford University Press, New York, pp 149-182.

Claessen, D., de Jong, W., Dijkhuizen, L., Wösten, H.A.B. (2006) Regulation of *Streptomyces* development: reach for the sky! *Trends Microbiol* **14**(7):313-319.

Colson, S., van Wezel, G.P., Craig, M., Noens, E.E., Nothaft, H., Mommaas, A.M., Titgemeyer, F., Joris, B., Rigali, S. (2008) The chitobiose-binding protein, DasA, acts as a link between chitin utilization and morphogenesis in *Streptomyces coelicolor*. *Microbiol* **154**:373-382.

Cui, Y.Q., Okkerse, W.J., van der Lans, R.G., Luyben, K.C. (1998) Modeling and measurements of fungal growth and morphology in submerged fermentations. *Biotechnol Bioeng* **60**(2):216-229.

Dabney-Smith, C., Mori, H., Cline, K. (2006) Oligomers of Tha4 organize at the thylakoid Tat translocase during protein transport. *J Biol Chem* **281**:5476-5483.

Dajkovic, A., Lutkenhaus, J. (2006) Z-ring as executor of bacterial cell division. *J Mol Microbiol Biotechnol* **11**:140-51.

de Boer, P.A. (2010) Advances in understanding *E. coli* cell fission. *Curr Opin Microbiol* **13**:730-7.

de Bruin, K., Ruthardt, N., von Gersdorff, K., Bausinger, R., Wagner, E., Ogris, M., Bräuchle, C. (2007) Cellular dynamics of EGF receptor-targeted synthetic viruses. *Mol Ther* **15**:1297-1305.

Defeu Soufo, H.J., Graumann, P.L. (2005) *Bacillus subtilis* actin-like protein MreB influences the positioning of the replication machinery and requires membrane proteins MreC/D and other actin-like proteins for proper localization. *BMC Cell Biology* **6**.

Defeu Soufo, H.J., Graumann, P.L. (2003) Actin-like proteins MreB and Mbl from *Bacillus subtilis* are required for bipolar positioning of replication origins. *Curr Biol* **13**:1916-20.

Dempwolff, F., H. M. Wischhusen, Specht, M., Graumann, P.L. (2012) The deletion of bacterial dynamin and flotillin genes results in pleiotropic effects on cell division, cell growth and in cell shape maintenance. *BMC Microbiol* **12**:298.

Domínguez-Escobar, J., Chastanet, A., Crevenna, A.H., Fromion, V., Wedlich-Söldner, R., Carballido-López, R. (2011) Processive movement of MreB-associated cell wall biosynthetic complexes in bacteria. *Science* **333**:225-8.

Dye, N.A., Pincus, Z., Theriot, J.A., Shapiro, L., Gitai, Z. (2005) Two independent spiral structures control cell shape in *Caulobacter*. *Proc Natl Acad Sci USA* **102**:18608-13.

Edwards, D.H., Errington, J. (1997) The *Bacillus subtilis* DivIVA protein targets to the division septum and controls the site specificity of cell division. *Mol Microbiol* **24**(5):905-915.

Ellis, R.J. (2001) Macromolecular crowding: obvious but underappreciated. *Trends Biochem Sci* **26**:597-604.

Erickson, H.P. (1995) FtsZ, a prokaryotic homolog of tubulin? *Cell* **80**:367-70.

Erickson, H.P. (1997) FtsZ, a tubulin homologue in prokaryote cell division. *Trends Cell Biol* **7**:362-7.

Erickson, H.P., Anderson, D.E., Osawa, M. (2010) FtsZ in bacterial cytokinesis: cytoskeleton and force generator all in one. *Microbiol Mol Biol Rev* **74**:504-528.

Erickson, H.P., Taylor, D.W., Taylor, K.A., Bramhill, D. (1996) Bacterial cell division protein FtsZ assembles into protofilament sheets and minirings, structural homologs of tubulin polymers. *Proc Natl Acad Sci USA* **93**:519-523.

Ericson, C. (2005) Real-time collision detection. Morgan Kaufmann series in interactive 3D technology. Elsevier, Amsterdam; Boston.

Eriksson, H.M., Wessman, P. et al. (2009) Massive formation of intracellular membrane vesicles in *Escherichia coli* by a monotopic membrane-bound lipid glycosyltransferase. *J Biol Chem* **284**(49):33904-33914.

Errington, J., Daniel, R.A., Scheffers, D.J. (2003) Cytokinesis in bacteria. *Microbiol Mol Biol Rev* **67**(1):52-65.

Fedoryshyn, M., Welle, E., Bechthold, A., Luzhetskyy, A. (2008) Functional expression of the Cre recombinase in actinomycetes. *Appl Microbiol Biotechnol* **78**(6):1065-1070.

Fernandez, M., Sanchez, J. (2001) Viability staining and terminal deoxyribonucleotide transferase-mediated dUTP nick end labelling of the mycelium in submerged cultures of *Streptomyces antibioticus* ETH7451. *J Microbiol Meth* **47**(3):293-298.

Fernández-Martínez, L.T., Del Sol, R., Evans, M.C., Fielding, S., Herron, P.R., Chandra, G., Dyson, P.J. (2011) A transposon insertion single-gene knockout library and new ordered cosmid library for the model organism *Streptomyces coelicolor* A3(2). *Anthonie van Leeuwenhoek* **99**(3):515-522.

Figge, R.M., Divakaruni, A.V., Gober, J.W. (2004) MreB, the cell shape-determining bacterial actin homologue, co-ordinates cell wall morphogenesis in *Caulobacter crescentus*. *Mol Microbiol* **51**:1321-32.

Fishov, I., Norris, V. (2012) Membrane heterogeneity created by transertion is a global regulator in bacteria. *Curr Opin Microbiol* **15**(6):724-730.

Fishov, I., Woldringh, C.L. (1999) Visualization of membrane domains in *Escherichia coli*. *Mol Microbiol* **32**(6):1166-1172.

Flärdh, K. (2003) Essential role of DivIVA in polar growth and morphogenesis in *Streptomyces coelicolor* A3(2). *Mol Microbiol* **49**(6):1523-1536.

Flärdh, K. (2003) Growth polarity and cell division in *Streptomyces*. *Curr Opin Microbiol* **6**(6):564-571.

Flärdh, K. (2010) Cell polarity and the control of apical growth in *Streptomyces*. *Curr Opin Microbiol* **13**(6):758-765.

Flärdh, K., Buttner, M.J. (2009) *Streptomyces* morphogenetics: dissecting differentiation in a filamentous bacterium. *Nat Rev Microbiol* **7**(1):36-49

Flärdh, K., Leibovitz, E., Buttner, M.J., Chater, K.F. (2000) Generation of a non-sporulating strain of *Streptomyces coelicolor* A3(2) by the manipulation of a developmentally controlled ftsZ promoter. *Mol Microbiol* **38**:737-49.

Floriano, B., Bibb, M.J. (1996) *afsR* is a pleiotropic but conditionally required regulatory gene for antibiotic production in *Streptomyces coelicolor* A3(2). *Mol Microbiol* **21**(2):385-396.

Frangakis, A.S., Hegerl, R. (2001) Noise reduction in electron tomographic reconstructions using nonlinear anisotropic diffusion. *J Struct Biol* **135**(3):239-250.

Fuchino, K., Bagchi, S., Cantlay, S., Sandblad, L., Wu, D., Bergman, J., Kamali-Moghaddam, M., Flärdh, K., Ausmees, N. (2013) Dynamic gradients of an intermediate filament-like cytoskeleton are recruited by a polarity landmark during apical growth. *Proc Natl Acad Sci USA* **110**(21):E1889-1897.

Garner, E.C., Bernard, R., Wang, W., Zhuang, X., Rudner, D.Z., Mitchison, T. (2011) Coupled, circumferential motions of the cell wall synthesis machinery and MreB filaments in *B. subtilis*. *Science* **333**:222-5.

Gayathri, P., Fujii, T., Møller-Jensen, J., van den Ent, F., Namba, K., Löwe, J. (2012) A bipolar spindle of antiparallel ParM filaments drives bacterial plasmid segregation. *Science* **338**:1334-7.

Gerdes, K., Howard, M., Szardenings, F. (2010) Pushing and pulling in prokaryotic DNA segregation. *Cell* **141**:927-42.

Gibbons, I. R., A. J. Rowe. (1965) Dynein: a protein with adenosine triphosphatase activity from cilia. *Science* **149**:424-6.

Gitai, Z., Dye, N., Shapiro, L. (2004) An actin-like gene can determine cell polarity in bacteria. *Proc Natl Acad Sci USA* **101**:8643-8.

Gitai, Z., Dye, N.A., Reisenauer, A., Wachi, M., Shapiro, L. (2005) MreB actin-mediated segregation of a specific region of a bacterial chromosome. *Cell* **120**:329-41.

Giudici, R., Pamboukian, C.R., Facciotti, M.C. (2004) Morphologically structured model for antitumoral retamycin production during batch and fed-batch cultivations of *Streptomyces olindensis*. *Biotechnol Bioeng* **86**(4):414-424.

Glauert, A.M., Hopwood, D.A. (1959) A membranous component of the cytoplasm in *Streptomyces coelicolor*. *J Biophys Biochem Cytol* **6**: 515-516.

Glauert, A.M., Hopwood, D.A. (1960) The fine structure of *Streptomyces coelicolor*. I. The cytoplasmic membrane system. *J Biophys Biochem Cytol* **7**: 479-488.

Glazebrook, M.A., Doull, J.L., Stuttard, C., Vining, L.C. (1990) Sporulation of *Streptomyces venezuelae* in submerged cultures. *J Gen Microbiol* **136**(Pt 3):581-588.

Goehring, N.W., Beckwith, J. (2005) Diverse paths to midcell: assembly of the bacterial cell division machinery. *Curr Biol* **15**(13):R514-526.

Grantcharova, N., Lustig, U., Flärdh, K. (2005) Dynamics of FtsZ assembly during sporulation in *Streptomyces coelicolor* A3(2). *J Bacteriol* **187**(9):3227-3237.

Grantcharova, N., Ubhayasekera, W., Mowbray, S.L., McCormick, J.R., Flärdh, K. (2003) A missense mutation in *ftsZ* differentially affects vegetative and developmentally controlled cell division in *Streptomyces coelicolor* A3(2). *Mol Microbiol* **47**(3):645-656.

Graumann, P.L. (2007) Cytoskeletal elements in bacteria. *Annu Rev Microbiol* **61**:589-618.

Graumann, P.L. (2009) Dynamics of bacterial cytoskeletal elements. *Cell Motil Cytoskeleton* **66**:909-14.

Gray, D.I., Gooday, G.W., Prosser, J.I. (1990) Apical hyphal extension in *Streptomyces coelicolor* A3(2). *J Gen Microbiol* **136**(6):1077-1084.

Grund, A.D., Ensign, J.C. (1982) Activation of *Streptomyces-Viridochromogenes* spores by detergents. *Curr Microbiol* **7**(4):223-228.

Gueiros-Filho, F.J., Losick, R. (2002) A widely conserved bacterial cell division protein that promotes assembly of the tubulin-like protein FtsZ. *Genes Dev* **16**:2544-56.

Hale, C.A., de Boer, P.A. (1997) Direct binding of FtsZ to ZipA, an essential component of the septal ring structure that mediates cell division in *E. coli*. *Cell* **88**:175-185.

Hamoen, L.W., Meile, J.C., de Jong, W., Noirot, P., Errington, J. (2006) SepF, a novel FtsZ-interacting protein required for a late step in cell division. *Mol Microbiol* **59**:989-99.

Hamon, L., Curmi, P.A., Pastre, D. (2010) High-resolution imaging of microtubules and cytoskeleton structures by atomic force microscopy. *Methods Cell Biol* **95**:157-74.

Harry, E., Monahan, L., Thompson, L. (2006) Bacterial cell division: the mechanism and its precison. *Int Rev Cytol* **253**:27-94.

Hayes, F., Barilla, D. (2006) The bacterial segrosome: a dynamic nucleoprotein machine for DNA trafficking and segregation. *Nat Rev Microbiol* **4**:133-43.

Heichlinger, A., Ammelburg, M., Kleinschnitz, E.M., Latus, A., Maldener, I., Flärdh, K., Wohlleben, W., Muth, G. (2011) The MreB-like protein Mbl of *Streptomyces coelicolor* A3(2) depends on MreB for proper localization and contributes to spore wall synthesis. *J Bacteriol* **193**:1533-42.

Hempel, A.M., Wang, S.B., Letek, M., Gil, J.A., Flärdh, K. (2008) Assemblies of DivIVA mark sites for hyphal branching and can establish new zones of cell wall growth in *Streptomyces coelicolor*. *J Bacteriol* **190**(22):7579-7583.

Herrmann, H., Aebi, U. (2004) Intermediate filaments: molecular structure, assembly mechanism, and integration into functionally distinct intracellular scaffolds. *Annu Rev Biochem* **73**:749-789.

Hicks, M.G., Guymer, D., Buchanan, G., Widdick, D.A., Caldelari, I., Berks, B.C., Palmer, T. (2006) Formation of functional Tat translocases from heterologous components. *BMC Microbiol* **6**:64.

Higgins, M.L., Tsien, H.C. et al. (1976) Organization of mesosomes in fixed and unfixed cells. *J Bacteriol* **127**(3): 1519-1523.

Hille, A., Neu, T.R., Hempel, D.C., Horn, H. (2005) Oxygen profiles and biomass distribution in biopellets of *Aspergillus niger*. *Biotechnol Bioeng* **92**(5):614-623.

Hinderhofer, M., Walker, C.A., Friemel, A., Stuermer, C.A.O., Möller, H.M., Reuter, A. (2009) Evolution of prokaryotic SPFH proteins. *BMC Evol Biol* **9**.

Holmes, N.A., Walshaw, J., Leggett, R.M., Thibessard, A., Dalton, K.A., Gillespie, M.D., Hemmings, A.M., Gust, B., Kelemen, G.H. (2013) Coiled-coil protein Scy is a key component of a multiprotein assembly controlling polarized growth in *Streptomyces*. *Proc Natl Acad Sci USA* **110**(5):E397-406.

Hopwood, D.A. (2007) *Streptomyces* in nature and medicine: the antibiotic makers. Oxford University Press, New York.

Horinouchi, S. (2007) Mining and polishing of the treasure trove in the bacterial genus *Streptomyces*. *Biosci Biotechnol Biochem* **71**:283-299.

Hu, Z., Lutkenhaus, J. (1999) Topological regulation of cell division in *Escherichia coli* involves rapid pole to pole oscillation of the division inhibitor MinC under the control of MinD and MinE. *Mol Microbiol* **34**:82-90.

Hui, M.P., Galkin, V.E., Yu, X., Stasiak, A.Z., Stasiak, A., Waldor, M.K., Egelman, E.H. (2010) ParA2, a *Vibrio cholerae* chromosome partitioning protein, forms left-handed helical filaments on DNA. *Proc Natl Acad Sci USA* **107**:4590-5.

Ingerson-Mahar, M., Briegel, A., Werner, J.N., Jensen, G.J., Gitai, Z. (2010) The metabolic enzyme CTP synthase forms cytoskeletal filaments. *Nat Cell Biol* **12**:739-46.

Ingerson-Mahar, M., Gitai, Z. (2012) A growing family: the expanding universe of the bacterial cytoskeleton. *FEMS Microbiol Rev* **36**:256-266.

Inoué, S., Sato, H. (1967. Cell motility by labile association of molecules - nature of mitotic spindle fibers and their role in chromosome movement. *J Gen Physiol* **50**:259.

Izard, J., McEwen, B.F., Barnard, R.M., Portuese, T., Samsonoff, W.A., Limberger, R.J. (2004) Tomographic reconstruction of treponemal cytoplasmic filaments reveals novel bridging and anchoring components. *Mol Microbiol* **51**:609-18.

Jack,R.J., Sargent, F., Berks, B.C., Sawers, G., Palmer, T. (2001) Constitutive expression of *Escherichia coli tat* genes indicates an important role for the twin-arginine translocase during aerobic and anaerobic growth. *J Bacteriol* **183**:1801-1804.

Jakimowicz, D., van Wezel, G.P. (2012) Cell division and DNA segregation in *Streptomyces*: how to build a septum in the middle of nowhere? *Mol Microbiol* **85**:393-404.

Janik, P. (2012) Under the Hood: Using WebGL to Accelerate Advanced Physics Simulations in the Browser. http://concord.org/publications/newsletter/2012-fall/under-the-hood.

Jenkins, C., Samudrala, R., Anderson, I., Hedlund, B.P., Petroni, G., Michailova, N., Pinel, N., Overbeek, R., Rosati, G., Staley, J.T. (2002) Genes for the cytoskeletal protein tubulin in the bacterial genus *Prosthecobacter*. *Proc Natl Acad Sci USA* **99**:17049-54.

Jones, L.J., Carballido-López, R., Errington, J. (2001) Control of cell shape in bacteria: helical, actin-like filaments in *Bacillus subtilis*. *Cell* **104**:913-22.

Jyothikumar, V., Tilley, E.J., Wali, R., Herron, P.R. (2008) Time-lapse microscopy of *Streptomyces coelicolor* growth and sporulation. *Appl Environ Microbiol* **74**:6774-6781.

Kaplan, G. (1977) Differences in the mode of phagocytosis with Fc and C3 receptors in macrophages. *Scand J Immunol* **6**:797-807.

Karr, J.R., Sanghvi, J.C., Macklin, D.N., Gutschow, M.V., Jacobs, J.M., Bolival, B. Jr., Assad-Garcia, N., Glass, J.I., Covert, M.W. (2012) A whole-cell computational model predicts phenotype from genotype. *Cell* **150**(2):389-401.

Kawamoto, S., Watanabe, H., Hesketh, A., Ensign, J.C., Ochi, K. (1997) Expression analysis of the *ssgA* gene product, associated with sporulation and cell division in *Streptomyces griseus*. *Microbiol* **143**:1077-1086.

Keijser, B.J., Noens, E.E., Kraal, B., Koerten, H.K., van Wezel, G.P. (2003) The *Streptomyces coelicolor ssgB* gene is required for early stages of sporulation. *FEMS Microbiol Lett* **225**:59-67.

Kendrick, K.E., Ensign, J.C. (1983) Sporulation of *Streptomyces griseus* in submerged culture. *J Bacteriol* **155**(1):357-366.

Kieser, T., Bibb, M.J., Buttner, M.J., Chater, K.F., Hopwood, D.A. (2000) Practical *Streptomyces* genetics. The John Innes Foundation, Norwich, United Kingdom.

Koning, R.I., Koster, A.J. (2009) Cryo-electron tomography in biology and medicine. *Ann Anat* **191**:427-45.

Koonin, E.V. (1993) A superfamily of ATPases with diverse functions containing either classical or deviant ATP-binding motif. *J Mol Biol* **229**:1165-74.

Kossen, N.W. (2000) The morphology of filamentous fungi. *Advances Biochem Eng Biotechnol* **70**:1-33.

Krabben, P., Nielsen, J. (1998) Modeling the mycelium morphology of *Penicillium* species in submerged cultures. *Advances Biochem Eng Biotechnol* **60**:125-152.

Kremer, J.R., Mastronarde, D.N., McIntosh, J.R. (1996) Computer visualization of three-dimensional image data using IMOD. *J Struct Biol* **116**(1):71-76.

Kruse, T., Bork-Jensen, J., Gerdes, K. (2005). The morphogenetic MreBCD proteins of *Escherichia coli* form an essential membrane-bound complex. *Mol Microbiol* **55**(1):78-89.

Kruse, T., Møller-Jensen, J., Løbner-Olesen, A., Gerdes, K. (2003) Dysfunctional MreB inhibits chromosome segregation in *Escherichia coli*. *EMBO J* **22**:5283-92.

Kühn, J., Briegel, A., Morschel, E., Kahnt, J., Leser, K., Wick, S., Jensen, G.J., Thanbichler, M. (2010) Bactofilins, a ubiquitous class of cytoskeletal proteins mediating polar localization of a cell wall synthase in *Caulobacter crescentus*. *EMBO J* **29**:327-39.

Kürner, J., Frangakis, A.S., Baumeister, W. (2005) Cryo-electron tomography reveals the cytoskeletal structure of *Spiroplasma melliferum*. *Science* **307**:436-8.

Lafontaine, C., Valleton, J.M., Orange, M., Norris, V., Mileykovskaya, E., Alexandre, S. (2007) Behaviour of bacterial division protein FtsZ under a monolayer with phospholipid domains. *Biochim Biophys Acta* **1768**(11):2812-2821.

Landgraf, D., Okumus, B., Chien, P., Baker, T.A., Paulsson, J. (2012) Segregation of molecules at cell division reveals native protein localization. *Nature Meth* **9**:480-U498.

Larsen, R.A., Cusumano, C., Fujioka, A., Lim-Fong, G., Patterson, P., Pogliano, J. (2007) Treadmilling of a prokaryotic tubulin-like protein, TubZ, required for plasmid stability in *Bacillus thuringiensis*. *Genes Dev* **21**:1340-52.

Larson, J.L., Hershberger, C.L. (1986) The minimal replicon of a streptomycete plasmid produces an ultrahigh level of plasmid DNA. *Plasmid* **15**(3):199-209.

Leake, M.C., Greene, N.P., Godun, R.M., Granjon, T., Buchanan, G., Chen, S., Berry, R.M., Palmer, T., Berks, B.C. (2008) Variable stoichiometry of the TatA component of the twin-arginine protein transport system observed by in vivo single-molecule imaging. *Proc Natl Acad Sci USA* **105**:15376-15381.

Lejeune, R., Baron, G.V. (1997) Simulation of growth of a filamentous fungus in 3 dimensions. *Biotechnol Bioeng* **53**(2):139-150.

Lenarcic, R., Halbedel, S., Visser, L., Shaw, M., Wu, L.J., Errington, J., Marenduzzo, D., Hamoen, L.W. (2009) Localisation of DivIVA by targeting to negatively curved membranes. *EMBO J* **28**(15):2272-2282.

Leonard, T.A., Butler, P.J., Löwe, J. (2004) Structural analysis of the chromosome segregation protein Spo0J from Thermus thermophilus. Mol Microbiol 53:419-32.

Leonard, T.A., Møller-Jensen, J., Löwe, J. (2005) Towards understanding the molecular basis of bacterial DNA segregation. *Philos T Roy Soc B* **360**:523-35.

Letek, M., Fiuza, M., Villadangos, A.F., Mateos, L.M., Gil, J.A. (2012) Cytoskeletal proteins of *Actinobacteria*. *Int J Cell Biol*.

Li, Z., Trimble, M.J., Brun, Y.V., Jensen, G.J. (2007) The structure of FtsZ filaments in vivo suggests a force-generating role in cell division. *EMBO J* **26**:4694-708.

Liu, G., Chater, K.F., Chandra, G., Niu, G., Tan, H. (2013) Molecular regulation of antibiotic biosynthesis in *Streptomyces*. *Microbiol Mol Biol Rev* **77**:112-143.

Liu, G., Xing, M., Han, Q.G. (2005) A population-based morphologically structured model for hyphal growth and product formation in streptomycin fermentation. *World J Microb Biot* **21**(8-9):1329-1338.

López, D., Kolter, R. (2010) Functional microdomains in bacterial membranes. *Genes Dev* **24**:1893-1902.

Lu, C. L., Stricker, J., Erickson, H.P. (2001) Site-specific mutations of FtsZ - effects on GTPase and assembly in vitro, and cell division in vivo. *Mol Biol Cell* **11**:190a-191a.

Lu, S., Cutting, S., Kroos, L. (1995) Sporulation protein SpoIVFB from *Bacillus subtilis* enhances processing of the sigma factor precursor Pro-σ^K in the absence of other sporulation gene products. *J Bacteriol* **177**(4):1082-1085.

Lucić, V., Förster, F., Baumeister, W. (2005) Structural studies by electron tomography: from cells to molecules. *Annu Rev Biochem* **74**:833-65.

Lupas, A., Van Dyke, M., Stock, J. (1991) Predicting coiled coils from protein sequences. *Science* **252**(5009):1162-1164.

Lutkenhaus, J., Addinall, S.G. (1997) Bacterial cell division and the Z-ring. *Annu Rev Biochem* **66**:93-116.

Löwe, J., Amos, L.A. (1998) Crystal structure of the bacterial cell-division protein FtsZ. *Nature* **391**:203-6.

MacNeil, D.J., Gewain, K.M., Ruby, C.L., Dezeny, G., Gibbons, P.H., MacNeil, T. (1992) Analysis of *Streptomyces avermitilis* genes required for avermectin biosynthesis utilizing a novel integration vector. *Gene* **111**(1):61-68.

Männik, J., Wu, F., Hol, F.J.H., Bisicchia, P., Sherratt, D.J., Keymer, J.E., Dekker, C. (2012) Robustness and accuracy of cell division in *Escherichia coli* in diverse cell shapes. *Proc Natl Acad Sci USA* **109**(18):6957-6962.

Manteca, A., Alvarez, R., Salazar, N., Yagüe, P., Sanchez, J. (2008) Mycelium differentiation and antibiotic production in submerged cultures of *Streptomyces coelicolor*. *Appl Environ Microbiol* **74**(12):3877-3886.

Marchler-Bauer, A., Zheng, C., Chitsaz, F., Derbyshire, M.K., Geer, L.Y., Geer, R.C., Gonzales, N.R., Gwadz, M., Hurwitz, D., Lanczycki, C.J., Lu, F., Lu, S., Marchler, G.H., Song, J.S., Thanki, N., Yamashita, R.A., Zhang, D., Bryant, S.H. (2013) CDD: conserved domains and protein three-dimensional structure. *Nucleic Acids Res* **41**(Database issue):D348-352.

Margolin, W. (2009) Sculpting the bacterial cell. *Curr Biol* **19**:R812-22.

Margolin, W. (2012) The price of tags in protein localization studies. *J Bacteriol* **194**:6369-71.

Marston, A. L., Thomaides, H.B., Edwards, D.H., Sharpe, M.E., Errington, J. (1998) Polar localization of the MinD protein of *Bacillus subtilis* and its role in selection of the mid-cell division site. *Genes Dev* **12**:3419-30.

Matsumoto, K., J. Kusaka, Nishibori, A., Hara, H. (2006) Lipid domains in bacterial membranes. *Mol Microbiol* **61**(5):1110-1117.

Mauriello, E.M., Mouhamar, F., Nan, B., Ducret, A., Dai, D., Zusman, D.R., Mignot, T. (2010) Bacterial motility complexes require the actin-like protein, MreB and the Ras homologue, MglA. *EMBO J* **29**:315-26.

Mazouni, K., Pehau-Arnaudet, G., England, P., Bourhy, P., Saint Girons, I., Picardeau, M. (2006) The Scc spirochetal coiled-coil protein forms helix-like filaments and binds to nucleic acids generating nucleoprotein structures. *J Bacteriol* **188**:469-76.

Mazza, P., Noens, E.E., Schirner, K., Grantcharova, N., Mommaas, A.M., Koerten, H.K., Muth, G., Flärdh, K., van Wezel, G.P., Wohlleben, W. (2006) MreB of *Streptomyces coelicolor* is not essential for vegetative growth but is required for the integrity of aerial hyphae and spores. *Mol Microbiol* **60**:838-52.

McCormick, J.R. (2009) Cell division is dispensable but not irrelevant in *Streptomyces*. *Curr Opin Microbiol* **12**:689-98.

McCormick, J.R., Flärdh, K. (2012) Signals and regulators that govern *Streptomyces* development. *FEMS Microbiol Rev* **36**:206-231.

McCormick, J.R., Su, E.P., Driks, A., Losick, R. (1994) Growth and viability of *Streptomyces coelicolor* mutant for the cell division gene *ftsZ*. *Mol Microbiol* **14**:243-54.

McIntosh, R., Nicastro, D., Mastronarde, D. (2005) New views of cells in 3D: an introduction to electron tomography. *Trends Cell Biol* **15**:43-51.

Megee, R.D. 3rd, Kinoshita, S., Fredrickson, A.G., Tsuchiya, H.M. (1970) Differentiation and product formation in molds. *Biotechnol Bioeng* **12**(5):771-801.

Meyer, P., Dworkin, J. (2007) Applications of fluorescence microscopy to single bacterial cells. *Res Microbiol* **158**:187-194.

Meyerhoff, J., Tiller, V., Bellgardt, K.H. (1995) Two mathematical models for the development of a single microbial pellet. *Biotechnol Bioeng* **12**:305-313

Michel, F.C. Jr., Grulke, E.A., Reddy, C.A. (1992) Determination of the respiration kinetics for mycelial pellets of P*hanerochaete chrysosporium*. *Appl Environ Microbiol* **58**(5):1740-1745.

Michie, K.A., Löwe, J. 2006. Dynamic filaments of the bacterial cytoskeleton. *Annu Rev Biochem* **75**:467-92.

Mignot, T. (2007) The elusive engine in *Myxococcus xanthus* gliding motility. *Cell Mol Life Sci* **64**:2733-45.

Mignot, T., Shaevitz, J.W., Hartzell, P.L., Zusman, D.R. (2007) Evidence that focal adhesion complexes power bacterial gliding motility. *Science* **315**:853-6.

Miguélez, E.M., Hardisson, C., Manzanal, M.B. (2000) Streptomycetes: a new model to study cell death. *Int Microbiol* **3**(3):153-158.

Mika, J.T., Poolman, B. (2011) Macromolecule diffusion and confinement in prokaryotic cells. *Curr Opin Biotechnol* **22**:117-126.

Mileykovskaya, E., Dowhan, W. (2005) Role of membrane lipids in bacterial division-site selection. *Curr Opin Microbiol* **8**(2):135-142.

Mileykovskaya, E., Sun, Q., Margolin, W., Dowhan, W. (1998) Localization and function of early cell division proteins in filamentous *Escherichia coli* cells lacking phosphatidylethanolamine. *J Bacteriol* **180**(16): 4252-4257.

Miyawaki, A., Llopis, J., Heim, R., McCaffery, J.M., Adams, J.A., Ikura, M., Tsien, R.Y. (1997) Fluorescent indicators for Ca^{2+} based on green fluorescent proteins and calmodulin. *Nature* **388**:882-7.

Møller-Jensen, J., Jensen, R.B., Löwe, J., Gerdes, K. (2002) Prokaryotic DNA segregation by an actin-like filament. *EMBO J* **21**:3119-27.

Mori, H., Cline, K. (2002) A twin arginine signal peptide and the pH gradient trigger reversible assembly of the thylakoid ΔpH/Tat translocase. *J Cell Biol* **157**:205-210.

Moriya, S., Rashid, R.A., Rodrigues, C.D., Harry, E.J. (2010) Influence of the nucleoid and the early stages of DNA replication on positioning the division site in *Bacillus subtilis*. *Mol Microbiol* **76**(3):634-647.

Mukherjee, P., Sureka, K., Datta, P., Hossain, T., Barik, S., Das, K.P., Kundu, M., Basu, J. (2009) Novel role of Wag31 in protection of mycobacteria under oxidative stress. *Mol Microbiol* **73**(1):103-119.

Müller, M., Klösgen, R.B. (2005) The Tat pathway in bacteria and chloroplasts (review). *Mol Membr Biol* **22**:113-121.

Müller-Reichert, T., Srayko, M., Hyman, A., O'Toole, E.T., McDonald, K. (2007) Correlative light and electron microscopy of early *Caenorhabditis elegans* embryos in mitosis. *Methods Cell Biol* **79**:101-19.

Murray, H., Errington, J. (2008) Dynamic control of the DNA replication initiation protein DnaA by Soj/ParA. *Cell* **135**:74-84.

Nan, B., Zusman, D.R. (2011) Uncovering the mystery of gliding motility in the myxobacteria. *Annu Rev Genet* **45**:21-39.

Nanninga, N. (1971) The mesosome of *Bacillus subtilis* as affected by chemical and physical fixation. *J Cell Biol* **48**(1):219-224.

Nielsen, J. (1993) A simple morphologically structured model describing the growth of filamentous microorganisms. *Biotechnol Bioeng* **41**(7):715-727.

Nielsen, J., Villadsen, J. (1992) Modeling of microbial kinetics. *Chem Eng Sci* **47**(17-18):4225-4270.

Nieminen, L., Webb, S., Smith, M.C., Hoskisson, P.A. (2013) A flexible mathematical model platform for studying branching networks: experimentally validated using the model actinomycete, *Streptomyces coelicolor*. *PLoS ONE* **8**:e54316.

Nishibori, A., Kusaka, J., Hara, H., Umeda, M., Matsumoto, K. (2005) Phosphatidylethanolamine domains and localization of phospholipid synthases in *Bacillus subtilis* membranes. *J Bacteriol* **187**(6):2163-2174.

Noens, E.E., Mersinias, V., Willemse, J., Traag, B.A., Laing, E., Chater, K.F., Smith, C.P., Koerten, H.K., van Wezel, G.P. (2007) Loss of the controlled localization of growth stage-specific cell-wall synthesis pleiotropically affects developmental gene expression in an *ssgA* mutant of *Streptomyces coelicolor*. *Mol Microbiol* **64**:1244-1259.

Noens, E.E., Mersinias, V., Traag, B.A., Smith, C.P., Koerten, H.K., van Wezel, G.P. (2005) SsgA-like proteins determine the fate of peptidoglycan during sporulation of *Streptomyces coelicolor*. *Mol Microbiol* **58**:929-44.

Norris, V., Woldringh, C., Mileykovskaya, E. (2004) A hypothesis to explain division site selection in *Escherichia coli* by combining nucleoid occlusion and Min. *FEBS Lett* **561**(1-3): 3-10.

Palmer, T., Berks, B.C. (2012) The twin-arginine translocation (Tat) protein export pathway. *Nat Rev Microbiol* **10**:483-496.

Pamboukian, C.R.D., Guimaraes, L.M., Facciotti, M.C.R. (2002) Applications of image analysis in the characterization of *Streptomyces olindensis* in submerged culture. *Braz J Microbiol* **33**(1):17-21.

Paul, G.C., Thomas, C.R. (1996) A structured model for hyphal differentiation and penicillin production using *Penicillium chrysogenum*. *Biotechnol Bioeng* **51**(5):558-572.

Pichoff, S., Lutkenhaus, J. (2002) Unique and overlapping roles for ZipA and FtsA in septal ring assembly in *Escherichia coli*. *EMBO J* **21**:685-93.

Piette, A., Derouaux, A., Gerkens, P., Noens, E.E., Mazzucchelli, G., Vion, S., Koerten, H.K., Titgemeyer, F., De Pauw, E., Leprince, P., van Wezel, G.P., Galleni, M., Rigali, S. (2005) From dormant to germinating spores of *Streptomyces coelicolor* A3(2): new perspectives from the *crp* null mutant. *J Proteome Res* **4**(5):1699-1708.

Pilhofer, M., Jensen, G.J. (2012) The bacterial cytoskeleton: more than twisted filaments. *Curr Opin Cell Biol* **25**:125-133.

Pilhofer, M., Ladinsky, M.S., McDowall, A.W., Petroni, G., Jensen, G.J. (2011) Microtubules in bacteria: ancient tubulins build a five-protofilament homolog of the eukaryotic cytoskeleton. *PLoS Biol* **9**:e1001213.

Plitzko, J.M., Rigort, A., Leis, A. (2009) Correlative cryo-light microscopy and cryo-electron tomography: from cellular territories to molecular landscapes. *Curr Opin Biotechnol* **20**:83-9.

Pogliano, J., N. Osborne, et al. (1999) A vital stain for studying membrane dynamics in bacteria: a novel mechanism controlling septation during *Bacillus subtilis* sporulation. *Mol Microbiol* **31**(4):1149-1159.

Ptacin, J.L., Lee, S.F., Garner, E.C., Toro, E., Eckart, M., Comolli, L.R., Moerner, W.E., Shapiro, L. (2010) A spindle-like apparatus guides bacterial chromosome segregation. *Nat Cell Biol* **12**:791-8.

Ramamurthi, K.S., Lecuyer, S., Stone, H.A., Losick, R. (2009) Geometric cue for protein localization in a bacterium. *Science* **323**(5919): 1354-1357.

Raskin, D.M., de Boer, P.A. (1997) The MinE ring: an FtsZ-independent cell structure required for selection of the correct division site in *E. coli*. *Cell* **91**:685-94.

Raskin, D.M., de Boer, P.A. (1999) Rapid pole-to-pole oscillation of a protein required for directing division to the middle of *Escherichia coli*. *Proc Natl Acad Sci USA* **96**:4971-4976.

RayChaudhuri, D. (1999) ZipA is a MAP-Tau homolog and is essential for structural integrity of the cytokinetic FtsZ ring during bacterial cell division. *EMBO J* **18**:2372-83.

Reichl, U., Yang, H., Gilles, E.D., Wolf, H. (1990) An improved method for measuring the interseptal spacing in hyphae of *Streptomyces tendae* by fluorescence microscopy coupled with image processing. *FEMS Microbiol Lett* **67** (1-2):207-209.

Reusch, V.M. Jr., Burger, M.M. (1973) The bacterial mesosome. *Biochim Biophys Acta* **300**(1):79-104.

Rodrigues, C.D., Harry, E.J. (2012) The Min system and nucleoid occlusion are not required for identifying the division site in *Bacillus subtilis* but ensure its efficient utilization. *PLoS Genet* **8**:e1002561.

Romberg, L., Levin, P.A. (2003) Assembly dynamics of the bacterial cell division protein FtsZ: poised at the edge of stability. *Annu Rev Microbiol* **57**:125-154.

Rothfield, L., Taghbalout, A., Shih, Y.L. (2005) Spatial control of bacterial division-site placement. *Nat Rev Microbiol* **3**(12): 959-968.

Ruban-Ośmiałowska, B., Jakimowicz, D., Smulczyk-Krawczyszyn, A., Chater, K.F., Zakrzewska-Czerwińska, J. (2006) Replisome localization in vegetative and aerial hyphae of *Streptomyces coelicolor*. *J Bacteriol* **188**:7311-7316.

Salje, J., Zuber, B., Löwe, J. (2009) Electron cryomicroscopy of *E. coli* reveals filament bundles involved in plasmid DNA segregation. *Science* **323**:509-12.

Salzberg, L.I., Helmann, J.D. (2008) Phenotypic and transcriptomic characterization of *Bacillus subtilis* mutants with grossly altered membrane composition. *J Bacteriol* **190**(23):7797-7807.

Sambrook, J., Fritsch, E.F., Maniatis, T. (1989) Molecular cloning: a laboratory manual. N.Y., Cold Spring Harbor Laboratory Press.

Sartori, A., Gatz, R., Beck, F., Rigort, A., Baumeister, W., Plitzko, J.M. (2007) Correlative microscopy: bridging the gap between fluorescence light microscopy and cryo-electron tomography. *J Struct Biol* **160**:135-45.

Saxena, R., Fingland, N., Patil, D., Sharma, A.K., Crooke, E. (2013) Crosstalk between DnaA protein, the initiator of *Escherichia coli* chromosomal replication, and acidic phospholipids present in bacterial membranes. *Int J Mol Sci* **14**(4):8517-8537.

Schaerlaekens, K., Schierova, M., Lammertyn, E., Geukens, N., Anné, J., van Mellaert, L. (2001) Twin-arginine translocation pathway in *Streptomyces lividans*. *J Bacteriol* **183**:6727-6732.

Schlieper, D., Oliva, M.A., Andreu, J.M., Löwe, J. (2005) Structure of bacterial tubulin BtubA/B: evidence for horizontal gene transfer. *Proc Natl Acad Sci USA* **102**:9170-5.

Scholefield, G., Errington, J., Murray, H. (2012) Soj/ParA stalls DNA replication by inhibiting helix formation of the initiator protein DnaA. *EMBO J* **31**:1542-55.

Schroeder, T.E. (1972) The contractile ring. II. Determining its brief existence, volumetric changes, and vital role in cleaving *Arbacia* eggs. *J Cell Biol* **53**:419-34.

Schwartz, C. L., V. I. Sarbash, F. I. Ataullakhanov, J. R. McIntosh, D. Nicastro. (2007) Cryo-fluorescence microscopy facilitates correlations between light and cryo-electron microscopy and reduces the rate of photobleaching. *J Microsc* **227**:98-109.

Schwedock, J., McCormick, J.R., Angert, E.R., Nodwell, J.R., Losick, R. (1997) Assembly of the cell division protein FtsZ into ladder-like structures in the aerial hyphae of *Streptomyces coelicolor*. *Mol Microbiol* **25**(5):847-858.

Shapiro, L., McAdams, H.H., Losick, R. (2009) Why and how bacteria localize proteins. *Science* **326**:1225-1228.

Shih, Y.L., Rothfield, L. (2006) The bacterial cytoskeleton. *Microbiol Mol Biol Rev* **70**:729-54.

Silva, M.T., Sousa, J.C.F., Polónia, J.J., Macedo, M.A.E., Parente, A.M. (1976) Bacterial mesosomes - real structures or artifacts. *Biochim Biophys Acta* **443**(1):92-105.

Sontag, C.A., Staley, J.T., Erickson, H.P. (2005) *In vitro* assembly and GTP hydrolysis by bacterial tubulins BtubA and BtubB. *J Cell Biol* **169**:233-8.

Specht, M., Schätzle, S., Graumann, P.L., Waidner, B. (2011) *Helicobacter pylori* possesses four coiled-coil rich proteins that form extended filamentous structures and control cell shape and motility. *J Bacteriol* **193**:4523-4530.

Srivastava, P., Demarre, G., Karpova, T.S., McNally, J., Chattoraj, D.K. (2007) Changes in nucleoid morphology and origin localization upon inhibition or alteration of the actin homolog, MreB, of *Vibrio cholerae*. *J Bacteriol* **189**:7450-63.

Steinberg, G. (2007) Hyphal growth: a tale of motors, lipids, and the Spitzenkörper. *Eukaryot Cell* **6**(3): 351-360.

Strahl, H., Hamoen, L.W. (2010) Membrane potential is important for bacterial cell division. *Proc Natl Acad Sci USA* **107**(27): 12281-12286.

Stuart, D.C. Jr. (1959) Fine structure of the nucleoid and internal membrane systems of *Streptomyces*. *J Bacteriol* **78**: 272-281.

Subramaniam, S. (2005) Bridging the imaging gap: visualizing subcellular architecture with electron tomography. *Curr Opin Microbiol* **8**:316-22.

Sun, M., Wartel, M., Cascales, E., Shaevitz, J.W., Mignot, T. (2011) Motor-driven intracellular transport powers bacterial gliding motility. *Proc Natl Acad Sci USA* **108**:7559-64.

Sun, Q., Margolin, W. (1998) FtsZ dynamics during the division cycle of live *Escherichia coli* cells. *J Bacteriol* **180**(8):2050-2056.

Swulius, M.T., Chen, S., Jane Ding, H., Li, Z., Briegel, A., Pilhofer, M., Tocheva, E.I., Lybarger, S.R., Johnson, T.L., Sandkvist, M., Jensen, G.J. (2011) Long helical filaments are not seen encircling cells in electron cryotomograms of rod-shaped bacteria. *Biochem Biophys Res Commun* **407**:650-5.

Swulius, M.T., Jensen, G.J. (2012) The helical MreB cytoskeleton in *E. coli* MC1000/pLE7 is an artifact of the N-terminal YFP tag. *J Bacteriol* **194**(23):6382-6.

Taivalsaari, A., Mikkonen, T., Antonnen, M., Salminen, A. (2011) The death of binary software: end-user software moves to the web. Ninth International Conference on Creating, Connecting and Collaborating through Computing, IEEE Computer Society: 17-23.

Tinsley, E., Khan, S.A. (2006) A novel FtsZ-like protein is involved in replication of the anthrax toxin-encoding pXO1 plasmid in *Bacillus anthracis*. *J Bacteriol* **188**:2829-35.

Tocheva, E.I., Li, Z., Jensen, G.J. (2010) Electron cryotomography. *Cold Spring Harb Perspect Biol* **2**(6):a003442.

Tough, A.J., Prosser, J.I. (1996) Experimental verification of a mathematical model for pelleted growth of *Streptomyces coelicolor* A3(2) in submerged batch culture. *Microbiol* **142**(3):639-648.

Traag, B.A., van Wezel, G.P. (2008) The SsgA-like proteins in actinomycetes: small proteins up to a big task. *Anthonie van Leeuwenhoek* **94**(1):85-97.

Tresner, H.D., Hayes, J.A., Backus, E.J. (1967) Morphology of submerged growth of streptomycetes as a taxonomic aid (I) Morphological development of *Streptomyces aureofaciens* in agitated liquid media. *Appl Microbiol* **15** (5):1185-1191.

Treuner-Lange, A., Aguiluz, K., van der Does, C., Gómez-Santos, N., Harms, A., Schumacher, D., Lenz, P., Hoppert, M., Kahnt, J., Munoz-Dorado, J., Søgaard-Andersen, L. (2012) PomZ, a ParA-like protein, regulates Z-ring formation and cell division in *Myxococcus xanthus*. *Mol Microbiol* **87**(2):235-53.

Vale, R.D., Reese, T.S., Sheetz, M.P. (1985) Identification of a novel force-generating protein, kinesin, involved in microtubule-based motility. *Cell* **42**:39-50.

van den Brink-van der Laan, E., Boots, J.W., Spelbrink, R.E., Kool, G.M., Breukink, E., Killian, J.A., de Kruijff, B. (2003) Membrane interaction of the glycosyltransferase MurG: a special role for cardiolipin. *J Bacteriol* **185**(13): 3773-3779.

van den Ent, F., Amos, L.A., Löwe, J. (2001) Prokaryotic origin of the actin cytoskeleton. *Nature* **413**:39-44.

van den Ent, F., Møller-Jensen, J., Amos, L.A., Gerdes, K., Löwe, J. (2002) F-actin-like filaments formed by plasmid segregation protein ParM. *EMBO J* **21**:6935-43.

van Driel, L.F., Valentijn, J.A., Valentijn, K.M., Koning, R.I., Koster, A.J. (2009) Tools for correlative cryo-fluorescence microscopy and cryo-electron tomography applied to whole mitochondria in human endothelial cells. *Eur J Cell Biol* **88**:669-84.

van Suijdam, J.C., Hols, H., Kossen, N.W. (1982) Unstructured model for growth of mycelial pellets in submerged cultures. *Biotechnol Bioeng* **24**(1):177-191.

van Teeffelen, S., Wang, S., Furchtgott, L., Huang, K.C., Wingreen, N.S., Shaevitz, J.W., Gitai, Z. (2011) The bacterial actin MreB rotates, and rotation depends on cell-wall assembly. *Proc Natl Acad Sci USA* **108**:15822-7.

van Wezel, G.P., Krabben, P., Traag, B.A., Keijser, B.J., Kerste, R., Vijgenboom, E., Heijnen, J.J., Kraal, B. (2006) Unlocking *Streptomyces* spp. for use as sustainable industrial production platforms by morphological engineering. *Appl Environ Microbiol* **72**:5283-8.

van Wezel, G.P., Mahr, K., Konig, M., Traag, B.A., Pimentell-Schmitt, E.F., Willimek, A., Titgemeyer, F. (2005) GlcP constitutes the major glucose uptake system of *Streptomyces coelicolor* A3(2). *Mol Microbiol* **55**(2):624-636.

van Wezel, G.P., McDowall, K.J. (2011) The regulation of the secondary metabolism of *Streptomyces*: new links and experimental advances. *Nat Prod Rep* **28**(7):1311-1333.

van Wezel, G.P., McKenzie, N.L., Nodwell, J.R. (2009) Chapter 5. Applying the genetics of secondary metabolism in model actinomycetes to the discovery of new antibiotics. *Methods Enzymol* **458**:117-141.

van Wezel, G.P., van der Meulen, J., Kawamoto, S., Luiten, R.G., Koerten, H.K., Kraal, B. (2000a) *ssgA* is essential for sporulation of *Streptomyces coelicolor* A3(2) and affects hyphal development by stimulating septum formation. *J Bacteriol* **182**(20):5653-5662.

van Wezel, G.P., van der Meulen, J., Taal, E., Koerten, H.K., Kraal, B. (2000b) Effects of increased and deregulated expression of cell division genes on the morphology and on antibiotic production of streptomycetes. *Anthonie van Leeuwenhoek* 78 (3-4):269-276.

van Wezel, G.P., White, J., Hoogvliet, G., Bibb, M.J. (2000c) Application of *redD*, the transcriptional activator gene of the undecylprodigiosin biosynthetic pathway, as a reporter for transcriptional activity in *Streptomyces coelicolor* A3(2) and *Streptomyces lividans*. *J Mol Microbiol Biotechnol* **2**:551-556.

Vara, J., Lewandowska-Skarbek, Wang, Y.G., Donadio, S., Hutchinson, C.R. (1989) Cloning of genes governing the deoxysugar portion of the erythromycin biosynthesis pathway in *Saccharopolyspora erythraea* (*Streptomyces erythreus*). *J Bacteriol* **171**(11):5872-5881.

Vats, P., Rothfield, L. (2007) Duplication and segregation of the actin (MreB) cytoskeleton during the prokaryotic cell cycle. *Proc Natl Acad Sci USA* **104**:17795-800.

Vats, P., Yu, J., Rothfield, L. (2009) The dynamic nature of the bacterial cytoskeleton. *Cell Mol Life Sci* **66**:3353-62.

Waidner, B., Specht, M., Dempwolff, F., Haeberer, K., Schaetzle, S., Speth, V., Kist, M., Graumann, P.L. (2009) A novel system of cytoskeletal elements in the human pathogen *Helicobacter pylori*. *PLoS Pathog* **5**(11):e1000669.

Walshaw, J., Gillespie, M.D., Keleman, G.H. (2010) A novel coiled-coil repeat variant in a class of bacterial cytoskeletal proteins. *J Struct Biol* **170**(2):202-215.

Wang, L., Khattar, M.K., Donachie, W.D., Lutkenhaus, J. (1998) FtsI and FtsW are localized to the septum in *Escherichia coli*. *J Bacteriol* **180**(11):2810-2816.

Wardell, J.N., Stocks, S.M., Thomas, C.R., Bushell, M.E. (2002) Decreasing the hyphal branching rate of *Saccharopolyspora erythraea* NRRL 2338 leads to increased resistance to breakage and increased antibiotic production. *Biotechnol Bioeng* **78**:141-146.

Widdick, D.A., Dilks, K., Chandra, G., Bottrill, A., Naldrett, M., Pohlschroder, M., Palmer, T. (2006) The twin-arginine translocation pathway is a major route of protein export in *Streptomyces coelicolor*. *Proc Natl Acad Sci USA* **103**:17927-17932.

Willemse, J., Borst, J.W., de Waal, E., Bisseling, T., van Wezel, G.P. (2011) Positive control of cell division: FtsZ is recruited by SsgB during sporulation of *Streptomyces*. *Genes Dev* **25**:89-99.

Willemse, J., Mommaas, A.M., van Wezel, G.P. (2012) Constitutive expression of ftsZ overrides the *whi* developmental genes to initiate sporulation of *Streptomyces coelicolor*. *Anthonie van Leeuwenhoek* **101**:619-32.

Willemse, J., Ruban-Ośmiałowska, B., Widdick, D., Celler. K., Hutchings, M.I., van Wezel, G.P., Palmer, T. (2012) Dynamic localization of Tat protein transport machinery components in *Streptomyces coelicolor*. *J Bacteriol* **194**:6272-6281.

Willemse, J., van Wezel, G.P. (2009) Imaging of *Streptomyces coelicolor* A3(2) with reduced autofluorescence reveals a novel stage of FtsZ localization. *PLoS One* **4**:e4242.

Wintrebert, P. (1931) La rotation immédiate de l'oeuf pondu et la rotation d'activation chez *Discoglossus pictus*. *Otth Comptes Rend Soc Biol* **106**:439-442.

Wolański, M., Wali, R., Tilley, E., Jakimowicz, D., Zakrzewska-Czerwińska, J., Herron, P. (2011) Replisome trafficking in growing vegetative hyphae of *Streptomyces coelicolor* A3(2). *J Bacteriol* **193**:1273-1275.

Woldringh, C.L., Mulder, E., Huls, P.G., Vischer, N. (1991) Toporegulation of bacterial division according to the nucleoid occlusion model. *Res Microbiol* **142**:309-20.

Wolgemuth, C., Hoiczyk, E., Kaiser, D., Oster, G. (2002) How myxobacteria glide. *Curr Biol* **12**:369-77.

Wright, C.S. (1984) Structural comparison of the two distinct sugar binding sites in wheat germ agglutinin isolectin II. *J Mol Biol* **178**(1):91-104.

Wu, L.J., Errington, J. (2004) Coordination of cell division and chromosome segregation by a nucleoid occlusion protein in *Bacillus subtilis*. *Cell* **117**:915-25.

Wu, L.J., Errington, J. (2011) Nucleoid occlusion and bacterial cell division. *Nat Rev Microbiol* **10**:8-12.

Xu, Q., B. A. Traag, B.A., Willemse, J., McMullan, D., Miller, M.D., Elsliger, M.A., Abdubek, P., Astakhova, T., Axelrod, H.L., Bakolitsa, C., Carlton, D., Chen, C., Chiu, H.J., Chruszcz, M., Clayton, T., Das, D., Deller, M.C., Duan, L., Ellrott, K., Ernst, D., Farr, C.L., Feuerhelm, J., Grant, J.C., Grzechnik, A., Grzechnik, S. K., Han, G.W., Jaroszewski, L., Jin, K.K., Klock, H.E., Knuth, M.W., Kozbial, P., Krishna, S.S., Kumar, A., Marciano, D., Minor, W., Mommaas, A.M., Morse, A.T., Nigoghossian, E., Nopakun, A., Okach, L., Oommachen, S., Paulsen, J., Puckett, C., Reyes, R., Rife, C.L., Sefcovic, N., Tien, H.J., Trame, C.B., van den Bedem, H., Wang, S., Weekes, D., Hodgson, K.O., Wooley, J., Deacon, A.M., Godzik, A., Lesley, S.A., Wilson, I.A., van Wezel, G.P. (2009) Structural and functional characterizations of SsgB, a conserved activator of developmental cell division in morphologically complex actinomycetes. *J Biol Chem* **284**:25268-79.

Yang, H., King, R., Reichl, U., Gilles, E.D. (1992a) Mathematical-model for apical growth, septation, and branching of mycelial microorganisms. *Biotechnol Bioeng* **39**(1):49-58.

Yang, H., Reichl, U., King, R., Gilles, E.D. (1992b) Measurement and simulation of the morphological development of filamentous microorganisms. *Biotechnol Bioeng* **39**(1):44-48.

Yang, R.F., Bartle, S., Otto, R., Stassinopoulos, A., Rogers, M., Plamann, L., Hartzell, P. (2004) AglZ is a filament-forming coiled-coil protein required for adventurous gliding motility of *Myxococcus xanthus*. *J Bacteriol* **186**:6168-6178.

You, Y., Elmore, S., Colton, L.L., Mackenzie, C., Stoops, J.K., Weinstock, G.M., Norris, S.J. (1996) Characterization of the cytoplasmic filament protein gene (*cfpA*) of *Treponema pallidum* subsp. *pallidum*. *J Bacteriol* **178**:3177-87.

Young, K.D. (2010) Bacterial shape: two-dimensional questions and possibilities. *Annu Rev Microbiol* **64**:223-40.

Zangirolami, T.C., Johansen, C.L., Nielsen, J., Jørgensen, S.B. (1996) Simulation of penicillin production in fed-batch cultivations using a morphologically structured model. *Biotechnol Bioeng* **56**(6):593-604.

CURRICULUM VITAE

Katherine Anna Celler was born on the 30th of July, 1985, in Vancouver, Canada. In 2002, she graduated from St. Thomas Aquinas High School in North Vancouver. Between 2002-2007 she studied at the University of British Columbia (UBC) in Vancouver, obtaining a Bachelor of Applied Sciences (BASc) in Chemical and Biological Engineering. During her studies she completed three internships, fulfilling the requirements for the UBC co-operative education option. These internships involved operation of several pilot-scale bioleaching extraction columns at Outokumpu Research Oy, in Pori, Finland; testing of anti-stiction coatings for acceleration Micro-Electro Mechanical Systems or MEMS at Robert BOSCH GmbH in Stuttgart, Germany; and quantifying metal extraction and circuit stage efficiency at the smelter operations of Teck Cominco Metals Ltd. in Trail, Canada. In 2009 she obtained her MSc in Chemical Engineering from the Delft University of Technology. Her MSc project, completed under the supervision of Dr. Cristian Picioreanu of the Environmental Biotechnology group, involved modeling the formation of microbial streamers in river biofilms. In the fall of 2009 she started as a PhD student at Leiden University, working in the Molecular Biotechnology group under the supervision of Prof. Dr. Gilles van Wezel. The work done as a PhD student is presented in this thesis.

LIST OF PUBLICATIONS

Celler, K., van Wezel, G.P., Willemse, J. (2013) Single particle tracking of dynamically localizing TatA complexes in *Streptomyces coelicolor. Biochemical and Biophysical Research Communications.* Aug; 438(1):38-42.

Celler, K., Koning, R.I., Koster, A.J., van Wezel, G.P. (2013) A multidimensional view of the bacterial cytoskeleton. *Journal of Bacteriology*. Apr; 195(8):1627-36.

Willemse, J., Ruban-Ośmiałowksa, B., Widdick, D., **Celler, K.**, Hitchings, M.I., van Wezel, G.P., Palmer, T. (2012) Dynamic localization of Tat protein transport machinery components in *Streptomyces coelicolor*. *Journal of Bacteriology*. Nov; 194(22):6272-81.

Celler, K., Picioreanu, C., van Loosdrecht, M.C.M., van Wezel, G.P. (2012) Structural morphological modeling as a Framework for Rational Strain Design of *Streptomyces* species. *Anthonie van Leeuwenhoek*. Oct; 102(3):409-23.